SLOPE STABILITY ANALYSIS ALONG SELECTED SECTION OF ARBAREKETE-GALAMSO ROAD, WEST HARARGE ZONE, EASTERN ETHIOPIA

Abdi Kamilo Umare

A Thesis Submitted to the Department of Applied Geology

School of Applied Natural Science

Presented in Partial Fulfillment of the Requirement for the Degree of Master of Science in Applied Geology

Office of Graduate Studies

Adama Science and Technology University

October, 2023

Adama, Ethiopia

Slope Stability Analysis along Selected Section of Arbarekete-Galamso Road, West Hararge Zone, Eastern Ethiopia

Abdi Kamilo Umare

Major Advisor: Dr. Yadeta Chemdesa

Co-Advisor: Tola Garo (MSc)

A Thesis Submitted to the Department of Applied Geology

School of Applied Natural Science

Presented in Partial Fulfillment of the Requirement for the Degree of Master of Science in Applied Geology

Office of Graduate Studies

Adama Science and Technology University

October, 2023

Adama, Ethiopia

Declaration

I hereby declared that this MSc thesis entitled "**Slope stability analysis along selected section of Arbarekete-Galamso road, west Hararge Zone, Eastern Ethiopia**" is my own work. That is, it has not been submitted for the award of any academic degree, diploma or certificate in any other university. All sources of material that are used for this thesis have been duly acknowledged through citation.

Abdi Kamilo	______________________	_______________
Name of student	Signature	Date

Recommendation of Advisors

We, the advisors of this thesis, hereby certify that we have closely advised the student while developing this thesis and read the revised version of the thesis entitled "**Slope stability analysis along selected section of Arbarekete-Galamso road, west Hararge Zone, Eastern Ethiopia**" prepared under our guidance by Abdi Kamilo. Therefore, we recommend the submission of revised version of the thesis to the department following the applicable procedures.

______________________	____________________	_____________
Major Advisor	Signature	Date
______________________	____________________	_____________
Co-advisor	Signature	Date

Approval sheet of advisors

We, the advisors of the thesis entitled "**Slope stability analysis along selected section of Arbarekete-Galamso road, west Hararge Zone, Eastern Ethiopia**" developed by Abdi Kamilo, hereby certify that the recommendation and suggestions made by the board of examiners are appropriately incorporated into the final version of the thesis.

______________________	______________________	______________
Major Advisor/Supervisor	Signature	Date
______________________	______________________	______________
Co-advisor/ Co-supervisor	Signature	Date

Approval of Board of Reviewers

We, the undersigned members of the Board of Examiners of the thesis by Abdi Kamilo, have read and evaluated the thesis entitled "**Slope stability analysis along selected section of Arbarekete-Galamso road, west Hararge Zone, Eastern Ethiopia**" and examined the candidate during open defense. This is, therefore, to certify that the thesis is accepted for partial fulfillment of the requirement of the degree of Master of Science in Applied geology.

______________________________	______________________	____________________
Chairperson	Signature	Date
______________________________	______________________	____________________
Reviewer 1	Signature	Date
______________________________	______________________	____________________
Reviewer 2	Signature	Date

Finally, approval and acceptance of the thesis is contingent upon Submission of its final copy to the Office of Postgraduate Studies (OPGS) through the Department Graduate Council (DGC) and School Graduate Committee (SGC).

______________________________	______________________	____________________
Department Head	Signature	Date
______________________________	______________________	____________________
School Dean	Signature	Date
______________________________	______________________	____________________
Office of Postgraduate Studies, Dean	Signature	Date

ACKNOWLEDGEMENTS

First and foremost, I would like to express my heartfelt gratitude and 'shukran' to the Almighty Allah for all the good graces and mercies He has blessed me with in my life. I am truly grateful for His guidance and for providing me with a successful path throughout my thesis work.

Next, I would like to extend my deepest appreciation to my advisor, Dr. Yadeta Chemdesa, and my co-advisor, Tola Garo (MSc), for their unwavering encouragement, invaluable advice, and continuous follow-up, which helped me complete this thesis. I would also like to thank the Geology department, School of Applied Natural Science, and Adama Science and Technology University for providing me with a conducive working environment and their entire supportive staff who were always ready to help me with whatever I needed on time.

I would like to offer my deepest thanks to my family, particularly to my wife and sisters-brothers, for their unwavering support and encouragement during my study. I am truly grateful for their sacrifices and understanding throughout my thesis work. Additionally, I would like to express my gratitude to my colleagues, particularly to Mr. Ditta Amano, and all others who gave me valuable shared ideas, materials, and support for my thesis work.

I would also like to thank Al-Asab organization and their Geotechnical Laboratory staff for the material and laboratory support they provided me, which helped me accomplish this thesis. Moreover, I would like to extend my appreciation to the Ethiopian minister of mine and energy, Ethiopian Geospatial Information Agency (EGIA) and the National Metrological Agency for providing me with the necessary data for my research work.

Lastly, I would like to express my acknowledgement to Oda Bultum University for their financial support, which helped me throughout my study. Their generosity has made a significant impact on my academic success, and I am truly grateful.

Table of Contents

LIST OF TABLES

LIST OF FIGURE

LIST OF ABBREVIATIONS AND ACRONYMS

ANS = Arabian Nubian shield

ASTM = American Society for Testing Materials Standard

DEM = Digital elevation model

EBCS = Ethiopian Building Code Standard

FEM = Finite element method

FOS = Factor of safety

GLEM= General Limit Equilibrium method

GPS = Geographic Positioning System

GSI = Geological strength index

ISRM = "International Society of Rock Mechanics" Standards

JCS= Joint Wall Compressive Strength

JV = Volumetric Joint Count

LEM = Limit equilibrium method

MDD = Maximum dry density

M.M. = Modified Mercalli

MB = Mozambique belts

OMC = Optimum moisture content

RMR = Rock Mass Rating

RQD = Rock Quality Designation

RSS = Rock Slope Section

SMR = Slope Mass Rating

SRF = Strength reduction factor

UCS = Uniaxial Compressive Strength

USCS = Unified Soil Classification Systems

ABSTRACT

Slope instabilities are among the most common natural geohazards in the world's hilly and mountainous terrains causing loss of life and damage to infrastructures. The Arbarekete-Galamso road is a critical area of road infrastructure construction that requires attention due to its traversing in hilly and mountainous terrains that can have issues with slope instability. So, the present study was conducted to identify and analyze the stability of the slope along selected Arbarekete-Galamso road sections and to suggest some remedial measures based on field investigation and analysis results. A detailed field investigation for this study includes a discontinuity survey, in situ rock testing, soil and rock sampling for laboratory analysis, slope geometry, and orientation measurements. Based on visual observation and some field manifestations, the study revealed seven critical rock slope sections along with two critical soil slope sections for stability analysis. A detailed stability analysis was carried out using kinematic, deterministic, limit equilibrium and finite element methods on these critical slope sections. Kinematic analyses performed with dips software showed wedge modes of rock slope failure occurring at slope sections RSS1 and RSS2, and planar modes of rock slope failure occurring at slope sections RSS1 and RSS5. Additionally, deterministic methods were conducted to determine the factor of safety by using Swedge and Rocplane for wedge and planar failures, respectively. Furthermore, the soil laboratory analysis result revealed that soils are classified as sand soils (medium to high plasticity) with moisture contents ranging from 11.5 to 20.7%, a liquid limit range of 44.42 to 67.24% and a plasticity index of 16.9 to 36.3%. The stability analysis was conducted for static dry, static saturated, dynamic dry, and dynamic saturated loading conditions using deterministic methods, limit equilibrium and finite element methods. The analysis revealed that changes in slope angle, height, and benching slope geometry can improve slope stability, and the installation of retaining walls, rock bolts, anchors, and drainage controls can prevent slope failure.

Keywords: *Factor of safety, Finite element method, Kinematic analysis, Limit equilibrium method, Slope stability analysis.*

CHAPTER ONE

1. INTRODUCTION

1.1 Background

Throughout the world, slope instabilities are one of the major natural hazards for human activities spatially, to the civil engineering structure such as road, tunnels, dams and open pit mines (Siddique, et al., 2019; Dietze, et al., 2022). It occurs in the form of rotational, translational and wedge mode of failure causing different impact on properties, lives, and blocking traffic activity (Kumar, 2022; Pantelidis, 2010).

Slope instabilities occur in natural slopes or man-modified slopes, and are triggered by various agents like rainfall, earthquakes, stream undercuts or excavations. The properties and orientation of a discontinuity in the rock mass are the most important factors in rock slope stability (Awang, et al., 2021). The type and filling material properties of joints, the external forces conditions, weathering, and groundwater level in tensional cracks are additional effective parameters that contribute to instability (Kumar & Raj Kumar, 2022; Bao, et al., 2022). The slope stability depends on the orientation of discontinuity in the rock mass. The slopes along the road cut may fail due to the presence of irregularly oriented discontinuities in the rock mass (Bekele & Meten, 2022; Roul, et al., 2021). According to Chen, et al. (2022) stability of the cut slope can be disturbed mainly by improper modification to natural slope during construction and widening of the road. And most of the time, there is a general lack of focus for detailed investigation and design for mitigation of slope instability related problems during design of the same road projects. According to Abramson, et al. (2002) the engineering solutions to slope instability problems require a good understanding of analytical methods, investigative tools, and stabilization measures.

In the past, many geotechnical engineers and engineering geologists have performed slope stability analyses using different techniques. In geo-mechanical engineering, to asses and analyze stability of the slope, some of the methods such as: Limit equilibrium method, Finite element method, Kinematic analysis and Rock mass classification systems, Deterministic, Probabilistic and Numerical methods (Vanneschi, et al., 2022; Pandit, et al., 2021) are used frequently.

The rock mass classification system is widely used in geotechnical engineering to assess the stability of rock slopes and aid in their design (Yang et al., 2022; Elmo & Stead, 2020). Various analytical and numerical modeling techniques have been employed by researchers, including kinematic analysis, limit equilibrium methods, and finite element methods (Azarafza et al., 2021; Rehmana et al., 2020). Kinematic analysis, performed using DIPS 6.0 software, helps to determine the geometric relationship between joint sets and the slope face to understand failure mechanisms (Khanna & Dubey, 2021; Ansari et al., 2020).

Slope stability evaluations can be conducted using the limit equilibrium method or the finite element approach with the shear strength reduction (SSR) technique to analyze the factor of safety (Mebrahtu et al., 2022). The factor of safety (FOS) is the ratio of resisting forces to driving forces and is used to describe slope stability (Renani & Martin, 2020; Sudani & Patil, 2022). For slope stability analysis, both the limit equilibrium method (LEM) and the finite element method (FEM) can be used, employing software such as Rocscience Slide v6.0 and Phase2 v8.0 (Komadja et al., 2021). The LEM can be divided into rigorous and non-rigorous techniques, and in this study, the Morgenstern and Price method was adopted, as it is a rigorous method that can handle any shape of slip surface and accurately satisfies the complete equilibrium criteria (Zheng, 2012). FEM is useful for solving complex problems involving stress and movement data, which are not be feasible with the limit equilibrium method (Martinelli et al., 2021).

Slope instability problems are widespread along roads that pass through mountainous terrenes/gorges/valleys in Ethiopia. Most of the Ethiopian plateau in the north, south, west and eastern parts of the country has a history of slope instability both at superficial materials and bedrock levels due to steep mountains and road cuts (Bekele & Meten, 2022). The current study area is situated along the eastern highland plateau very close to the Eastern Rift Margin and partly lies within the northwestern extreme end of Ogaden basin. Hence, stability analysis of cut slope was performed to have information on the slope deformation, state of stresses at critically unstable failure zones, different mode failures and safe functional design of excavated slopes using different slope stability analysis methods.

The present study was conducted to evaluate the stability of slope along selected section of Arbarekete-Galamso road using kinematic analysis, limit equilibrium and finite element method. For this purpose, determining the engineering properties of soils and rocks through extensive field survey, discontinuity measurements and sampling, in situ tests, literature review and correlation, and laboratory experiments were performed in order to extract necessary data. Finally, appropriate remedial measures were recommended based on the analysis results.

1.2 Statement of Problem

Slope instability is one of the most hazardous processes in the world which was caused by failure of soil, rock or combination of soil and rock along the road section (Gao, et al., 2022). Slope stability analyzing is an important tool for designing and constructing road infrastructure along steep slopes (Andualem, et al., 2022; Kabeta, et al., 2020). Slope instability along road cuts that built in Ethiopia's highlands cross valleys, hills, and mountains is a common problem. This can cause damage to human beings as well as properties. According to Bekele & Meten (2022), previous studies have shown that slopes along roads are repeatedly affected by slope instability (landslide) problems. The main triggers of slope instability are various environmental factors (e.g., heavy summer rains), geological and structural factors (weak rocks, sliding debris, weak soils, shear bands, and faults), and characteristics of difficult roads (narrow roads). According to the previous studies, the failure of slopes and Landslides hazards have been causing loss of human life, failure of engineering structures and damage to agricultural lands and the natural environments (Haile Fekadu, et al., 2022). Hence, slope stability analysis is crucial to identify critical slope sections and apply different remedial measures.

The present study was undertaken along the road between the Arbarekete and Badesa town**.** Nevertheless, the road is affected by frequent slope instability problems during and after its construction. The problem is intensified mainly during rainy season in which different mode of rock slope failure such as planar, wedge and rock falls fall onto the road. In addition, some part of the road was also subjected to soil slope failures which nearly have circular shape. The stated slope stability problem along the road section hinders day to day traffic activities by blocking and damaging the road. Furthermore, there was no research and other investigation done on slope stability along the road section to identify, analyze and recommend proper remedial measures.

Therefore, this work aims to fill this gap by studying geological and geotechnical condition of materials of the slope section to identify, locate and analyze slope stability problems along selected road section using different approaches such as: Kinematic analysis, Limit equilibrium and Finite element methods. Finally, appropriate remedial measures were recommended based on the analysis results.

1.3 Objective of the Study

1.3.1 General Objective

The main objective of this study is to analyze the slope stability condition along selected section of Arbarekete-Galamso road.

1.3.2 Specific Objective

The specific objectives of this research are:

- To identify and locate the potential slope to instability problems along selected road sections.
- To determine geological and geotechnical properties of soils and rock of the critical slope sections.
- To determine the factor of safety and failure probability of the critical slope sections.
- To identify the causative or triggering factors responsible for slope instability.
- To suggest the possible remedial measures for the identified problems.

1.4 Significance of the Study

The findings of the study are highly significant as it provide detailed information on the stability condition of the area and suggest potential remedial measures. The slope analysis results will be crucial in designing the road corridor optimally to minimize the risk of sliding slope mass while also ensuring a safe and cost-effective environment for its intended purpose. The study has been thoroughly examined the stability condition of the site and the underlying causes of instability in the study area. This will be instrumental in understanding possible slope instabilities that have occurred along the selected section of the road corridor.

1.5. Limitations of the Research

Several rock slope failures were found along the road segments in the current study area. However, because of time, resource, and financial constraints, the investigations were limited to only a subsection of the slopes that showed high potential instability. As a result, only nine (9) critical slope sections were chosen and analyzed in the current study. Furthermore, the present study area lacks the sufficient secondary data such as drill log geophysical data to understand the subsurface geology.

CHAPTER TWO

2. LITERATURE REVIEW

2.1 INTRODUCTION

Slope failures pose a significant natural hazard in construction projects worldwide, leading to infrastructure damage and potential risks to human lives (Panchal & Shrivastava, 2022). These failures can lead to severe damage to critical structures such as dams, buildings, roads, and railroads (Dadi & Chala, 2022). Slope failures can be attributed to several factors, including material strength, slope geometry, geo-hydrological conditions, weathering, and heavy rainfall (Sousa, et al., 2022). These factors can weaken the stability of slopes, making them susceptible to failure (Filice, et al., 2022). In Ethiopia, ground slope instability, surface flooding, soil erosion, and natural geological variations are prevalent contributors to the damage of constructed infrastructure, particularly along roads passing through mountainous regions (Fikadu, 2021). Therefore, it is crucial to implement preventative measures and employ strategies like rock mechanics studies to mitigate the effects of slope instability (Laimer, 2021). This essay aims to explore the factors contributing to slope instability, various analysis methods used to assess slope failure, and common remedial measures employed to mitigate the effects. Additionally, it will discuss failure criteria for both soil and rock, as well as software applications that can aid in addressing this critical issue.

2.2 Slope Instability Governing Factors

A majority of rock slope instability in the past has been driven by natural processes (Savi, et al., 2021). When the downward movements of material due to gravity and shear stresses exceed the shear strength slope failure will occurred. Instability of the slope deals the relationship between shear stress and shear strength forces (Kumar, 2022). Some factors enhance and increase stress force; whereas, others add to the resisting force. The stability analysis of rock slopes, especially regarding the plane mode of failure, heavily relies on the influences of two governing factors - internal and external. These factors play a crucial role in determining the overall stability of the rock slopes and should not be overlooked. It is essential to carefully consider all the governing factors to ensure the safety of the rock slopes and surrounding areas. The combination of both internal and external factors mentioned above will be responsible for defining the stability condition of the slope.

2.2.1 Internal Factors

According to Bekele & Meten (2022), the main internal governing factors are the geometry of the slope, potential failure plane characteristics, surface drainage, and groundwater condition.

The geometry of the slope: The geometry of the slope is defined by the inclination of the slope, upper slope surface inclination, slope height, potential failure plane dip amount and dip direction, tension crack or upper release joint, and the lateral release surfaces (Zheng, et al., 2018). The main driving force acting on the slope is the gravitational force which is directly proportional to the slope inclination. The steeper slope will be more susceptible than the gentler slope to instability (Hamza & Raghuvanshi, 2017). According to Mamot, et al. (2018), due to the increase in shear stress and a decrease in normal stress on the potential rupture plane steep slopes have a greater risk of instability. Also, the possibility of slope failure or landslide occurrence will increase with increasing slope height.

The potential failing planes: One of the factors which determine the stability of the rock and soil slope is the potential failure plane. The characteristics of discontinuities and their inter-relationship with the slope geometry affect the stability condition of rock slopes (Havaej & Stead, 2016). The main characteristics of discontinuities that control the stability of rock slopes are spacing, orientation, persistence, surface characteristics, separation of discontinuity surface, and thickness of material filled in discontinuities. Similarly, in soil slopes weak layers of soil which sometimes rest on hard strata serve as failure planes. For the specific mode of rock slope failure to occur, the dip of the potential failure plane should be less than the dip of the slope face but greater than the friction angle along the failure plane (Hoek and Bray, 1981; Willy and Mah, 2004).

Drainage of surface water and groundwater conditions: The increased pore water pressure along potential failure plane can reduce the shear strength, and the water can also lubricate the surface, making it easier for things to slide around (Yang, et al., 2018). According to Ermias, et al. (2017), increases in groundwater in soil slope results in the development of pore water pressure which reduces the shear strength in the soil mass.

2.2.3 External Factors

Rainfall, seismicity, and manmade activities are the external slope instability governing factors (Ermias, et al., 2017).

The rainfall: Most of the time, the main reason for slope failure occurrence is the influence of rainfall which is one of the external and triggering factors of slope instability (Abbate, et al., 2019; Chen, et al., 2021). Rainfall is the main triggering factor for slope instability in rock slopes (Ermias, et al., 2017). The rainfall, which infiltrates into the slope, increases the instability of the potential failure plane by reducing shear strength (Gallage, et al., 2021; Raghuvanshi, 2017). One of the impacts of rainfall is it increases the elevation of groundwater level. Groundwater in turn affects the stability of the rock slope for the following reason (Wyllie and Mah, 2004). Water pressure affects the stability of the rock slope by decreasing resisting force along the failure plane. A change in moisture content of the rock accelerates weathering and then decreases the shear strength of the rock. Freezing of groundwater and surface water in tension crack can causes a buildup of water pressure which in turn decreases the stability of the slope. It's important to note that increasing the degree of weathering in the rock can have a negative impact on the stability of the slope, specifically the toe of the slope. When evaluating the impact of groundwater on slope stability, one of the methods is to determine the recharge and discharge areas concerning the location of unstable rock slopes. This can help in understanding how groundwater affects the stability of the slope and can be useful in planning any construction or development in the area (Wyllie and Mah, 2004).

The seismicity: Seismic activity is another triggering factor of slope stability especially in active seismic zone (Mebrahtu, et al., 2022). According to Zhao & Karim (2018), slope failures that happened by the earthquake may occur due to an increase in driving movement and reducing the shear strength According to Karray, et al. (2018) the slopes which are stable during static conditions may fail during dynamic seismic loading. The minimum magnitude of an earthquake to cause slope failure is approximately 4-5MM (BAYOU, 2020). From the safety point of view, it is recommended that seismicity is taken into consideration for critical structures like steep slopes (Caroles, 2023). Since horizontal seismic acceleration adds to driving force along failure plane, planar mode of rock slope failures will be easily destabilized under seismic loading conditions (Raghuvanshi, 2017).

Human activities: Human activity like improper modifications and excavations of the slope can trigger the stability of the slope. Most of the time human activities which can cause the slope to fail are: cutting the slope in an unplanned manner, steepening the slope gradient, improper excavation on the toe of the slope, and adding an extra load (Raghuvanshi, 2017).

The natural slope stability is disturbed and loses its stability in slope due to man-made activities (Pradhan, et al., 2018).

2.2.4 Geotechnical Properties of Soils and Rocks

Geotechnical factors like porosity, gradation factors, dry density, saturated permeability, and shear strength have been identified to contribute to the predictions of slope failures from the physical-based approach (Gidday, et al., 2023; Gutierrez-Martin, 2020). The soil composition depth shear strength (which is dependent on density, cohesion, plasticity, dilatancy, and the angle of internal friction), porosity, permeability, grading, moisture content, and organic matter content are some of the important geotechnical parameters of soils that control slope stability (Kamal, et al., 2022). The strength parameters of the rock change by mechanical and chemical weathering. Weathering reduces the mechanical properties of rocks and causes rock slope failures according to Endalu and Rao (2018). The cohesion and angle of internal friction are the shear strength parameters of the slope material, and they are the key factors that define resisting force acting normal to the failure plane (Raghuvanshi, 2017).

Lithology: lithology is strongly related to slope instability by weathering processes, water percolation, and interaction of rock mass. Weathered rock mass allows percolation of water via joints and fractures which can promote slope failure. The properties of rock materials such as strength and permeability are related to the degree of weathering and internal structure of the rock.

Geological discontinuity: The most significant variable for assessing rock slope stability is discontinuity strength than orientation (Khanna & Dubey, 2021; Asmare & Hailemariam, 2021). The characteristics of discontinuities and their inter-relationship with the slope geometry affect the stability condition of rock slopes (Carter & Marinos, 2020). The main characteristics of discontinuities that control the stability of rock slopes are spacing orientation, persistence, surface characteristics, separation of discontinuity surface, and thickness of material filled in discontinuities. The tectonic setting of the area also contributes to slope instability by fracturing, faulting, jointing, and foliation structures (Wolter, 2020). Fault and fracture zones indicate weak zones; therefore, they may be favorable planes of weakness where failures occur.

2.3 Type of Slope Failures

Slope failures can occur in a variety of ways depending on the cause of failure, geometry, material properties, and rate of movement (Aydan, 2016). According to Idrees & Pradhan (2018), depending on the type and degree of structural control, the modes of rock slope failures are mostly classified into circular, planar, wedge, and toppling mode of failures. There are necessary structural conditions that must be fulfilled for the kinematic admissibility of a planar and wedge mode of failure.

2.3.1 Circular (Rotational) Failure

Circular failure occurs when the individual particles in the soil or rock mass are very smaller than the size of the slope and are not interlocked due to their shape. Then, crushed rock in a large waste dump tends to behave as soil and the failures occur following a circular mode (Singh, et al., 2022).

2.3.2 Plane Failure

The planar type of failure is down-dip sliding on a single discrete discontinuity surface whose orientation concerning the face of the slope plays crucial in its analyses (Mebrahtu, 2021). Kinematic admissibility of a planar mode of failure requires four necessary structural conditions according to (Hoek and Bray, 1981; Goodman, 1989; Wyllie and Norrish, 1996; Wyllie and Mah, 2004). The favorable conditions of plane failure are: Firstly, the sliding plane and the slope face must have parallel strikes with each other within a range of ±20°. Secondly, the dip of the discontinuity should be less than the dip of the slope, and the failure plane should daylight on the slope face. Thirdly, the angle of friction on the surface should be less than the dip of the planar discontinuity. Lastly, the upper end of the sliding surface must either intersect the upper slope or terminate in a tension crack. By satisfying all of these favorable conditions, the plane failure can be successfully achieved.

2.3.3 Wedge Failure

Wedge failure occurs when two discontinuities strike obliquely into the slope face of the rock and form a slide of a wedge-shaped block along the line of intersection of these two planes (Ahmed, et al., 2023; Bowa, 2020). In order for wedge failure to be kinematically admissible, there are certain structural conditions that must be met. For example, the dip of the slope needs to be steeper than the dip of the line of intersection of the two discontinuities. Additionally, the line of intersection must daylight on the slope face, and the dip of the line of intersections needs to be greater than the angle of friction of the surface. Finally, the upper ends of the line of intersections need to either intersect the upper slope or terminate in a tension crack. These conditions must all be fulfilled for the planar mode of failure to occur.

2.3.4 Toppling

According to Bowa & Samson (2022), toppling failure is an overturning of a rock block through a pivot point found below its center of gravity. It is a type of failure that mainly occurs in rock masses that are sub-divided into a series of slabs or columns formed by a set of fractures that strike almost parallel to the slope face and steeply dip into the rock mass (Mebrahtu, 2021).

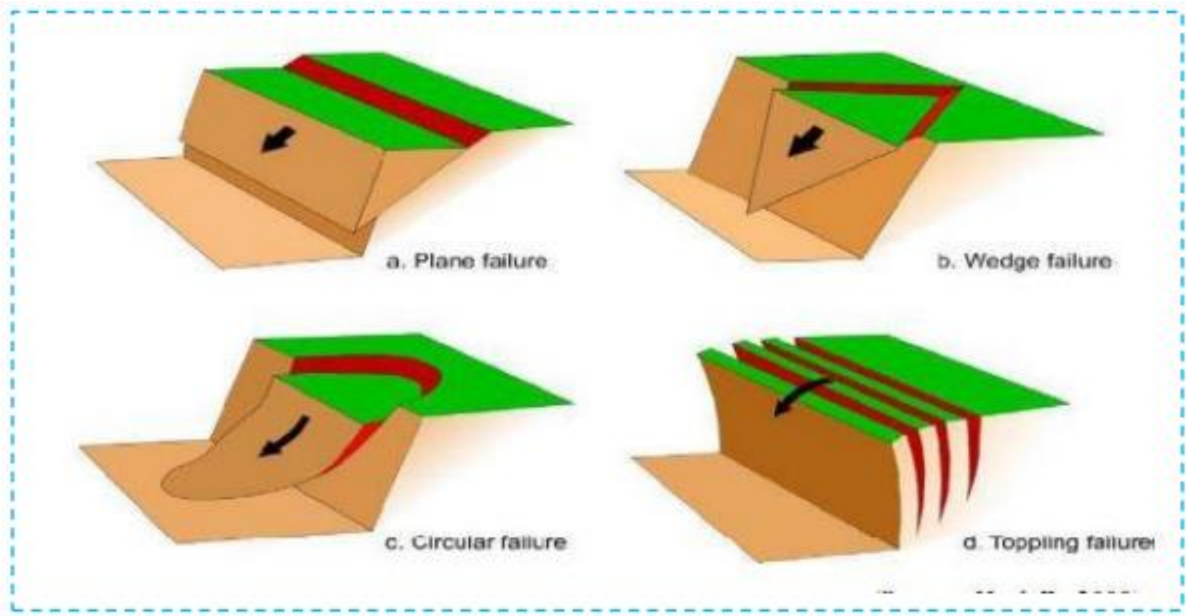

Figure2.1: Simplified image of the most common types of slope failure (Hoek, 2009).

2.4 Failure Criteria of Soil and Rock

Different types of criteria can define failure mechanisms. Some of these criteria depend on strain level, but most of them are based on the shear stress when compared to the shear strength.

2.4.1 Mohr-Coulomb Failure Criterion

The Mohr-Coulomb failure criterion is the most common and widely used in soil mechanics. This model is a perfectly elastic-plastic model and has been mostly used in geotechnical applications (Ambassa & Amba, 2022). Mohr-coulomb gives a failure criterion of soil material by using a critical combination of normal and shear stress (Pauli, et al., 2021). The linear empirical equation of the Mohr-Coulomb criterion relates the shear strength of the material on the failure plane with the cohesion, normal stress, and angle of internal friction of the material (Eq .2.1).

$$\tau f = c + \sigma n \tan\emptyset \qquad \text{Eq.2.1}$$

Where, τ = is the shear stress, σ= is the normal stress, c= is the cohesion of the material, and ϕ is the material angle of friction.

2.4.2 Hoek-Brown Failure Criterion

Hoek–Brown criterion started from the properties of intact rock and then introduced factors to diminish these properties based on the characteristics of joints in a rock mass (Hoek, et al., 2002). It was developed as a means to estimate the strength of rock mass by scaling the relationship derived according to the geological conditions present (ISRM, 2014). The edition of the 2002 Hoek–Brown criterion utilizes the following equation (Eq.2.2)

$$\sigma 1 = \sigma 3 + \sigma ci \left(\mathrm{mb}\ \frac{\sigma 3}{\sigma \mathrm{ci}} + \mathrm{s}\right)^{\mathrm{a}} \qquad \text{Eq.2.2}$$

Where σ1 and σ3 are the maximum and the minimum effective principal stresses at failure respectively, mb, s, and α are the values of Hoek-Brown constants for the rock mass, σci is the uniaxial compressive strength of the intact rock.

2.4.3. Barton-Bandis Failure Criterion

According to Barton's (1973) empirical law of basic friction angle, the shear strength of discontinuities in rock slopes can be determined by taking into account several factors, including surface roughness, rock strength at the surface, applied normal stress, and the amount of shear displacement (Barton, et al., 2023). These combined effects play a crucial role in determining the shear strength of discontinuity surfaces. The Barton-Bandis failure Criterion can be expressed in the following way (Eq. 2.3):

$$\tau = \partial n * \tan \{\mathrm{JRC} * \log 10\ (cs\ \sigma n) + \phi r\} \qquad \text{Eq. 2.3}$$

Where: τ = Peak shear strength, ∂n = Effective normal stress, JRC = Joint roughness coefficient, JCS = Joint wall compressive strength, ϕr = Residual friction angle

Joint wall compressive strength (JCS) is the strength of a layer of rock adjacent to a joint and it controls the strength and deformation properties of the rock mass (Barton, et al., 2023). According to Barton, et, al. (2023), the joint roughness coefficient (JRC) is the coefficient of joint surface roughness with a value ranging from 0- 20 (smoothest to roughest). A basic friction angle (ϕb) is an angle with a flat, planar, and un-weathered rock surface in which its value ranges from 25º-35º.

2.5 Methods for Slope Stability Analysis

As demand for better awareness of the failure mechanism of both man-made and natural slopes increases, slope stability analysis has become a common task in geotechnical engineering. To aid in this process, various scholars and organizations have created a variety of rock slope stability assessment procedures or techniques (Alhamdi & Albusoda, 2021). These techniques include conventional methods such as Slope mass rating, Kinematic analysis, and limit equilibrium, as well as numerical methods such as finite element methods (Abramson, et al., 2002).

2.6 Conventional Method

2.6.1 Rock Mass Classifications Systems

Rock Mass Classification Systems are an important tool for assessing rock mass quality and rock slope stability. These systems are used to classify and group rock masses into classes based on defined relationships, such as composition, strength, and deformation properties (Bieniawski, 1989). Rock Mass Rating (RMR), Rock Mass Quality Designation (RQD), and Geological Strength Index (GSI) are among the rock mass classification systems that have gained international recognition (Hussian, et al., 2020; Zhang, et al., 2019). The purpose of these systems is to classify rock masses based on qualitative parameters such as strength, discontinuity condition, weathering condition, and structural orientation. This information is then used to estimate deformability and strength properties, as well as provide measurable data for support estimation and communication between researchers, designers, engineers, and contractors (Bieniawski, 1989). Additionally, rock mass classification is useful for assessing the performance of rock-cut slopes using the most important inherent and structural parameters (Fereidooni, et al., 2015). Overall, rock mass classification systems are an essential tool for engineers to ensure the safe and efficient construction of engineering structures in rock masses.

2.6.1.1 Rock Mass Rating (RMR)

The Rock Mass Rating is a classification system used to assess the stability and support requirements of tunnels. It was originally developed by Prof. Z.T. Bieniawski in 1973 based on his experience with shallow tunnels in sedimentary rocks. Since then, the system has undergone several significant changes and modifications, including in 1979 and 1989 (Palin, et al., 2020). The most widely used version of the classification system is Bieniawski's 1989 version, which divides the rock mass into several structural regions and classifies each region separately (Edelbro, 2004). To classify the rock mass using the RMR system, six parameters are used, including uniaxial compressive strength, rock quality designation, joint spacing, joint condition, joint orientation, and groundwater condition. The five parameters mentioned earlier represent the RMRbasic parameters, and joint spacing, joint condition, and groundwater condition can be estimated in the field by visual observation and using instruments such as a tape meter.

2.6.1.2 Uniaxial Compressive Strength (UCS) of Intact Rock

Determining the uniaxial compressive strength of rock material is a crucial factor in rock engineering practice (Beran, 2008). Core samples or Schmidt hammer strength tests in the field can be used to estimate the value of uniaxial compressive strength (UCS) of the intact rock (Omar, 2017; Jalali, et al., 2017). Additionally, empirical formulas such as Broch and Franklin's (1972) formula can be used to estimate UCS from the point load strength index Is(50) or Schmidt hammer rebound hardness value (R) measurements in laboratory and insitu tests (Aydin, 2009). Schmidt hammer hardness values (N-values) are also used in laboratory and in situ tests to evaluate the UCS and modulus of elasticity (E) of intact rock (Rahim et al. 2021). Correlations have been proposed between rebound number and UCS, such as the one suggested by Miller (1965) for use in rock quality. Furthermore, Barton and Choubey (1977) proposed an empirical equation for calculating the rock UCS by multiplying the rebound number by the dry density of the rock using the empirical equation below.

$$\log 10\ (UCS) = 0.00088\ \gamma R + 1.01 \qquad \text{Eq.2.4}$$

Where; UCS is the uniaxial compressive strength in Mpa, γ is the dry rock densities in KN/m3 and R is the average rebound value of Schmidt hammer.

2.6.1.3. Point Load Strength Index

According to the information provided, the point load test is a cost-effective and practical method for determining the strength of rocks. This test involves measuring the applied force (P) and distance (D) between conical platens when a core specimen or irregular rock is placed between them until failure occurs (ASTM D5731, 1995). This method is useful because it is simple to perform on straight or cut blocks and irregular (ASTM, 2008). Many studies have been conducted to understand the relationship between UCS and point load index for various rock types. Broch and Franklin's equation provides a useful formula for describing this relationshipas as the following equation 2.5:

$$UCS = 24 * Is\,(50) \qquad \text{Eq. 2.5}$$

Where Is (50) is the size corrected point load strength

2.6.1.4 Rock Quality Designation

The Rock Quality Designation (RQD) index is a useful tool for assessing the quality of rock masses based on drill core logs. It was developed by Deere (1988) and is calculated as the percentage of core pieces longer than 100 mm (10 cm) that are still intact as shown in Eq. below. This provides a quantitative measure of the rock mass quality, which can be used to determine the best course of action for any given project. By analyzing the RQD index, engineers and geologists can gain valuable insights into the strength and stability of the rock beneath the surface, which is crucial for ensuring the safety and success of any construction or mining operation.

$$\text{RQD} = \frac{\sum \text{Length of core pieces} > 10\text{cm}}{\text{Total length of core}} * 100 \qquad \text{Eq.2.6}$$

The RQD determined from the above equation is used only when core drill samples are available and not applicable for surface exposure of rock quality estimation. When no core is available but discontinuity traces are visible in surface exposures the RQD can be estimated using the volumetric count method proposed by Palmström (1982). Under this condition, RQD is estimated using the following formula:-

$$\text{RQD} = 115 - 3.3\text{Jv} \qquad \text{Eq.2.7}$$

Where, Jv is the total number of discontinuities more than 10 cm long in 1 x 1 m exposed rock face (Volumetric Joint count) or Jv is obtained from following equation

$$\text{Jv} = \left(\frac{1}{S1}\right) + \left(\frac{1}{S2}\right) + \left(\frac{1}{S3}\right) + \ldots\ldots + \left(\frac{1}{Sn}\right) \qquad \text{Eq.2.8}$$

Where S1, S2, and S3 are the average spacing for the joint sets.

2.6.1.5 Geological Strength Index (GSI)

The Geological Strength Index (GSI) is a rock mass classification system that was developed by Hoek (1994) and further refined by Hoek, Kaiser, and Bawden (1995). This system provides a way to estimate the reduction in rock mass strength under different geological conditions. The GSI grouping system is widely used to assess the strength and deformation characteristics of extensively jointed rock masses, as it separates the rock mass into five categories based on field observations of its structure (Ambassa & Amba, 2022). These observations range from blocky to fragmented, and help to determine the GSI value (Ambassa & Amba, 2022). According to Wyllie and Mah (2004), the GSI value is determined by observing the weathering condition of the discontinuity surface, rock mass structure, and interlocking of rock blocks in the study area. Once the Geological Strength Index and mi have been estimated, the rock mass strength parameters used to describe its characteristics are calculated using the following formula.

$$\text{Mb} = \text{mi} \exp\left(\frac{GIS-100}{28-14D}\right) \qquad \text{Eq.2.9}$$

Mi. for intact rock is determined from lab triaxial test or the tabulated data proposed by Hoek, Kaiser, and Bawden (1995) for different types of rock.

2.6.1.6 Slope Mass Rating

The slope mass rating (SMR) is a modification to the rock mass rating that was first developed by Romana in 1985 (Dahiya, et al., 2022). Initially, it was only used for planar and toppling modes of failure. However, Anbalagan and his team modified the method in 1992 to account for the wedge mode of failure as well. To obtain SMR, adjustment factors derived from joint-slope relationship and method of excavation were added to the basic rock mass rating (RMR). Based on stability class and probability of failures, the relationship below can be used to determine the stability of a rock slope.

$$\text{SMR} = \text{RMRbasic} + (F1 * F2 * F3) + F4 \qquad \text{Eq. 2.10}$$

Where RMRbasic is basic rock mass rating according to Bieniawski (1989), F1 – depends upon Parallelism between joints and slope face strikes (αj - αs) where αj is the joint strike and αs is strike of slope. F2 – refers to joint dip angle (βj) or plunge of line of intersection of two wedge forming planes (βi). F3 – depends upon relationship between joint dip or plunge of the line of intersection of two wedge forming planes and slope inclination (βj - βs) or (βi - βs) where βs is the inclination of the slope. F4 – Method of Excavation. It includes the natural slope, or the cut slope excavated by pre-splitting, smooth blasting, normal blasting, poor blasting, and mechanical excavation.

2.6.2 Kinematic Analysis

Kinematic analyses is a method used to analyze the potential for the various modes of rock slope failures (plane, wedge, toppling failures), that occur due to the presence of unfavorably oriented discontinuities along road, hilly and pit slope (Hoek and Bray, 1981; Wyllie and Mah, 2004). It shows the motion of bodies without reference to the forces that cause them to move (Goodman, 1989). Kinematic analyses were done to identify several mode of rock slope failure by plotting discontinuity orientation on stereonet using software like (Dips 6.0 & Rocscience, 2004). The analysis was done by importing friction angle (friction cone), dip and dip directions of slope and discontinuities into dips software. Then, the software undergo the kinematic analyses by identifying main joint, daylight envelope, lateral limits and mode of rock slope failure (Goodman, 1989; Hudson and Harrison, 1997; and Willy and Mah, 2004).

To consider the kinematic admissibility of planar mode of failure the following criteria must be satisfied:

- ✓ The plane on which sliding occurs must strike near parallel to the slope face (within approx. ±20°).
- ✓ Release surfaces (that provide negligible resistance to sliding) must be present to define the lateral slide boundaries.
- ✓ The sliding plane must “daylight” in the slope face.
- ✓ The dip of the sliding plane must be greater than the angle of friction.
- ✓ The upper end of the sliding surface either intersects the upper slope, or terminates in a tension crack.

Similar to planar failures, several conditions relating to the line of intersection must be met for wedge failure to be kinematically admissible:

- ✓ The dip of the slope must exceed the dip of the line of intersection of the two wedge forming discontinuity planes.
- ✓ The line of intersection must “daylight” on the slope face.

- ✓ The dip of the line of intersection must be such that the strength of the two planes is reached.
- ✓ The upper end of the line of intersection either intersects the upper slope, or terminates in a tension crack.

In addition, toppling mode of failure may occur when the dip direction of the slope face is approximately towards the opposite orientation of the dip direction of the discontinuity plane, but toppling will not occur when the difference between the strike of the slope face and the strike of the plane of the discontinuities is relatively big; say more than 20º (Qin & Zhou, 2023). The necessary conditions for toppling failure to occur can be summarized as follows (Hoek and Bray, 1981):

- ✓ The strike of the layers must be approximately parallel to the slope face. Differences in these orientations of them is between 15 and 30 degrees have been quoted by various workers, but for consistency with other modes of failure, a value of 20 degrees seems appropriate.
- ✓ The dip of the layers must be into the slope face.

2.6.3 Limit Equilibrium Method

Based on the research of Wu et al. (2022), it was suggested that Limit Equilibrium methods (LEM) are a suitable option for analyzing slope failure in plane mode. As Tang et al. (2016), these methods are relatively simple compared to numerical methods. The Limit Equilibrium method evaluates the different forces responsible for the rock mass movement and the resisting forces. The factor of safety (FOS) is then defined by the ratio of resisting forces to driving forces at equilibrium (Price, 2009). This technique is used to determine factors of safety for stability analysis (Qin & Zhou, 2023). Once the mode of rock slope failure is identified using kinematic analysis, the factor of safety can be determined by considering the force leading the rock mass to fail along the failure surface and the force resisting the rock mass to fail (Qin & Zhou, 2023).

In the case of soil slope stability analysis, there is no predefined failure surface as with rock slope failures. The soil tends to have a circular shape failure (Qin & Zhou, 2023). The factor of safety of the circular mode of failure in soil slope can be determined from the ratio of shear strength to shear stress, as stated by Hossain in 2011. According to Hossain (2011), the stability of the slope depends on the factor of safety, with a value greater than 1 suggesting a stable slope, less than 1 indicating an unstable slope, and equal to 1 suggesting the slope is in a critical state of equilibrium.

According to Abramson et al. (2002), Limit equilibrium techniques are performed using safety factors by dividing the soil mass into different slices, and normal and shear inter-slice force and equilibrium can be determined from it. Some slice's methods of limit equilibrium are used to determine the factor of safety for a mode of failure. Wang et al. (2020), noted that there are different limit equilibrium methods for slope stability analysis, including Swedish Circle, Bishop's modified method, Janbu's generalized method of a slice, Spencer's method, and Morgenstern and Price's method. The generalized Limit Equilibrium (GLE) method is used for circular and noncircular failure surfaces and satisfies both force and moment equilibrium, encompassing most of the assumptions used by various LEMs.

2.7 Numerical Method

When it comes to analyzing slope stability, conventional methods can be limited in their scope of application. These methods are typically only effective for simple slope geometries and basic loading conditions, and can provide limited analyses regarding the mechanism of slope failure. However, a numerical modeling approach has been developed to address this issue and provide an approximate solution to problems that would have otherwise been difficult to solve using conventional methods (Abramson et al., 2002). This approach involves solving slope stability through mathematical calculation while taking deformation into account. There are three main types of numerical slope stability analyses approach, including continuum, discontinue, and hybrid modeling approach, and they are primarily used for rock slope stability analysis (Abramson et al., 2002).

2.7.1 Continuum Modeling

For the analysis of slopes that are made up of homogeneous, massive, weak rocks, and soil-like or heavily jointed rock masses, a numerical modeling approach is ideal (Eberhardt, 2003). This approach involves solving slope stability through mathematical calculation while taking deformation into account. The continuum modeling approach is one of the main types of numerical slope stability analyses and is best suited for this type of analysis. Shear strength parameters along the failure plane, surface and groundwater conditions, and in-situ stress are the main input parameters for continuum modeling (Raghuvanshi, 2017).

2.7.2 Finite Element Methods

Gosz (2017) suggests that the Finite element method (FEM) is a powerful numerical tool that can be used to solve many engineering problems, depending on the mechanical behavior of slope materials. With recent advancements in computer technology, the finite element method has become a preferable alternative to traditional methods in geotechnical engineering. The gravity increase method and strength reduction techniques are widely utilized in finite element methods. The gravity forces and weight gradually increase until the slope becomes unstable when using the gravity increase method. The factor of safety is then determined from the ratio between gravitational acceleration in failure time and actual gravitational acceleration. During the strength reduction method, the strength parameters of the slope decrease until the slope becomes unstable. The factor of safety for this method is obtained from the ratio of actual strength parameters and critical strength parameters. Slope stability analyses using the finite element method depend on the shear strength reduction (SSR) technique, which is helpful in determining the factor of safety and the improvement after strengthening (Wanstreet, 2007). The finite element method is used in engineering as verification or benchmark for newly proposed analysis methods (Shao, et al., 2021). It is preferable to the limit equilibrium method for slope analysis due to its ability to analyze any geometry of slope in two and three-dimension, linear and nonlinear problems, as well as its ability to give a factor of safety without pre-assumptions about the shape and position of the sliding plane and employ various soil material models. It can also consider the stress-strain relationship of the materials (Burman et al., 2015).

2.8 Remedial Measures for Slope Instability Problems

Before deciding on a slope stabilization method, it's important to evaluate the current conditions of the slope and identify the underlying causes of instability. Once the causes have been determined, the appropriate remedial measure can be selected based on factors such as feasibility, stability, and economy (Kazmi, et al., 2017). According to Kazmi et al. (2017), there are several remedial measures that can be considered to stabilize an unstable slope, including surface protection and drainage, subsurface drainage, slope regarding, retaining structures, structural reinforcement, strengthening of slope-forming material, vegetation and bioengineering, and removal of hazards. Out of these methods, some of the most effective ones are discussed below.

2. 8.1 Drainage Systems

It has been discovered that the main cause of slope failure is due to a build-up of saturation and pore water pressure in the subsoil. Fortunately, there is a solution to this problem. According to Mizal-Azzmi (2011), implementing a proper drainage system can effectively stabilize the slope by reducing the pore water pressure and saturation of subsoil. The drainage system technique is often used in conjunction with other methods and is only applicable in conditions where proper maintenance of surface and sub-surface drains is performed. If excess pore water pressure is present, it is a significant factor that contributes to the instability of the slope. However, with the appropriate design of surface and subsurface drainage systems, the build-up of pore water pressure in subsoil can be eliminated, and the stability of the slope can be improved.

2.8.2 Geometrical Method

In areas with steep slopes, there is a high risk of slope material sliding due to gravity and increasing its speed (Ibrahim, et al., 2022). This can be addressed through the geometrical method, which is simple and cost-effective, but requires sufficient space. Another way to improve slope stability is by converting steeper slopes into gentler ones, which can be achieved by cutting the slope to reduce excess loading. The stability of the slope can be further enhanced through flattening or backfilling at the toe of the slope (Kazmi, et al., 2017). However, the effectiveness of this method is highly dependent on the conditions of the site and may not be suitable for all situations.

2.8.3 Retaining Structures Method

One effective method for resisting the downward forces of soil masses is through the use of retaining structures. There are several types of retaining structures available, including gravity and cantilever retaining walls, as well as contiguous bored piles and nailing to help stabilize slopes. While this method may be more expensive, it is often the most popular choice due to its flexibility in constrained sites (Kazmi, et al., 2017)

2.9 Software Applications

2.9.1 Slide Software

This software is a great tool for analyzing slope stability of both soil and rock slopes. It was initially proposed by Rocscience Inc. Toronto, Canada, and is called the Slide software. With this program, you can easily model slopes with various loading conditions such as surcharge, pseudo-static earthquake, groundwater condition, and support conditions. The software allows you to perform slope stability analysis by vertical slice using different types of limit equilibrium method analysis such as Bishop, Spencer, and Ordinary/Fellenies methods. Additionally, it has features such as searching for critical surfaces, modeling multiple, anisotropic, and non-linear Mohr-Coulomb materials, defining and analyzing groundwater problems, and viewing detailed analysis results (Slide, 2003). This software is definitely worth considering for anyone who needs to evaluate the stability of both circular and non-circular failure surfaces because it is a computer-based program for 2D limit equilibrium (Slide, 2003).

2.9.2 Rocscience Software

Rocscience software is one of the software used for stability analysis of both rock and soil slopes based on the limit equilibrium method. This software was developed by Rocscience Inc., a company based in Toronto, Canada. It has different sub-program like, Swedge, Rocplane, Dips, Roclab, Rocdata, and Slide software. Swedge 4.0 and Rocplane 4.0 are used to analyze the stability of wedge and planar mode of rock slope failure, respectively (Tesfaye, et al., 2023). Similarly, Dips 6.0 and Slide 6.0 software are used to determine stereographic projection and stability analysis of soil slopes, respectively (Rocscience, 2004). Rocdata3.0 software (Rocscience, 2004) is also used to determine shear strength parameters along the failure plane. The Rocdata software determines the shear strength parameters along the failure plane using failure criteria (Barton-Bandis, 1990). Under this study, Rocscience software like Dips, Swedge, Rocplane, Rocdata, and Slide were utilized to undergo stability analysis of the slope.

2.9.3 Phase Software

Phase 2 Software is a widely-used tool in geotechnical and mining engineering for designing and analyzing tunnel surface excavation and supports (Rahman, et al., 2022). The software is developed by Rocscience Inc, based in Toronto, Canada. It relies on the finite element method to analyze soil and rock slope stability, and it includes several FEM models and four main sub-procedures: inputs, calculations, outputs, and curve plots. It's a versatile tool that can be used for deformation and stability analyses for various geotechnical applications (Rahman, et al., 2022). The software automatically reduces strength parameters until the final calculation step results in a fully developed failure mechanism.

CHAPTER TREE

3. DESCRIPTION OF THE STUDY AREA

3.1 Location and Accessibility of Study Area

The study area, Arbarekete-Galamso road, is situated in west Hararge zone of Oromia regional state in eastern Ethiopia. It is bounded between $8^0$52'0'' – $9^0$3'45'' N latitude and $40^0$44'10'' - $40^0$56'25'' E longitude. The start of the project is 325-km far from Addis Ababa along Addis–Chiro – Dire Dawa main highway or 8.5-km from Chiro towards Dire Dawa side. From this junction the project road traverses in south west direction until it reach the end of the project, Kortu River Bridge near the outskirt of Machara town.

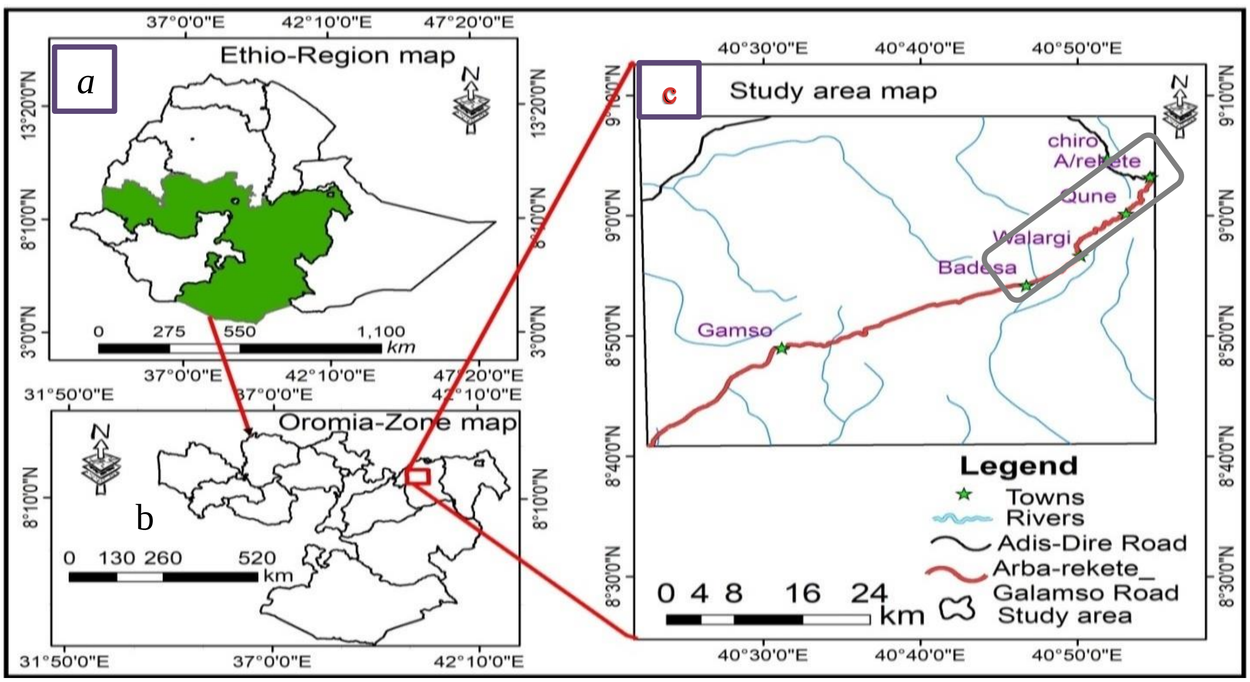

Figure3.1**:** Location maps of study area: (a) Ethiopian regional boundary b) Oromia zone boundary and c) study area boundary

3.2. Physiography of the Study Area

Physiography is strongly related to the geological setting and geomorphological history of rock (Jain, et al., 2020). The study area is part of eastern highland plateau very close to the eastern rift margin and partly lies within the northwestern extreme end of Ogaden basin and the area contains high cliffs formed on basalt rock formations, moderate slopes, and topographic breaks on basalt rocks. In the study area, different physiographic features such as ridges, cliffs, and plains are the result of past volcanic and tectonic activity. The road that connects Arbarekete and Baddesa town passes along Charchar mountain terrain which has a moderately to steep slope where the several slope of rock mass failures were observed during field work.

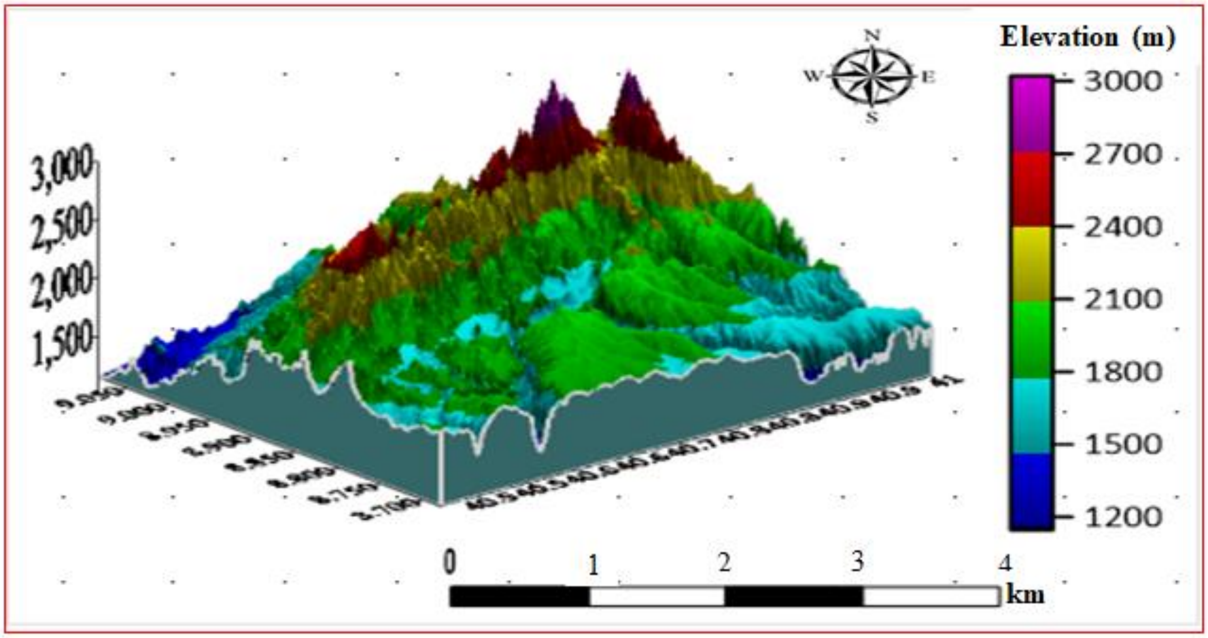

Figure3.2: Physiographic map of the study area

3.3. Drainage Pattern

The study area is located on the eastern highland of Ethiopian plateau which contains the small rivers and their tributaries. Several small tributary streams run through the study area and intersect at various points and drain to Galeyti River. The road pass through the steep slope and the drainages are flow easily from the escarpment to the rivers in the lowland area. All the local drainages in the study area flow towards the southeastern and southern direction. The drainage pattern of the studied area is characterized by parallel to subparallel dendritic patterns. The structures and topographic landscapes of the study area control the flow direction and distribution of the drainage pattern.

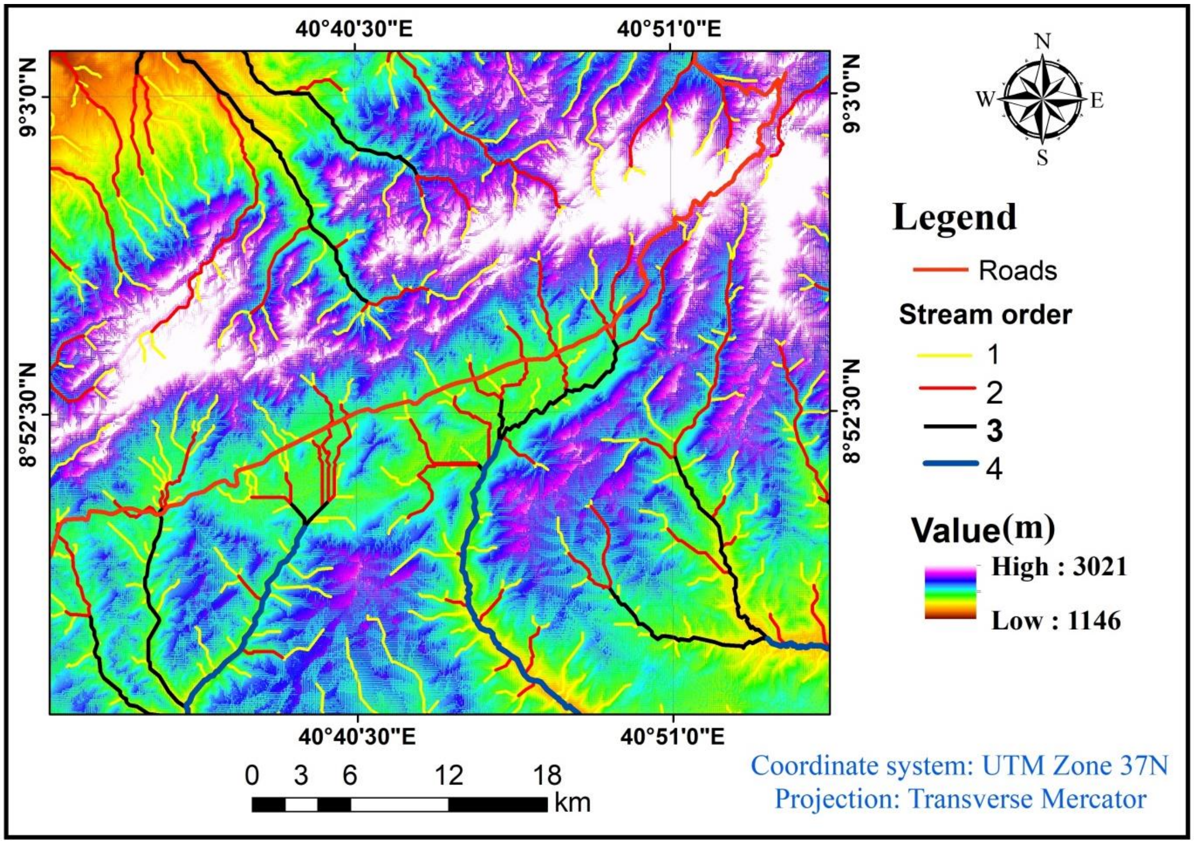

Figure3.3**:** Drainage pattern and stream order of the study area

3.4. Seismicity of the Study Area

It's important to be aware of the potential risks associated with seismic activity, especially in active seismic zones (Mebrahtu, et al., 2022). Research has shown that when rock slopes are subjected to ground accelerations, the resulting structural discontinuities can lead to reduced shear strength and increased slope failure (He, et al., 2023). In fact, the seismic risk map of Ethiopia for a hundred-year return period indicates that the study area falls within a zone with high seismic hazards as shown in Fig 1.4. The predicted earthquake acceleration is average of 0.08g based on the Modified Mercalli intensity scale (Luna, et al., 2010). Hence, the present study area fell into zones (zone 3) with high seismic hazards. This means that there is a significant chance for slope instability problems to occur in the area, particularly if triggered by seismic activity. It's crucial to take this into consideration when planning and implementing any projects or developments in the region.

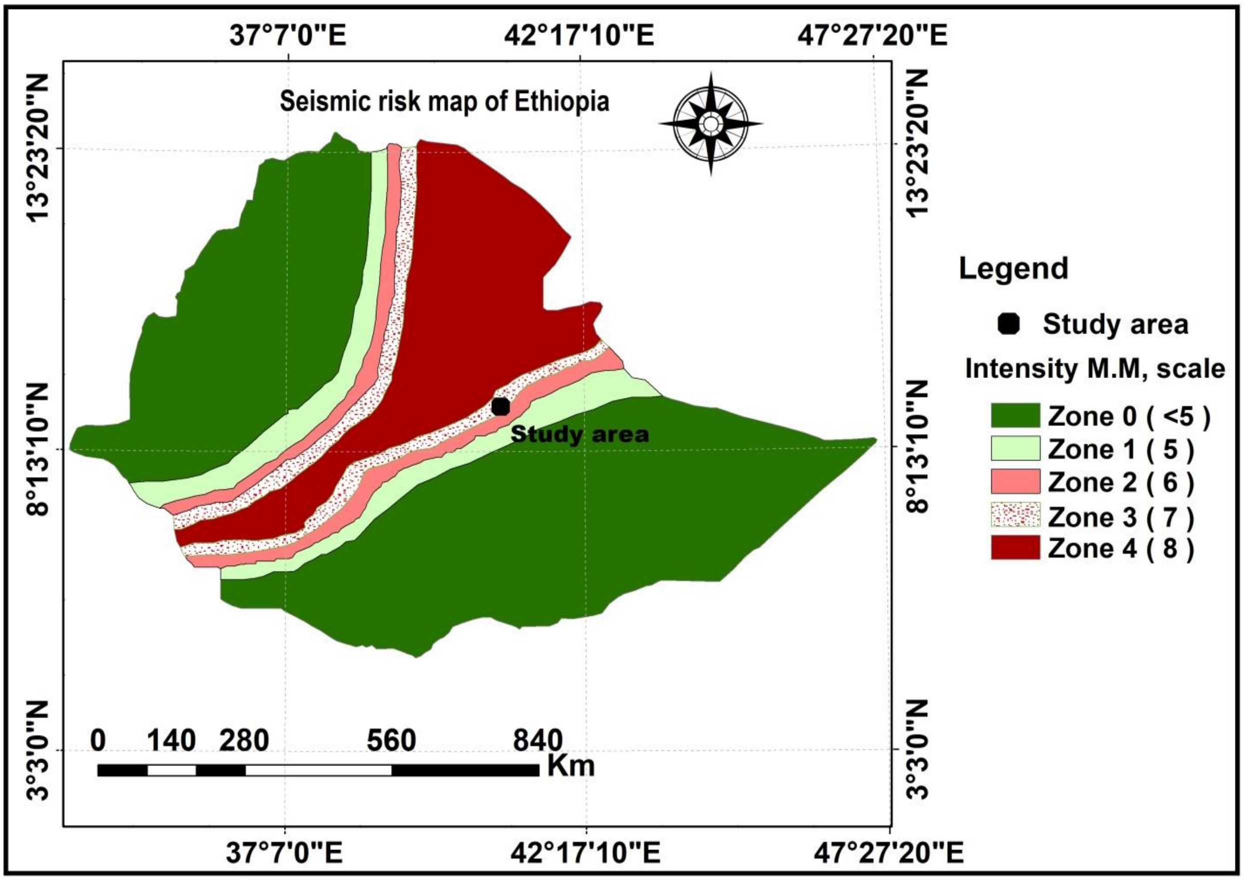

Figure3.4**:** Seismic hazard map of Ethiopia for 100-year return period as per EBCS 8: 1995 (Stewart, et al., 2003)

3.5. The Climate Condition of the Study Area

The climate of study area contains the average temperature (Fig.1.5) and precipitation conditions (Fig.1.6). Ethiopia has a variety of rainfall distributions. According to Ayelew (1999), the Lowland locations have lower precipitation records and the highland areas have over 70% of yearly rainfall. There are two recognized climate components: precipitation amount and distribution of temperature conditions according to Ayelew (1999) description.

3.5.1. Temperature

According to data obtained from the National Meteorological Agency of Ethiopia, the maximum and minimum mean annual temperatures in the study area were recorded at the Qunne and Baddessa town stations. The maximum and minimum average annual temperatures for Qunne were 31.10ºC and 9.95ºC, respectively, while for Baddessa, they were 32.33ºC and 6.74ºC, as illustrated in Fig.1.5.

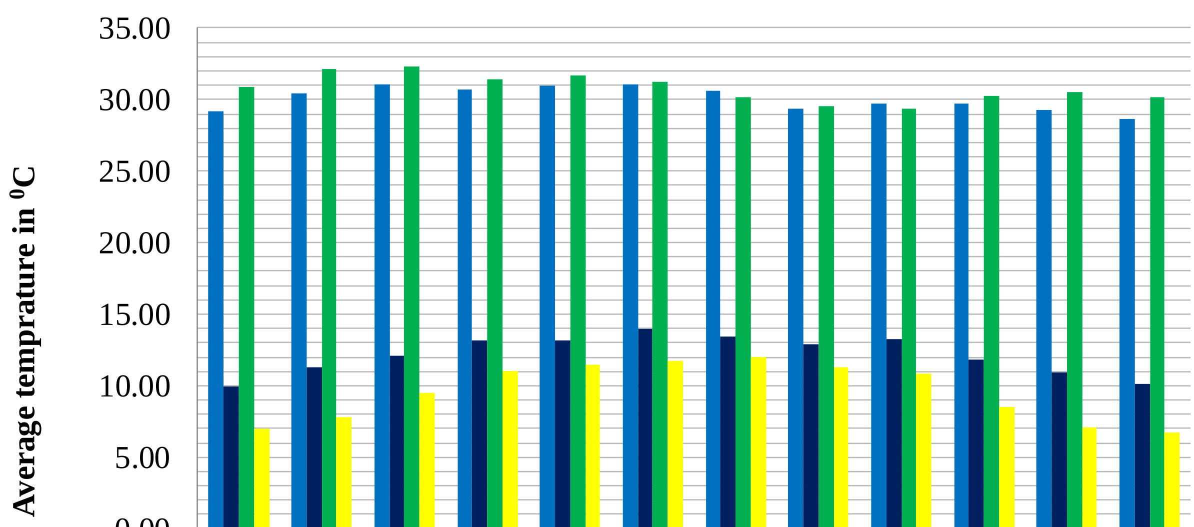

	Jan	Feb	Mar	Apr	May	Jun	Jul	Aug	Sep	Oct	Nov	Dec
Qune max	29.22	30.40	31.02	30.70	30.94	31.10	30.66	29.36	29.70	29.76	29.25	28.61
Qune min	9.95	11.31	12.10	13.14	13.15	13.99	13.47	12.94	13.23	11.81	10.95	10.11
Badesa max	30.91	32.17	32.33	31.40	31.65	31.21	30.12	29.53	29.40	30.22	30.49	30.15
Badesa min	6.95	7.77	9.52	11.03	11.43	11.70	12.04	11.27	10.87	8.52	7.04	6.74

Months

Figure3.5**:** Mean average temperature of the study area (2000-2022). (Sources: National Meteorological Agency of Ethiopia).

3.5.2. Rainfall of the Study Area

Based on research conducted by (Chango, et al., 2021), it has been found that heavy rainfall is the most common cause of slope failures. In particular, the Ethiopian highlands are susceptible to slope instability due to a range of factors such as topography, geology, hydrology, and land use conditions. According to (Getachew & Meten , 2021), the majority of landslides in the area are caused by heavy rainfall. During these events, the distribution of pore water pressures in the soil can vary widely depending on factors such as hydraulic conductivity, topography, weathering, and soil types. The meteorological conditions in the study area range from tropical to subtropical, and slope instability tends to occur during the rainy season. Rainfall data for the study area was obtained from the National Meteorological Agency of Ethiopia, specifically for Chiro, Qunne, and Baddesa stations. The maximum and minimum mean monthly rainfall at Qunne station was 197.1mm and 17.68mm, respectively (Fig.1.6). Meanwhile, at Baddesa stations, the average monthly rainfall ranged from 16.47 mm to 155.6mm. It is important to note that the study area's rainfall is not consistent throughout the year, as shown in Fig.3.6. Based on field observations, it appears that slope instability in the study area is more likely to occur during July and August, which are characterized by heavy rainfalls (Fig.3.6).

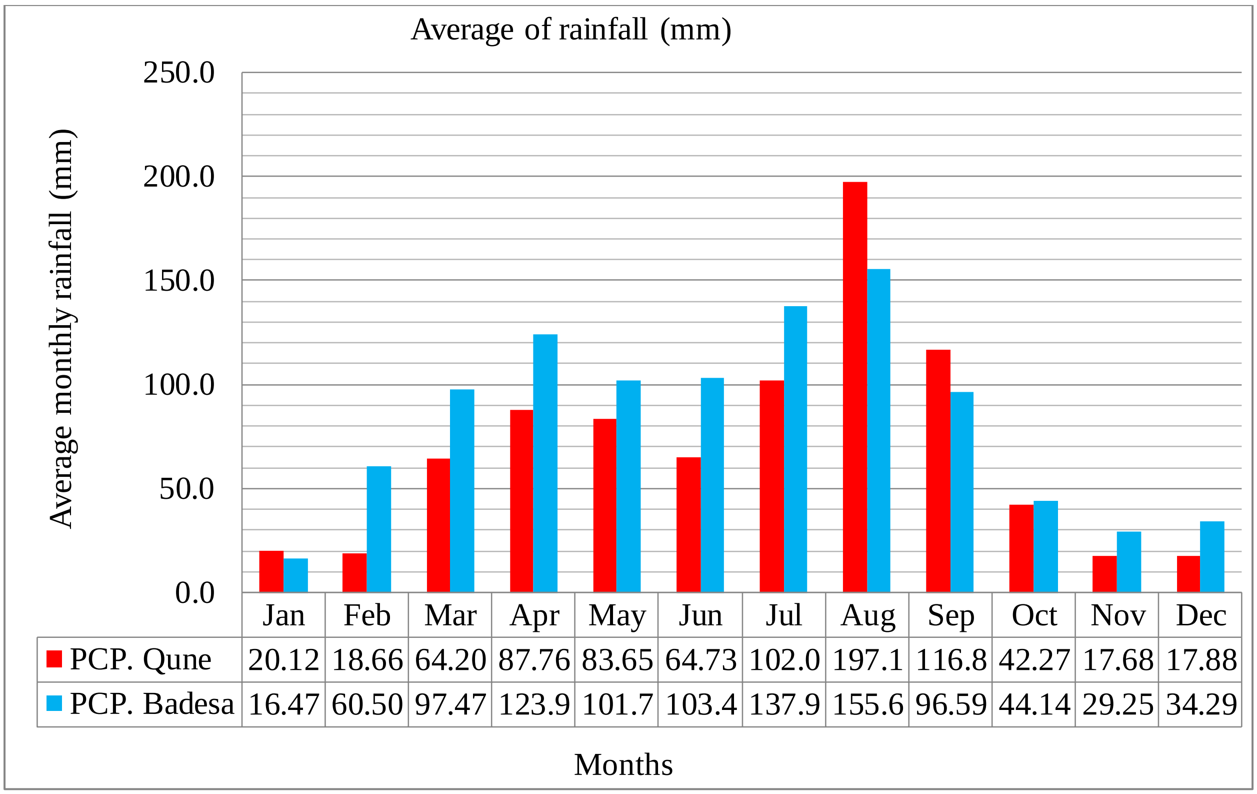

Figure3.6**:** Monthly Rainfall data **o**f the study area (2000-2022) (Source: National Meteorological Agency of Ethiopia.

3.6 GEOLOGY OF THE AREA

3.6.1 Introductions

The study area is situated in the southeastern part of Ethiopia, near the Eastern Rift Margin, and partially falls within the northwestern end of the Ogaden Basin of the Ethiopia Physiography Region. Ethiopia's major lithological units are Precambrian basements, Paleozoic to Tertiary sediments, and Cenozoic volcanoes and sediments associated with them (Tefera, et al., 1996). The geology of the Bedesa area represents the northern part of Ogaden Basin, which mainly comprises a Jurassic sedimentary sequence with minor Precambrian metamorphic basement and Cenozoic Volcanic cover (ALEMU, 2010). The area is affected by the younger Main Ethiopian Rift and Afar structures with prominent topographic features in the northwest and northern part. It's interesting to note that the Arabian-Nubian Shield (ANS) and the Mozambique Belt (MB) are exposed in the north and south, respectively, as the Precambrian bedrocks of Ethiopia belong to the East African orogeny. The physiographic features of Ethiopia are characterized by extensive northwestern and southeastern plateaus, the Main Ethiopian Rift Valley (MER), and the Afar Depression (Tefera, et al., 1996). Because of these features the Ogaden Basin is one of the countries' most important sedimentary basins located in the southeastern Ethiopia.

The Ogaden Basin, where our study area is located, is one of the African Phanerozoic Basins and covers an area of 350,000 km2 in southeast Ethiopia (Tadesse, 2007). It contains a thick succession of sediments that were formed between the Upper Permian and Lower Tertiary. Additionally, Cenozoic volcanic rocks have occurred in the north and south peripheries of the map sheet. In the northern part, the rocks are exposed from northwest to northeast corner, scattered here and there. These rocks form important topographic highs, particularly in the northwest part (in the area north of Gelemso and Bedesa), where they represent part of the eastern shoulder of the Main Ethiopian Rift (MER), known as the Chercher Mountain Chain, with a summit exceeding 2500m.

3.6.2. Regional Geology of Study Area

The geology of Bedesa area represents the northern part of Ogaden Basin comprehending mainly a Jurassic sedimentary sequence with minor Precambrian metamorphic basement and Cenozoic Volcanic cover (ALEMU, 2010).

Precambrian Crystalline Basement Units

The Precambrian crystalline basement exposed to the north, within the deep cut canyons of major Wabe Shebele tributaries. They are the least exposed rocks in the mapped area. Based on the outcrop distribution, the Precambrian basement in the project area is described to comprehend a north-south trending low grade volcano sedimentary belt bounded by two gneissic blocks in the east and the west. The rocks in the Western Block are exposed in several streams, whereas, the outcrops of low grade rocks and that of the Eastern Block gneisses are very limited. The low grade rocks are observed only in Ramis Stream and its tributaries. The basement rocks in the Eastern Block are represented by biotite gneiss that observed at the northeast tip corner of the sheet, Mudena Stream.

Mesozoic Sedimentary Units

The Mesozoic sediments of the mapped area represent the northern part of Ogaden Basin accumulated during late triassic-jurassic time. The total sedimentary succession in the area is estimated to thick more than 800m increasing to the south. The complete sedimentary pile is distinguished into: Adigrat Formation, Hamanlei Formation, Urandab Formation, Gabredare Formation, and Gerbaharre Formation (from bottom to top).

Field data analysis confirms that this straigraphic column defines a complete transgression-regression cycle. The continental sediments of Adigrat are fluviatiles formed whene the sea was much far from Bedesa, at the early rifting stage of lithospheric extension. The overlying succession of Hamanlei, Urandab, Gabredare and Garbaharre Formations are mainly marines, deposited in the conditions ranging from tidal flats and near shore areas to the more deeper, open sea environments. Because their feicies assemblage confirms a continuous sea level rise, Hamanlei and Urandab Formations constitute the Transgressive System Tracts (TST) separated from Gabredare and Garbaharre Formations by a condensed section. The later two, hence, mark the Highstand System Tracts (HST). The contact between Adigrat and Hamanlei is an erosinal transgressive surface, and between Hamanlei and Urandab is also another transgressive surface caused by sudden deepening of the sea. On the other hand, the thin (not more than 100m) aggradational limestone succession of Gabredare has a gradational contact with the overlying progradational clastic wedge of Garbaharre Sandstone.

Cenozoic Volcanic Units

The volcanic rocks occurred, generally in the north and south peripheries of the map sheet. In the northern part, the rocks are exposed from northwest to northeast corner scattered here and there. In all cases, the rocks form important topographic highs. Specially, in the northwest part (in the area north of Gelemso and Bedesa) they represent part of eastern shoulder of Main Ethiopian Rift (MER), known as Chercher Mountain Chain, with a summit exceeding 2500m.

In the north and northeastern part, the volcanic rocks are mapped as fringe of the mountain chain including some local fault controlled and isolate volcanic centers. Most of the rocks are basaltic flows and are believed to relate with the rift processes. Based on age data from (Kazmin & Seifemichael, 1979; Kazmin, 1972; Mengesha, et al., 1996), the rocks are classified and described as Tertiary Basalts (Alaji and Termaber Basalt) and Quaternary Basalts (part of Ginir Formation). The lava flows are either, lying unconformably, on the Mesozoic sediments or cut the sediments, where they appear as local intrusives.

A. Tertiary Basalts

The basaltic rocks occurred in the northern part of the area mark the margin of MER and Afar. Limited age data indicates that these rocks are older than that of the southern volcanics. The type area of Tertiary basaltic rocks is the northwest corner of the map sheet, where thick succession of flows is recorded and two stratigraphic units: Alaji and Termaber Basalts have been distinguished. The two basalts are separated in the field by topographic breaks, thin paleosol layers and small springs. With respect to the rift margin, the two basaltic units show characteristic distribution. The Termaber Basalt is restricted within the rift indicating its syn-to post-rifting emplacement. The Alaji Basalt, on the contrary, occurred both outside and inside the rift. The rift faults, with a northeast southwest trend affect these Tertiary basalts rendering the fault blocks to incline northwards (rift wards). The major rift boundary fault forms a graben in which Gelemso and Bedesa towns are located. The volcanic pile also becomes thick towards the rift (to north), where the total thickness is estimated to be more than 600m.

B. Quaternary Covers (Qel & Qal)

Recent deposits are widely developed above any lithologic units. Commonly, they are soil horizons distinguished in to two named as Elluvial Deposits (Qel) those sediments exercised little or no transportation, and Alluvial Deposits (Qal) that are evidently confirm a remarkable transportation processes.

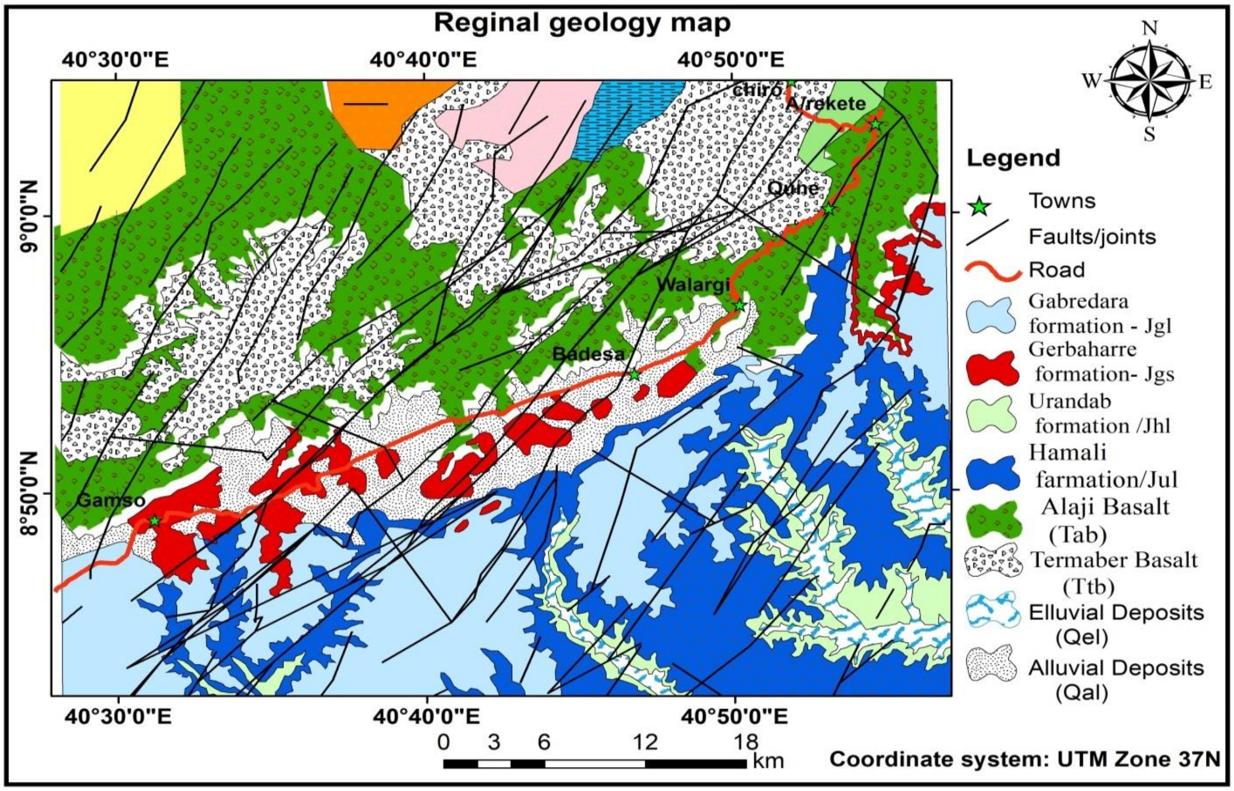

Figure3.7:- Regional geological map of the study area (Minister of mine and Energy of Ethiopia, 2008)

3.6.3. Local Geology of the Study Area

During the journey from Arbarekete to Badessa, a wide range of geology was observed from Mesozoic sediments to Tertiary basalts. The study area is located within the southeastern Ethiopian plateau and northern parts of the Ogaden basin. According to Tefera et al. (1996), the study area mainly consists of Cenozoic volcanic rocks and Quaternary deposits. The volcanic lavas and Quaternary deposits are arranged in a condensed sequence from bottom to top. In the study area, various major lithological units were observed along road sections, as follows:

Basaltic Unit

In the study area, there is a rock unit called the Basaltic Unit that can be found overlying the upper sandstone. This unit is known for forming a gentler slope and a steep cliff, and it has moderate to steep topography. It is mostly exposed along road cut section because of its top soil covering. Basalt rocks in this unit have a dark gray color, fine-grained texture, and large columnar joints, but they are also fractured and weathered. The basaltic rock units along the road sections in the study area are characterized by slightly to moderately weathered inclined columnar fractures, as well as highly fractured rocks with multiple closely to moderately spaced, small, nonpermanent, open and partially filled, steep to gently sloping fracture sets. The escarpments along the mountain chain form this rock unit, and the most critical rock slope sections were found within it. The study area consists of the upper and lower basalt units, which were briefly discussed as follows.

A. Upper Basalt Unit

At the top of the mountain range, there is upper Basalt unit that is well exposed. It has a dark grey color and thin columnar jointing, with the joints being mostly vertical to steeply sloping. Additionally, there are open fractures with high persistence and open-filled columnar joints. The unit is moderately to steeply sloping and is slightly weathered and fractured. In fresh samples, it has a light dark grey color and a light bluish grey color on weathered surfaces. The unit consists of olivine and plagioclase phyric, which is dark gray to black in color, medium to coarse-grained in texture, and sometimes fine-grained in texture. It is positioned above the lower basalt in the study area.

Figure3.8:- Upper basalt rock of the study area

B. Lower Basalt

In the study area, this basaltic rock unit along the road sections is characterized by slightly to moderately weathered inclined columnar fractures, highly fractured rocks with multiple closely to moderately spaced, small nonpermanent open and partially filled, steep to moderate sloping fracture sets are found with the rock slope wall along the road sections. This type of rock usually occupies the lower part of the mountain chain and is made up of a number of flows separated by thin layers of soil. One peculiar feature of this basalt is its porphyritic texture that is expressed by large plagioclase phenocrysts. In some places, it is seen to include tuff beds and aphanitic basalts in the upper part. Locally, it also appears to be vesicular filled by silica. While columnar jointing is rarely found, where present, the columns are large, reaching up to 0.8-1.0m diameter with 5 and 6 faces. Fresh samples of this rock are light dark grey, while weathered surfaces have a light bluish grey color. Spheroidal weathering in this unit usually leaves behind large blocks of weathering cores, whose diameter commonly exceeds 30cm. The rock is seen to include olivine, plagioclase, and pyroxene. It seems that this rock unit is highly susceptible to different slope instability problems as the rock is intensively fractured and jointed with parallel dipping of fractures and joints with the slope face.

Figure3.9:- Lower basalt rock of the study area

Alluvial Deposit: The study area has an alluvial deposit in the river channel, consisting of silt clay to coarse sands, gravel, and boulders. The alluvium is reddish-brown to dark brown to gray in color. Erosion and transport of various rocks caused the deposition of Quaternary alluvium in the river and stream course. However, it only covers a small part of the study area, making it difficult to map.

Residual soil: On the other hand, residual soils are formed from parent rocks of basalt rocks in the original place by physical and chemical weathering processes. The soils in the study area are red to brown in color and mixtures of variable particle sizes ranging from clay to gravel. It can be found over the higher elevations with near-flat land and in some places with moderately sloping escarpments.

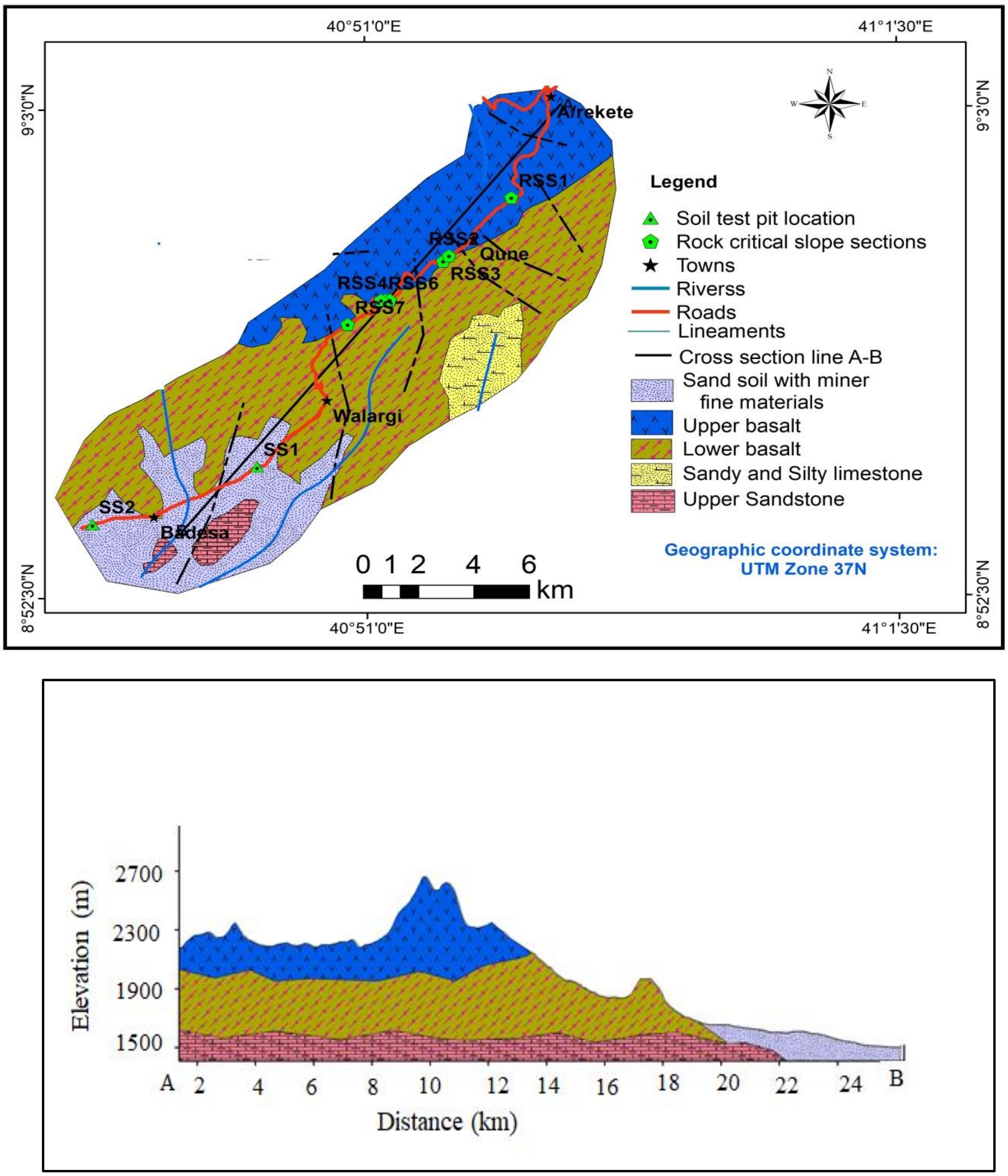

Figure3.10:- Geological map of the study area with its cross-section along A-B

3.7 Geological Structures

3.7.1 Regional Geological Structures

The tectonic history of the study area is mainly related to the development of Main Ethiopian Rift and Afar. The major structural elements are rift-related volcano tectonics, and there are three sets of faults trending NE-SW, E-W and N-S (NNW-SSE) that are observed in the area. Each type of fault occurs in a particular part of the sheet, with the NE-SW trending faults being the most prominent. These are part of the Main Ethiopian Rift faults and are younger structures that developed with the association of Tertiary basalts, at the northeast corner of the area. In this part of the area, such faults are expressed forming continuous cliffs (in the mountain range), fault blocks, abrupt lithological changes, and the Bedesa basin. The boundary fault trending east-west around Gelemso and Bedesa, and turning to north and northeast around Kuni, forms a wide depression zone between the two blocks running curvy linearly for about 60km starting from Gelemso. The depression between these fault blocks is described as Bedesa Graben filled by recent alluvial deposits with a number of sandstone blocks standing at the middle. The thickness of the alluvial sediments may reach up to 50m, according to Bekele et al. (1992).

3.7.2 Local Geological Structures

The study area has a variety of geological structures, including joints, fractures and Lineaments along the lithological units of the road section that were identified during the fieldwork.

A. Joints

The fracture set conditions play a vital role in identifying the stability conditions of the slope rock mass (Hack et al., 2003). In the study area, the lower basaltic units have steeply dipping joints that are found most frequently. The study area has three major joint sets with strikes in the NW-SE, NE-SW, and E-W directions. During the fieldwork, the dip and dip direction of the joints were measured on the field to determine their general orientation and its impact on slope stability. The rock slope's critical sections were observed that were characterized by different sets of discontinuities in the slope face wall. The fractured columnar joint is the most frequently observed joint type of basaltic rock along the road sections. A Rosset plot was used, as shown in Fig.3.11, to determine the general strike direction of the joint sets along the road section.

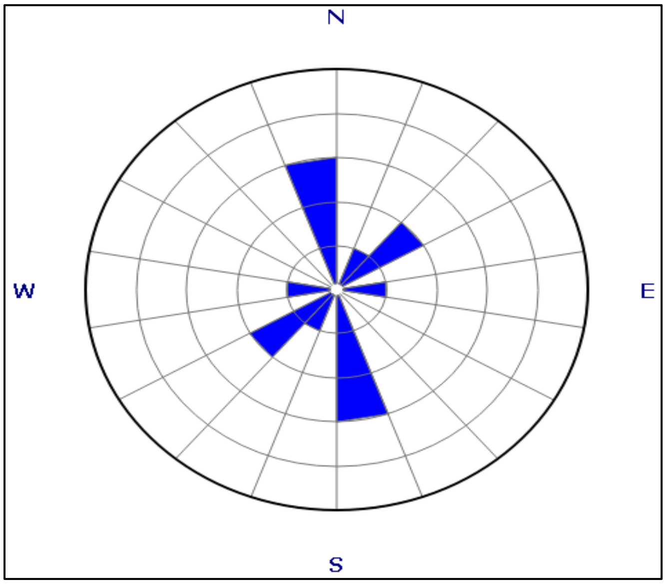

Figure3.11:- Rosset plotted diagram which indicate the joint orientation along the road sections

B. Lineaments

Lineaments are large-scale topographical features such as valleys controlled by mountain ranges, ridges and isolated hills. Many lineaments influence stream and river courses and ridge alignments in the study area. They run from N to S, and join main stream and run NE to SW with variable lengths and straight to curvilinear trends (see Fig.3.10).

CHAPTER FOUR

4. METHODOLOGY AND MATERIALS

4.1 METHODOLOGY

To obtain accurate and comprehensive information on the engineering geological and slope stability conditions of the study area, different appropriate methods were utilized. The data acquisition processes and general working principles of these techniques are presented in this section. The methods and approaches used in this study included secondary data collection and field survey, detailed fieldwork and sampling, laboratory testing and data processing. Slope stability analysis was conducted using kinematic analysis, deterministic, limit equilibrium and finite element methods. The primary and secondary data were integrated to analyze, summarize and present the results. The approaches and some applications of those aforementioned methodologies are discussed in detail as follows.

4.2 Secondary Data Collection and Field Survey

As part of this phase, important and relevant data that are used for slope stability analysis was able to be gathered from various reputable institutions, such as the Ethiopian Geospatial Agency, the National Metrological Agency, and minister of mine and energy of Ethiopia. This included secondary data like meteorological data, topographical maps, and regional geological maps and their reports. The investigation included a reconnaissance study and a thorough literature review on various causes and mechanisms of slope failure. This information, which was obtained from the Ethiopian Geospatial Information Agency (EGIA), was then utilized to create a base map of the study area through the use of ArcGIS 10.8 software. Additionally, regional geological maps and their reports were gathered from the minister of mine and energy of Ethiopia, as well as climatic data from the National Meteorological Agency of Ethiopia. With the regional geological maps and structures of the study area in mind, the most appropriate traverses for lithologic unit mapping were then selected and field survey was conducted along the selected traverses. A slope failure is most frequently caused by heavy rainfall (Abebe et al., 2010). The graphs of average monthly precipitation data from 2000 up to 2022 at Qunne and Baddesa stations were drawn using Microsoft Excel (Fig.1.6). Similarly, the temperature data for the same period of time at Qunne and Baddesa stations were presented using Microsoft Excel (Fig.1.5)

4.3 Detailed Field Work and Sampling

Based on the detailed field investigation, it was found that the slope was in an unstable state and required further stability analysis. During the fieldwork, the primary data was collected from the study area and information on geological structures, discontinuity characteristics, rock mass characteristics, and drainage conditions were identified. Primary data was also collected from the study area through discontinuity surveying, in-situ strength test, mapping, and sampling for laboratory tests. A critical slope section was identified based on field failure manifestations such as removal of slope toe, development of tension crack, tilting of slope face, existences of some springs and orientation of discontinuity. These critical slope sections were then further observed to identify possible failure phenomena such as slope inclination, drainage status, types of slope material, weathering conditions, and orientation of discontinuity. Further field observations were conducted to analyze the slope stability after identifying critical slope sections.

4.3.1. Discontinuity Survey

Based on the field investigation carried out on rocks found along the road section of the study area, potential slope instabilities were identified. The failure mechanism was either structurally controlled failure or non-structural controlled failure. A detailed discontinuity survey was conducted, and the rock discontinuity conditions such as joint orientation, joint spacing, joint fill, and opening, joint roughness, groundwater, and weathering conditions of the rocks along the road section were identified and measured. To measure the orientations of the discontinuities and the slope face orientation, a Brunton compass was used. The spacing of discontinuities, aperture, the persistence of the set of discontinuities, and slope height were measured using a tape meter. Various parameters related to discontinuities were assessed in the field, such as surface roughness, infill material, weathering conditions, and groundwater status. The strength and orientation of discontinuities are the most important properties for analyzing rock slope stability (Ismail, et al., 2022). During the discontinuity measurement, special attention was given to the discontinuity sets with a favorable orientation for the rock slope instability.

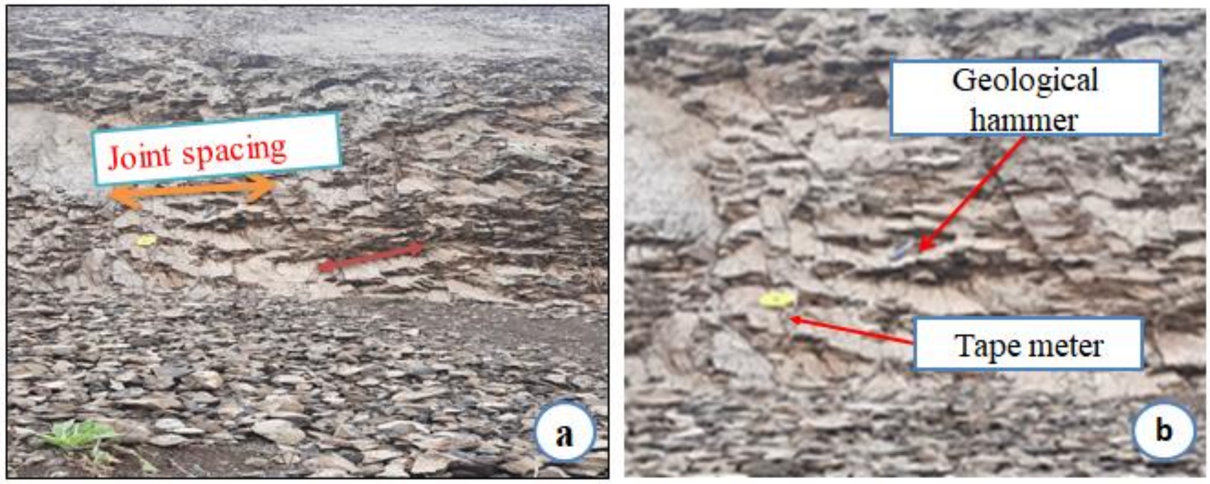

Figure4.1: Joint spacing measurement using tape meter and measuring degree of weathering using geological hammer in the field

4.3.2 Geological Mapping

In order to gain a more comprehensive understanding of the lithological units and geological structures in the study area, a geological map was prepared at a scale of 1:50,000. Various references were used, including a preliminary geological map, drainage map, and existing regional geological information of the study area, to gather information for this map. After conducting a reconnaissance survey, the best traverse lines were selected for the mapping and detailed geological mapping was carried out along those lines. During the fieldwork, geological materials were described in terms of their color, orientation, degree of weathering, thickness, and other relevant factors. Once the fieldwork was completed, ArcGIS software was used to convert the collected information into a geological map of the study area.

4.3.3 In-situ Strength Test

The strength of intact rock, also known as the Uniaxial Compressive Strength (UCS), was determined in the field using the Schmidt hammer rebound test (Hayat, et al., 2019). The guidelines for this test were provided by ISRM (1978) and ASTM (2001). The hammer was applied in a direction perpendicular to the test surface and gradually pushed until it impacted the surface. The test was conducted twice, with 10 readings taken at each sample location. The readings were taken at each trial test section, leaving a 25mm gap between two impact test points for all trials. The corresponding rebound values were recorded and a representative rebound value was determined by averaging the readings that did not differ from the average of 10 readings by more or less than 7 units. If any readings differed from the average by more or less than 7 units, they were excluded from the calculation of the representative rebound value. If more than two readings differed from the average by more or less than 7 units, all readings were rejected, and rebound values were determined at other nearby locations. Finally, the representative rebound values were converted into the UCS of rocks using empirical equations (Eq.4.1) that were suggested by (Barton & Choubey, 1977).

$$\text{Log10 (UCS)} = 0.00088*\gamma*R + 1.01 \tag{4.1}$$

Where: UCS- is the uniaxial compressive strength of rocks in Mpa, γ is the dry rock densities in kN/m3, and R average Schmidt hammer rebound value.

Figure4.2: In-situ strength rock test using Schmidt hammer rebound value for the estimation of uniaxial compressive strength (UCS).

4.4 Sampling of Soil and Rocks for Laboratory Test

In order to better understand the engineering properties of the soils and rocks in the study area, representative samples were collected from the field for laboratory testing. Both rock and soil samples were collected for index and strength tests, ensuring a comprehensive understanding of the materials. To account for the variability of weathering degrees, rock samples were also taken from multiple locations for the determination of unit weight using the buoyancy technique. These methods allowed for a thorough characterization of the materials and will inform future decision-making in the study area.

4.4.1 Soil Sampling

To properly analyze the stability of the slopes, disturbed soil samples were collected from selected critical sections as shown in Fig. 4.3. Two representative soil samples were taken for index and strength tests. To achieve this, two soil test pits were dug with a maximum depth of one meter, and collected the soil samples. The soil samples were placed in plastic bags to preserve their natural moisture content. The purpose of soil sampling was to obtain samples for laboratory testing. These soil investigations were conducted to characterize the materials and determine related parameters to better analysis slope stability.

Figure4.3: Pits for soil sampling at a) SS1 and b) SS2

4.4.2 Rock Sampling

The engineering properties of rocks in the study area were determined by collecting representative samples for laboratory testing of rock units along the road sections. For the study, seven critical rock slope sections were selected to determine the rock engineering properties for slope stability analysis. The degree of weathering of the exposed rock along the section of the road was determined using geological hammer blows based on ISRM (1978). Rock samples with different degrees of weathering were collected from seven different locations of the critical slope sections to determine the unit weight and point load test in the laboratory. Additionally, the engineering properties of rocks found near the road section of the study area were described**.**

Figure3.4: Rock sampling at critical slope sections

4.5 Laboratory Testing of Soils and Rocks

After conducting field sampling, various geotechnical laboratory tests were performed on representative soil and rock samples. These laboratory tests were carried out on soil samples to determine particle size analysis using sieve and hydrometer analysis, specific gravity, natural moisture content, atterberg limit (liquid and plastic limit), compaction, and shear strength. In addition, rock samples were subjected to unit weight and point load testing. The types of tests that were carried out on these soils and rocks, along with the standards used for testing, were discussed in great detail in the following sections.

4.5.1 Soil Laboratory Tests

The laboratory tests were performed on soil samples to evaluate the strength and index properties of the soil in the study area. Tests performed in the laboratory on soil samples included grain size analyses (sieve and hydrometer analyses), specific gravity tests, natural moisture contents Atterberg limit (liquid and plastic limit), compaction and shear strength tests (cohesion and angle of internal friction).

4.5.1.1 Grain Sizes Analysis

Based on the grain size analysis of the two soil samples taken from the critical slopes sections of the study area, it was found that there are both large and fine particles present. The analysis was conducted using both sieves and hydrometers. This data is crucial in understanding the characteristics of the soil and can be used to inform decisions regarding construction or other land use activities in the area.

A) Sieve Analysis: The sieve analysis was conducted following ASTM D422 (1998), which is a standard test procedure for determining soil particle size (Fig.3.5a). The purpose of the test was to determine the distribution of coarser grain sizes that are greater than 75 µm in diameter. To conduct the test in the laboratory, dry soil samples were first prepared and crushed into appropriate small sizes using a hammer and pestle grinder. Once the samples were ready, a stack of sieves was cleaned with a brush and a set of sieves were placed with progressively smaller openings from top to bottom, with the pan at the bottom of the finest sieve. After 15 minutes, the soil retained on each sieve and pan was measured using a digital balance. The dry mass of soil grains from individual sieving was used to find the percent passing and accordingly, the percent retained in each sieve size. The recorded data was then analyzed on a

Microsoft Excel datasheet and the grain size distribution curve was drawn from the diameter versus percent finer using the sieve analysis result (Fig. 5.1).

B) Hydrometer Analysis: In order to determine the distribution of fine particle sizes smaller than 75 µm in diameter, a hydrometer analysis was conducted following ASTM D422 (1998) standard test. The test was performed in the laboratory by first weighing 50 g of fine-grain soil retained on the pan and placing it in a beaker with water, into which 125 ml of dispersing agent (sodium hexametaphosphate) mixture with the soil was added. The soil slurry was then transferred into an empty sedimentation cylinder and distilled water was added up to the mark. The cylinder was covered and turned upside down for one minute, then observed for 24 hours by reading the top of the meniscus-formed suspension hydrometer (Hossain, et al., 2021). The cylinder was placed in a constant-temperature water bath during these tests. The grain diameter was computed by referring to the calibrated curves and the grain size distribution curve was drawn from the diameter versus percent finer using the analysis result.

4.5.1.2 Atterberg Limit Test

The atterberg limit test is used to determine the liquid limit (LL) and plastic limit (PL) of soils. The liquid limit is the percentage (%) of moisture at which the soil changes from a liquid state to a plastic state, and the plastic limit is the percentage (%) of moisture at which the soil changes from plastic state to a semi-solid (El Jazouli, et al., 2022). The test was performed according to ASTM D 4318 (1998). The Atterberg limit test was determined on soil samples that passed the 40 sieve (0.425 mm) and distilled water was added to perform the casagrande test. The laboratory test is carried out according to the following flow and yield test procedure.

A) Liquid limit test: The liquid limit (LL) is the point at which the soil changes from a liquid state to a plastic state. For this analysis, a portion of the soil sample that passed through the pore size of sieve #40 (0.425 mm) was placed in the evaporator dish. The soil sample is mixed with water and stirred with a spatula to create a smooth soil surface. The soil mixture is then divided into two parts using a grooving tool and rotating the handle at 2 rpm until it contacts the bottom of the trench at a distance of 13mm. The number of hits required to close two sections of a 13 mm soil sample was recorded. A representative sample was taken from the flow section and placed in wet boxes that were oven-dried for 24 h at 105°C. Next, moisten the can to determine the moisture content. Finally, the moisture content of each soil sample was recorded and analyzed.

B) Plastic limit test: The plastic limit (PL) is the percentage moisture content (%) at which the soil changes from a plastic state to a semi-solid state. This test is made from sample for liquidity limit test. The soil sample is placed on a glass dish and rolled with a finger to form a thread of uniform diameter. The wire is then rolled up until its diameter reaches 3 mm and crumbles. Debris samples were collected in containers and digitally weighed then placed in the oven for 24 h and the oven temperature was set at 105°C. Finally, the humidity boxes are removed from the oven and the results of each sample are recorded and analyzed. Finally, from the yield and plastic limit tests, the plastic index (PI) of the soil is determined according to Equation 4.2 as follows.

$$PI = LL\text{-}PL \quad (4.2)$$

Figure4.5: Sieve and Atterberg limit tests of soils

4.5.1.3. Natural Moisture Contents Tests

The natural moisture content of the soil is an important factor in determining its condition in the field. According to Arezou et al. (2020), cohesive soils are particularly affected by moisture content, which can impact their engineering behavior. To test the moisture content, fresh soil samples were taken and subjected to the ASTM D 2216 (1998) standard using the oven drying technique. In addition, representative soil samples were also collected from two critical slope sections and preserved in plastic bags to maintain their in-situ natural moisture content. The wet mass of the samples (Mw) was determined using a digital balance, and the dry mass was obtained by oven-drying the samples (Md) for 24 hours at 105°C. Using equation 4.3, the natural moisture content of the soil was able to be calculated.

$$W\ (\%) = \frac{M_W - M_d}{M_d} \times 100 \qquad (3.3)$$

Where: W is the natural moisture content in (%), Mw is the mass of wet soil samples in (g), and Md is the mass of oven-dried soil samples in (g).

4.5.1.4 Specific Gravity

The specific gravity of soil at the selected slope section was determined using a pycnometer with distilled water at a specific temperature (Diro, et al., 2020). This test was performed according to the ASTM D 854 (1998) standard procedure to determine the specific gravity of soil using oven-dry techniques. To begin, the weight of the empty, clean, and dry pycnometer was determined and recorded. Then, the dry soil sample that passed through sieve No. 10 was placed in the pycnometer and its weight was determined (Md). Distilled water was then added to the pycnometer to fill just above the soil level and soaked for 10 minutes. Any entrapped air was removed through boiling. Finally, the pycnometer was filled with distilled water up to the calibration mark and its corresponding mass was measured (Mc). After emptying and cleaning the pycnometer, it was filled with distilled water up to the calibration mark to obtain the mass of the pycnometer filled with water (Ma).

$$G = \frac{M_d}{M_d + (M_a - M_c)} \qquad (4.4)$$

Where G is specific gravity, Md is mass of dry soil+ pycnometer, Ma is mass of pycnometer filled with water, Mc is mass of pycnometer filled with soil and water.

Figure4.6: Specific gravity test of soils

4.5.1.5 Compaction Tests

The compaction tests determine the maximum dry density and optimal moisture content of the soil used in the shear strength test. Proctor tests are used to determine how soil compaction changes with moisture content. Tests were conducted in accordance with ASTM D698-07 (1998) on two soil samples taken along the critical slope section of the study area. To conduct the test, 5kg of the soil sample passing through the No. # 4 sieve was taken and mixed thoroughly with a measured amount of water. Determine the weight of compaction molds within the base (M1). The soil sample was then filled in the cylinder mold in three layers within 25 blows for each layer. Remove the collar, trim, and level of excess compacted soil beyond the rim of the mold. The weight of the compacted soil within its molds and base was recorded (M2) and the soil compacted from the molds was removed using a mechanical extrude. A sample from the bottom and top of the moisture cans was taken and put in the oven at 105 ° C for 24 hours. The bulk density and dry density of the soil were then determined using equations 4.5 and 4.6 respectively.

$$\gamma b = \frac{M2 - M1}{v} \tag{4.5}$$

$$\gamma d = \frac{\gamma b}{(1+\frac{w}{100})} \tag{4.6}$$

Where: γd is dry unit weight, γb is the bulk unit weight, M2- the mass of soil after being compacted with mold, M1- the mass of the mold, V is the volume of the mold and W is the moisture contents of soils. Finally, the results of the recorded data were analyzed on Microsoft Excel datasheet and plotted the graph of the dry density versus moisture contents for analysis result (see Fig.5.4).

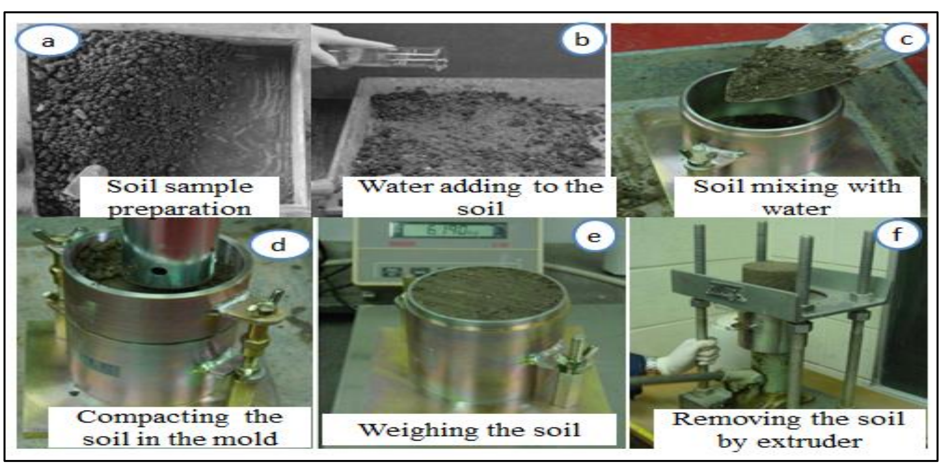

Figure4.7: Compacted test of the soil from critical slope section of the study area.

4.5.1.6 Unit Weight of Soils

When evaluating soil slope stability, one of the important input parameters is the unit weight of soil. To obtain this value, both the bulk (γb) and dry (γd) unit weights of soil were calculated. The laboratory test results of the soil are used to determine the saturated and dry unit weights of the soil, which were derived from the corresponding density and the acceleration of gravity (g). In this study, the unit weight of soil used for slope stability analysis is acquired through laboratory tests conducted on soil samples collected from a critical location where the slope has been cut and remolded for the shear strength test. First, the bulk and dry density are determined through laboratory tests. Then, using the bulk and dry density results, the unit weight of the soil is calculated using the formula provided bellow.

Bulk unit weight = Bulk density*g and Dry unit weight = Dry density*g.

4.5.1.7 Shear Strength Tests

Shear strength is the maximum soil resistance to shear stresses just before failure. The shear strength is one of the most important engineering properties of soil. In this study, shear strength parameters such as cohesion and angle of internal friction in the selected failed slope sections have been determined from the direct shear strength test. The test was performed on two soil samples measuring 60 x 60 x 25 mm that was compacted and remolded at their compaction tests moisture contents using ASTM D3080 (2002) standards at Addis Ababa Science and Technology University Geotechnical laboratory. The apparatus consists of a square brass box split horizontally at the level of the center of the soil sample which is held between metal grilles and porous stones as shown in. The vertical load is applied to the sample as shown in the figure and is held constant during a test. A gradually increasing horizontal load is applied to the bottom of the box until the sample fails in shear. For each normal load applied at regular intervals, the horizontal and vertical shear displacements were recorded. Shear stress and normal stress were calculated and plotted in the graph based on the test results. Finally, the Mohr-Coulomb failure criterion described the relationship between soil shear strength at a point on a particular plane and its normal stress as follows in equation 4.7.

$$\tau = c+\partial \tan\phi \qquad (4.7)$$

Where: C is the cohesion and ϕ is internal angle friction of the soil particles

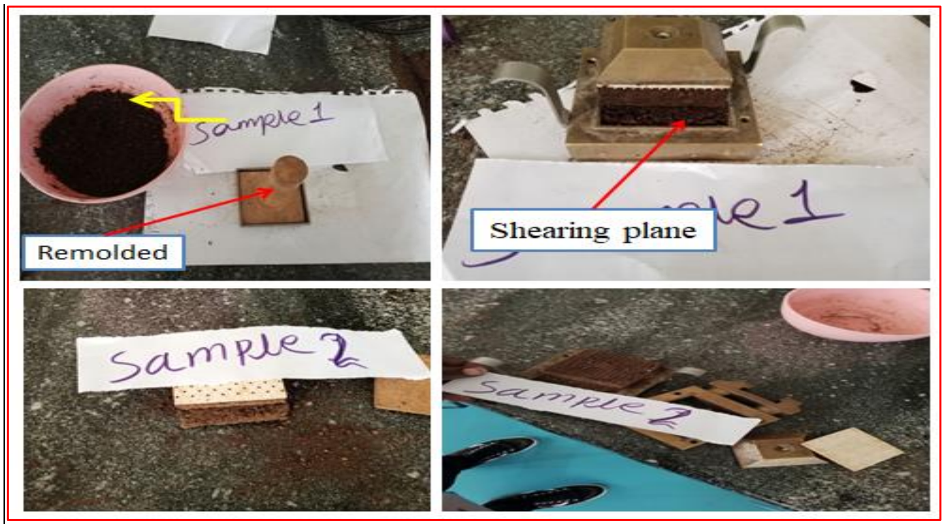

Figure4.8: Direct shear tests of soil slope sections in the study area

4.5.2 Laboratory Testing on Rocks Sample

The laboratory tests were performed on rock samples, including point load strength, density, and unit weight tests. Each of these tests was discussed as follows.

4.5.2.1 Point Load Tests

A point load strength test was performed to determine the unconfined compressive strength of intact rock. The tests were conducted according to ASTM D5731-16 (1995) standards to determine the strength of irregular rock samples at Al-asab geotechnical laboratory. The test was carried out under natural moisture content conditions on a minimum of three to four irregular rock samples taken at each selected critical slope section and a total of 26 lump rock samples for all slope sections were tested as follows:

- ✓ Before starting the test, a geological hammer was used to prepare irregular rock specimens with the correct size and shape for the point load testing machine (Fig.4.9a).
- ✓ The height, width, and length of the irregular rock samples were recorded before the start of the test (Fig.4.9b).
- ✓ Then place a rock sample in the test devices and apply the load continuously until the failures appear and the peak values of the failure load (P) are recorded (Fig.4.9d).
- ✓ Later, the average of the corrected point load strength was converted to the uniaxial compressive strength of the rock using the empirical equation proposed by (Broch & Franklin, 1972) which showed the relationship between the corrected point load strength and the uniaxial compressive strength of the rock (Eq. 2.5).

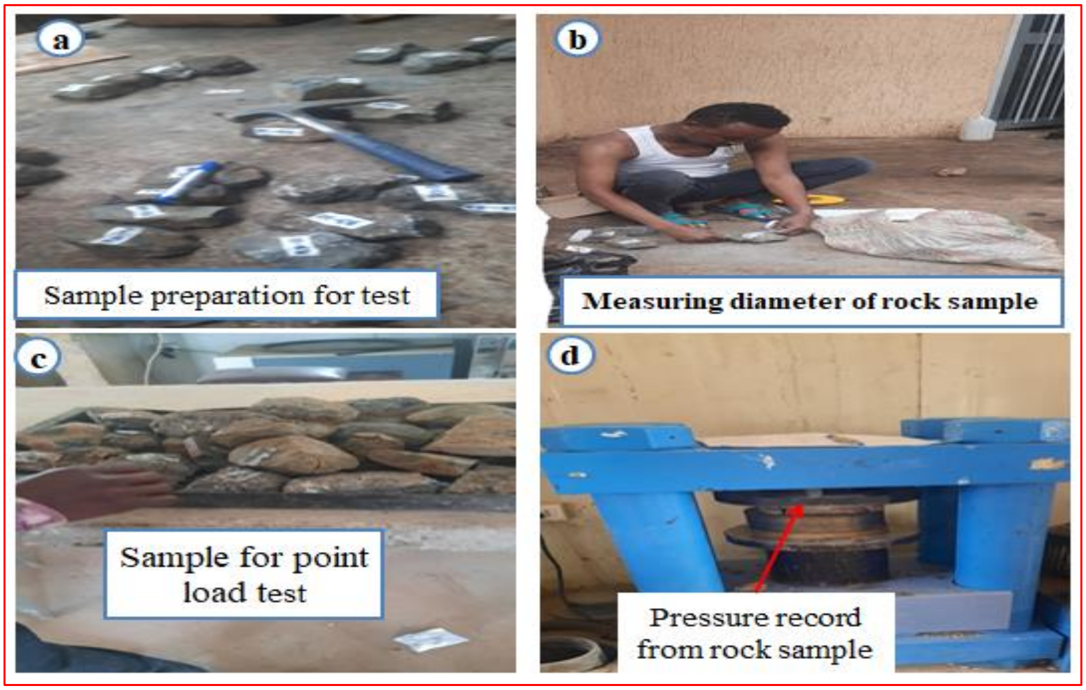

Figure4.9: point load strength test of intact rocks

4.5.2.2 Density and Unit Weight Rock

The unit weight of the rock is a crucial factor in determining the stress within the rock mass. It is also an important input parameter in calculating the safety factor for rock slope stability analyses. Moreover, the unit weight of the rock can be used in the conversion of Schmidt hammer rebound value to UCS of rocks using (Eq. 2.4). To determine the unit weight of the rock, at least three irregular rock samples were taken from a critical rock slope section using buoyancy techniques at Al-asab Geotechnical Laboratory (Fig.4.10) according to ISRM (1978) standard as follows:

- To determine the changed volume of irregular rock samples, the samples were first labeled and weighed (M1) while they were at their natural moisture content. Subsequently, the samples were dried in an oven for 24 hours at 105°C, and the weight of the oven-dried samples was recorded (M2).
- Afterward, a cylinder was filled with water, and the initial water volume (V1 in ml) was recorded. The oven-dried rock samples were then placed in the water-filled cylinder, and the volume change (V2 in ml) was recorded.

- By subtracting the initial water volume (V1) from the final water volume (V2), one can calculate the changed volume of the sample as follows: $\Delta V = V2 - V1$
- Finally, the dry density (γd) and bulk unit weight (γb) of each rock sample were determined using Equations 4.8 and 4.9, respectively.

$$Pd = \frac{M_d}{V_2 - V_1} \quad (4.8)$$

$$\gamma b = \rho d * g \quad (4.9)$$

Where, γd is the dry density of the rock samples in g/cm3, M2 is the mass of rock samples after being oven-dried in (g), ΔV is the difference between the water volume after the rock sample is placed and the water volume before the rock sample is placed in the cylinder γb is the unit weight of rock in KN/m3, and g is the gravitational accelerations (in m/s2).

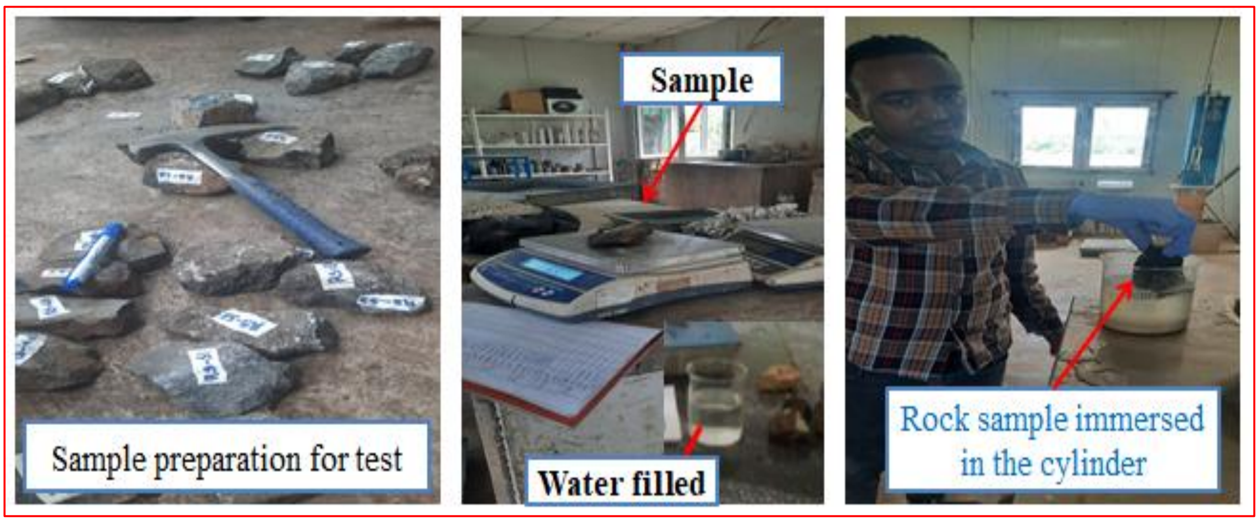

Figure4.10: Unit weight testing of rock samples

Table4.1: **Summary of laboratory tests for rock**

Types of tests	Number of tests	Standard of tests
Point load test	26	ASTM D5731-16(1995)
Unit weight	26	ISRM (1978)

4.6 Data processing and Analyzing

The data obtained from primary and secondary sources via desk study reconnaissance and compressive field survey, laboratory test and literature review was structured and processed in such a way that it could be suitably accessed during successive slope stability evaluations.

4.6.1 Rock Mass Classifications Method

In the field of rock engineering, the most commonly used empirical classification is rock mass classification (Gottron & Henk, 2021). It is used to evaluate rock-cut slopes based on critical characteristics and to quantify the rock mass condition (Khanna & Dubey, 2021). This study utilized the Bieniawski (1989) rock mass rating system to classify the rock quality and critical rock slope stability analysis. The rock mass was classified based on five basic rock mass rating parameters such as uniaxial compressive strength of intact rock, rock quality designation (RQD), discontinuity spacing, condition of discontinuity, and groundwater conditions. The study used a point load strength test to measure the uniaxial compressive strength of intact rock. RQD index was determined using the volumetric joint count method. Discontinuity spacing was measured in the field by taking the average value of the distance between adjacent spacing. The conditions of discontinuities such as persistence, aperture, roughness, infilling, and weathering condition of the wall rock were also estimated in the field. The condition of groundwater was visually determined as dry, damp, or wet observing the flow of water from a slope or the presence of water stains on the slope face (Khanna & Dubey, 2021). Finally, the Rating for five basic rock mass rating parameters was added to together to classify the rock mass of the study area according to Bieniawski (1989) as shown in eq. 4.10 below.

$$\text{RMRbasic} = R1 + R2 + R3 + R4 + R5 \tag{4.10}$$

Where: R1 is the Uniaxial compressive strength of intact rocks, R2 is rock quality designation, R3is the discontinuity spacing, R4 is the condition of discontinuity and R5 is the condition of the groundwater.

4.6.2. Shear Strength Parameter of Rock Mass

When evaluating the stability of rock slopes, it is important to consider the shear strength characteristics such as cohesion and angle of internal friction (Cala & Flisiak, 2020). In this study, equation 4.11 that is already included into the RocData software was used to predict the shear strength characteristics of the rocks (cohesion and friction angle) along the discontinuity plane based on an empirically derived correlation stated by Barton-Bandis (1973).

$$\tau = \partial n * \tan \{\text{JRC} * \log 10\ (\text{JCS}) + \phi b\} \tag{4.11}$$

Where: τ = Peak shear strength, ∂n = Effective normal stress, JRC = Joint roughness coefficient, JCS = Joint wall compressive strength, ϕb = basic friction angle.

The primary input parameters of Rocdata software, according to Barton and Bandis (1990) shear strength requirements, are basic friction angle (ϕb), joint roughness coefficient profile (JRC), joint wall compressive strength (JCS), slope height, and unit weight of the rock. The un-weathered joint wall compressive strength (JCS) equals the unconfined compressive strength of intact rock (Barton, 1976). For weathered rock surfaces, JCS will become a fraction of the uniaxial compressive strength of the rock approximately (1/4σc) (Barton, 1976). During the fieldwork, joint roughness coefficient was determined visually by comparing discontinuity surfaces to joint roughness profiles developed by Barton and Choubey (1977). The value of basic friction angle (ϕb) is between 25 and 35 for most smooth and un-weathered rock surfaces (Barton and Choubey, 1977). In addition, Heok- Brown failure criterion was used to determine shear strength and deformation parameters of the rock mass. According to Hoek et al. (2002), the cohesion (C) and internal friction angle (ϕ) of rock mass were determined with Rocdata software using generalized Hoek-Brown failure criteria. Rocdata software allows users to easily estimate rock mass properties and shear strength parameters (Hoek, 2006). The Geological Strength Index (GSI), uniaxial compressive strength of intact rocks (UCS), material constant of intact rock (mi) and Disturbance factor (D) were the input parameters for the Rocdata software. Furthermore, the Rocdata software requires the unit weight of rock and slope height (H) for slope application (Rocsciences, 2004). For this study, the uniaxial compressive strength of rock intact rock was determined from the point load strength index in the laboratory using ASTM D5631-16 (1995). The GSI was estimated in the field according to (Hoek and Marinos, 2000) by considering the weathering conditions of the discontinuity surface rock mass structure and interlocking of rock blocks. The material constant of intact rock (mi) was taken from the standard table of the Rocdata software (Hoek et al., 2002). The disturbance factor was obtained from the guideline of (Wyllie and Mah, 2004) based on the degree of disturbance of the rock mass subjected to mechanical excavation. In addition, the rock unit weight was determined in the laboratory test using buoyancy techniques (ISRM, 1978) and the slope height was measured in the field using a tap meter. Finally, results from output parameters from Rocdata software were used as input parameters in the slope stability analyses.

4.7 Slope stability Analysis Method

The slope stability analysis for this present study was performed using kinematics, Deterministic, limit equilibrium and finite element methods. The slope models were developed by compiling various geotechnical data gathered from field surveys and laboratory tests. This section provides a brief overview of each method for ensuring slope stability analysis

4.7.1 Kinematic Analysis Methods

In this study, the kinematic analysis was conducted using Dips software, which allowed for the evaluation of various failure mechanisms including planar, wedge, and toppling failure (Khanna and Dubey, 2021; Siddique and Pradhan, 2020). By analyzing the field manifestations and kinematic data, the rock slope failure modes were primarily determined (Park and West, 2001). The study utilized Dips 6.0 software (Rocscience, 2004) to analyze the kinematics of a rock slope for structurally controlled failure. The plotted structural data and daylight envelopes were used to determine the stability of the rock slope and identify the potential for failure zones (Seyed et al., 2011). To run the Dips software, slope orientations and major joint sets dip and dip directions, as well as the friction angle, were inputted (Raghuvanshi, 2017; Khanna and Dubey, 2021). These parameters were measured using a Brunton compass in the field. Finally, the kinematic analysis of the main plane was conducted using Dip's software to determine the mode of slope failure in the critical rock slope sections of the study area.

4.7.2 Deterministic Slope Stability Modelling Method

The safety factor for different anticipated conditions was calculated using the deterministic method (Park and West, 2001). The stability analysis for three modes of rock slope failures was evaluated using Rocplane, Swedge, and Roctopple software (Rocscience, 2004). The planar rock slope failure analysis was carried out using Rocplane software, whereas the stability analysis of the wedge mode of rock slope failure was evaluated using Swedge software. The input parameters used for the stability analysis included slope geometry, orientation of discontinuities, shear strength parameter, and unit weight of the rock. The safety factor was calculated for various conditions such as static dry, dynamic dry, static saturated and dynamic saturated conditions. The results were obtained based on the non-linear failure criteria of Barton-Bandis (1990).

4.7.3 Limit Equilibrium Method

The safety factor of rock and soil slope failures was analyzed using various methods. The limiting equilibrium approach was used to compare the shear strength adjacent to the sliding surface and the force needed to maintain the slope's equilibrium (Ullah et al., 2020). A limiting equilibrium method was used to analyze the stability of rock and soil slope failures using Rocscience slide software. The Morgenstern-Price method considers force and moment equilibrium, making it suitable for analyzing potential failure surfaces on both circular and noncircular surfaces (Raji Pant, 2021). For this study, the limit equilibrium method of the slide 6.0 software was used to model and compute the factor safety for rock and soil-selected slope sections (Rocscience, 2004). The input parameters for slide software include the shear strength parameter of rock and soil, the Unit weight of rocks, slope geometry, and external force. The shear strength of the rock mass-selected slope section was determined from the Hoek-Brown failure criteria using Rocdata software whereas the shear strength of soil was obtained from direct shear tests. The unit weight of the rock was obtained from the laboratory test using buoyancy techniques ISRM, the slope geometry was measured in the field using a tap meter and the horizontal earthquake coefficient was taken from EBCS 8 (1995). Finally, the General Limit Equilibrium (GLEM)/Morgenstern Price approach was used to compute the factor of safety of the limit equilibrium method under static dry, static saturated, dynamic dry, and dynamic saturated conditions.

4.7.4. Finite Element Method

The finite element method is a numerical method that is used to evaluate the stability of both natural and manmade slopes. Finite element analysis can be performed using Phase2 software, which uses a shear strength reduction technique to determine slope stability (Matsu and San, 1992; Griffith and Lane, 1999). This study used the Phase2 software (Rocscience, 2004) to determine slope stability, which is a strong finite element tool that can be used in a variety of situations (You et al., 2018). The data preparation and phase 2 software analyses includes the determination of the uniaxial compressive strength of intact rocks and the unit weight of rocks which are obtained from laboratory tests. The Geological strength index and slope height were determined in the field. The material constant of intact rock (mi) was taken from the standard table of the Rocdata software (Hoek et al., 2002). The shear strength parameters (cohesion and angle of friction) along the plane of failure of the rocks was determined using Rocdata 3.0

software (Rocscience, 2004), and the shear strength parameters (cohesion and angle of friction) along the plane of failure of soil materials were determined from a direct shear test. The Hoek Brown parameters were obtained also from the Rocdata 3.0 software (Rocsciences, 2004). The disturbance factor was obtained from the guideline of Wyllie and Mah (2004) based on the degree of disturbance of the rock mass. For this study, the Poisson's ratio of the rock mass can be calculated using the relationship between the material constant (mi) and the geological strength index Equation (4.12) proposed by Balazs (2009).

$$Vrm = -0.002GSI - 0.003mi + 0.457 \qquad (4.12)$$

Where: Vrm is the Poisson's ratio of the rock mass, mi is the material constant of intact rock (mi) and GSI is the Geological strength index of rocks which can be estimated in the field.

For this study the deformation modulus of the rock mass was determined by using General Hoek Brown failure criterion from Rocdata 3.0 software (Rocsicence, 2004). According to Hoek and Brown (1997), the deformation modulus of rock mass was determined using equations 4.13 and 4.14 below.

$$Ed = (1-\frac{D}{2}\sqrt{\frac{UCS}{100}}(10^{\frac{(GSI-10)}{40}})) \qquad \text{where UCS<100MPa} \qquad (4.13)$$

$$Ed = (1-\frac{D}{2})\ 10^{\frac{(GSI-10)}{40}} \qquad \text{UCS >100MPa} \qquad (4.14)$$

Cohesive soils (such as Clay soils) are characterized by a very low number of dilatancy angles ($\psi \approx 0$). The formula $\psi = \varphi - 30°$ can be used to estimate the dilatancy angle for non-cohesive soils (sand, gravel) with the angle of internal friction $\varphi > 30°$.

Hoek and Brown (1997) suggested that for very good, average, and very poor quality rock masses, the dilatancy angle can be approximated as a fraction of the friction angle. They recommended using values such as $\psi = \varphi/4$, $\psi = \varphi/8$, and $\psi = 0$ for very good, average, and very poor quality rock masses respectively.

Furthermore, soil's elasticity modulus (E) and Poisson's ratio (v) are used to analyze deformation in numerical modeling. Accordingly, suitable values of these parameters were derived from numerical correlations and literature review. The standard penetration test (SPT) has been used to correlate different soil parameters such as unit weight (γ), angle of internal friction (φ) and undrained compressive strength (qu) for estimating the stress-strain modulus elasticity of soils (Peck et. al., 1974; Bowles, 1977). For this study the SPT N, values were correlated with the saturated unit weight of soils (Bowles, 1977). The drained poisons ratio of granular soils can be calculated by using equation 4.15 as suggested by Bowles (1996). This study calculated the corrected standard penetration test N value to an average energy ratio of N60 using equation (Eq.4.16) proposed by Terzaghi and Pecks, (1967). The modulus of elasticity of the soil was calculated from the SPT N60 value as suggested by Das (1995) and Ameratunga et al., (2016) using equation 4.17 as follows:

$$Vd = 0.1+0.3\left(\frac{\phi - 25}{20}\right) \quad \text{For } \phi < 45^{\circ} \qquad (4.15)$$

$$\phi\ (\text{Deg}) = 27.1+0.3N_{60} - 0.00054N^{2}_{60} \qquad (4.16)$$

$$E = 1200(N+6)\ KN/m^{2} \quad \text{for } N<15 \qquad (4.17)$$

$$E = 4000+1200(N-6)\ KN/m^{2} \quad \text{for } N>15 \qquad (4.18)$$

In addition, horizontal earthquake coefficient was taken from EBCS 8 (1995). Finally, by importing the input parameter into the software, the safety factor was analyzed for various predicted situations such as dynamic dry, dynamic saturated static dry and static saturated conditions.

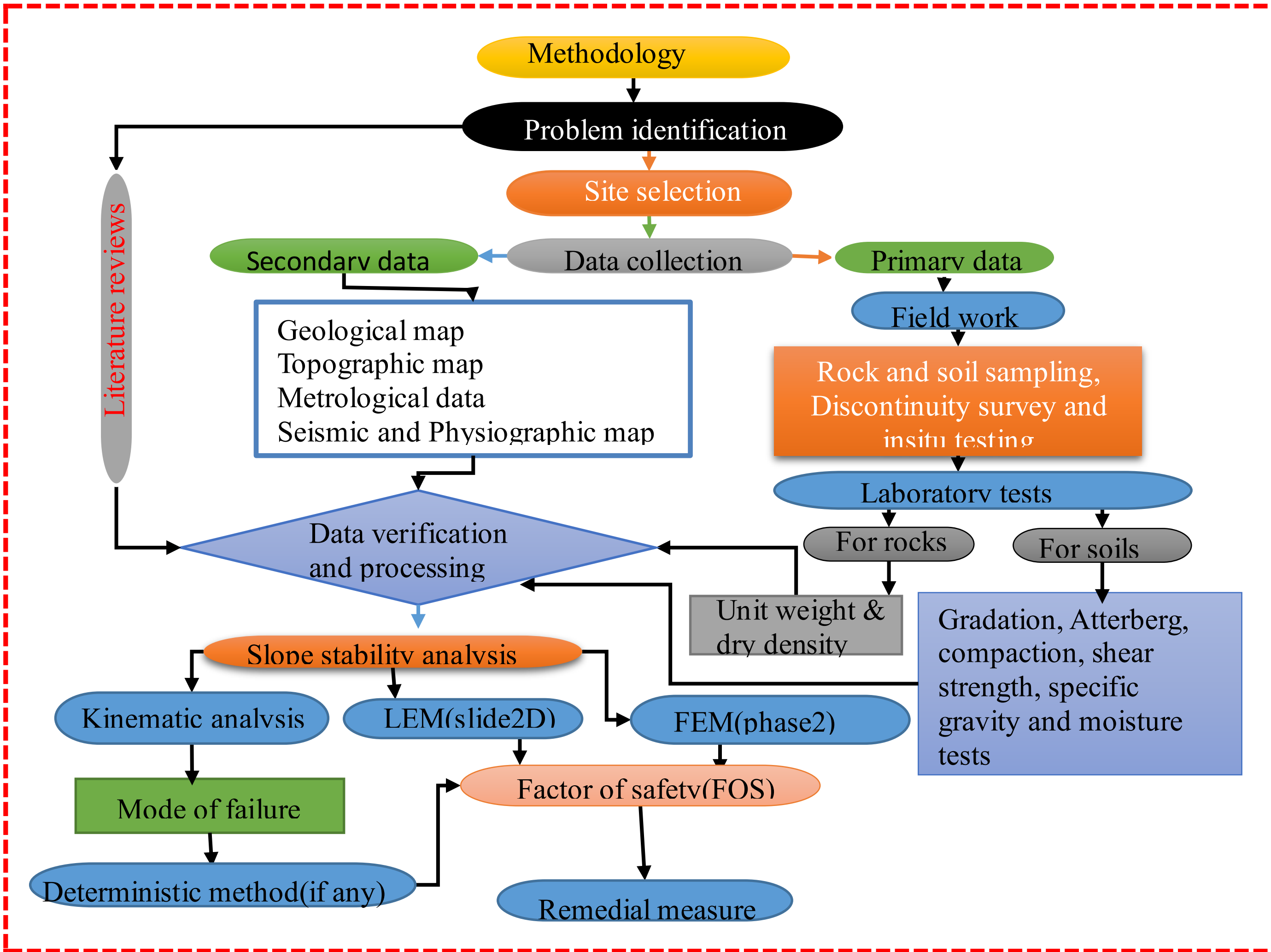

Figure4.11: General methodology flow chart

4.8 Materials

The material and equipment that were used for this research work include both laboratory and field equipment. The field equipment that were used for field data collection, measurement and testing include GPS, compass, a geological hammer, tape meter and Schmidt hammer for the in-situ test of rock strength. Soil mechanics laboratory equipments were used for shear strength, sieve analysis, specific gravity; natural moisture content and atterberg limit tests. A cylinder with known volume was used to determine the unit weight of the rock. For the preparation of map and data analysis, different software such as Arc GIS 10.8, Surfer 23, Google earth pro and Dip6.0, Slide 2D and phase 2 and Rockplane 6.0 were utilized.

CHAPTER- FIVE

5. RESULT AND DISCUSSION

5.1. Engineering Properties of Soils

The engineering properties of soils are used as input parameters for slope stability analysis of soils at critical slope section of the study area and also to correlate, classify and characterize the soils. The Soil samples collected from the field survey were tested in the laboratory to determine the physical properties of soil such as grain size analysis, Atterberg limit tests, Natural moisture contents, specific gravity tests, density and unit weight, compaction test and the shear strength tests were performed on the representative soil sample collected from the study area along the road section. Each parameter was discussed as follows.

5.1.1. Grain Size Analysis

Grain size analysis was performed to identify the percentage of different particle sizes in the soil from composes of critical soil slope located along the road. The laboratory test was conducted on the two disturbed soil samples collected from the test pits in the field. This test was carried out utilizing the mechanical sieve analysis and hydrometer analysis depending on the particle size soils. The mechanical sieve analysis was used for particle size larger than 0.075mm diameter (No.200 Sieve) and hydrometer analyses were employed for particle size smaller than 0.075mm diameter, (No.200 Sieve). Based on the particle size analysis results, the particle size diameter vs percent finer (particle size distribution curve) was plotted for each soil sample as shows on Fig.5.1. The grain size analysis results showed that the soil samples contained 10.07-30.86% of gravel, 67.25-86.47% of sand and 1.89-3.46% silt and clay. According to the results of grain size analysis, the soil of critical slope sections was classified as sand soil at both SS1 and SS2 of study area. The summary percentage of soil particles of each sample was shown in Table 5.1 below.

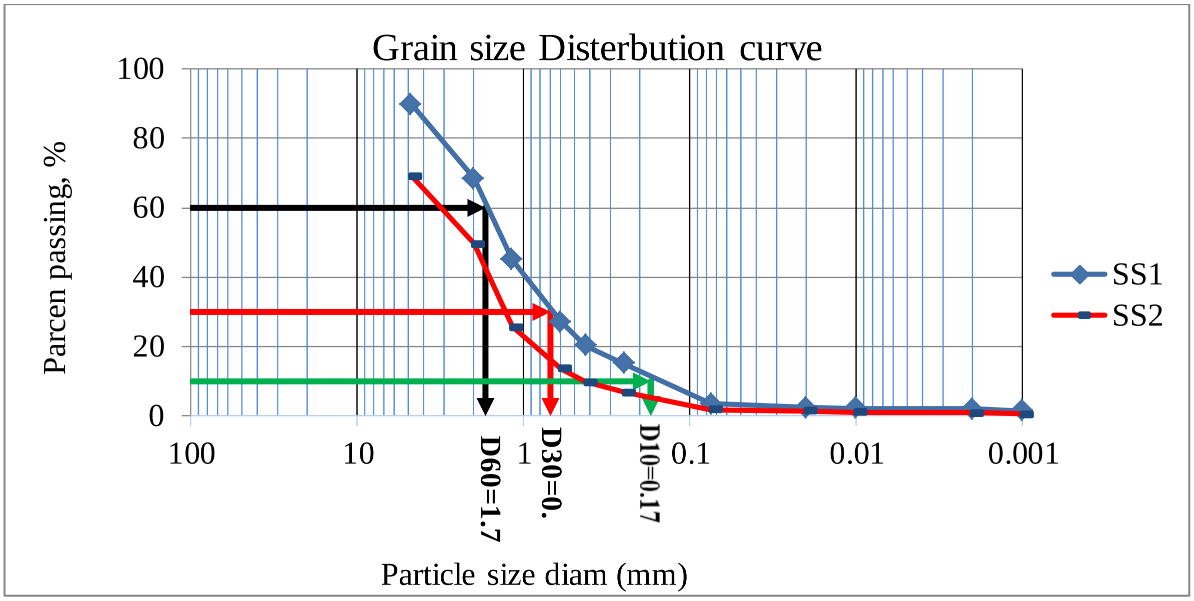

Figure5.1: Particle size distribution curve from sieve and hydrometer analyses

Table5.1: Grain size Analysis result of the soil slope sections of the study area.

Slope section	Depth (m)	The percentage of the soil particles		
		% Gravel	% Sand	% Silt and Clay
SSS1	1	10.07	86.47	3.46
SSS2	1	30.86	67.25	1.89
SSS = soil slope section				

5.1.2. Atterberg Limit Test

The Atterberg limit test was conducted on soil samples from the critical slope sections using the (ASTM D 4318, 1998) standard procedure and the Casagrande technique. This test is used to evaluate the liquid limit, plastic limit, and plasticity index of fine-grained soil and to classify soil using the Unified Soil Classification System (Moreno-Maroto & Alonso-Azcarate, 2022). The Liquid limit test was performed to determine the amount of water required for the soils to lose their cohesion and flow like a liquid. From the liquid limit determination chart (Fig.5.2) this test corresponds to 25 numbers of blows. A plastic limit test was conducted to determine the amount of water required for the soil to crumble. Furthermore, the plasticity index was determined from liquid and plastic limits (Table 5.2) to give the range over which the soils in the study area. The plasticity index of the soils in the study area ranges from 16.92 % to 36.29 % which indicates a medium to high plasticity soils and the liquid limit values are range from 44.42% to 67.24 % as shown in Fig.5.2. In addition, the minimum and maximum plasticity limits of the soil study area are 27.5 % and 30.95 % respectively as shows in Table 5.2 below.

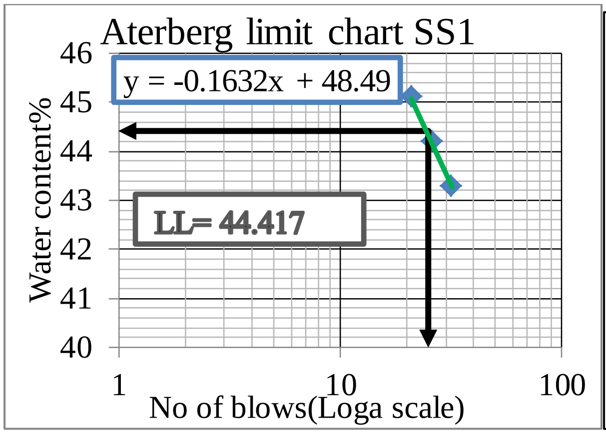

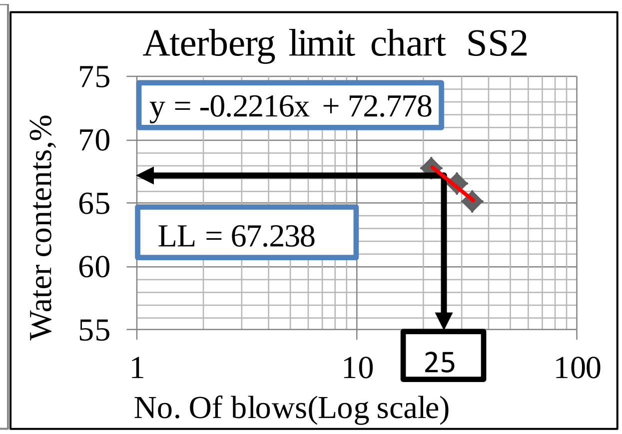

Figure5.2: Liquid limit chart the critical soil slope of the study area a) SS1 and b) SS2

Table5.2: Atterberg limit tests and plasticity index result of soil at critical slope sections

Slope sections	Depth(m)	Sample types	Atterberg limit tests			Plasticity Class according to Das, (2002)
			LL%	PL%	PI%	
SSS1	1	Disturbed	44.42	27.5	16.92	Medium plasticity
SSS2	1	Disturbed	67.24	30.95	36.29	High plasticity
SS = Soil slope section, LL = Liquid limit, PL = plastic limits, PI= Plasticity index						

5.1.3. Natural Moisture Contents

Natural moisture content (w) is the in-situ water content of soils determined using freshly excavated soil samples before exposing them to air. The test was conducted using fresh soil samples collected from two critical slope sections in accordance with (ASTM D2216, 1998). In the study area, the natural moisture content of the soils of critical slope section ranged from 12% to 25.6 % as shown in (Table 5.3). This demonstrates that the majority of soils are in dry state and the moisture holding capacity of the soils in the study area is low.

5.1.4. Specific Gravity of Soils

The specific gravity of soils in a selected slope section of the study area was evaluated using a pycnometer and distilled water at a specific temperature. For each sample, the specific gravity of the soil can be analyzed using the (ASTM D 854, 1998) standard. The specific gravity of soils at selected slope sections in the study area ranges from 2.64- 2.83 as shown in (Table 5.3).

Table5.3: Specific gravity and Natural moisture content of the soil slope sections

Slope section	Depth of sample (m)	Natural moisture contents (NMC%)	Specific gravity (Gs)
SSS1	1	25.6	2.64
SSS2	1	12	2.83

5.1.5. Unit Weight of Soils

The unit weight of the soil, both saturated and dry unit weight at critical slope section was determined from the laboratory test result of the collected soil samples from the fields. This test is performed for two soil samples that have been taken at different depth intervals of the study area. The result of the tests has been presented in Table 5.4. For this study, the unit weight utilized as an input parameter in slope stability analysis of the soil slope sections.

Table5.4: Shear strength parameters of soils for the soil slope section at SS1 and SS2

Slope sections	Soil description	Unit weight of soils	
		γ_d(KN/m^3)	γ_{sat}(KN/m^3)
SSS1	Well graded sand	9.41	11.37
SSS2	Well graded sand	11.14	13.45
SSS = Soil slope section, γ_d = dry unit weight of soil γ_{sat} = saturated unit weight of soil			

5.1.6. Standard Compaction Tests

The Standard proctor compaction test is performed to determine the relationship between the moisture content and the dry density of a specific soil sample at a specified compactive effort. This test was performed on two soil samples collected from the critical slope sections of the study area using a standard proctor test. The maximum dry density (MDD) and optimum moisture content (OMC) of the soil is used to remold the soil for the shear strength test were analyzed based on the results of the compaction test. The laboratory test results and the corresponding compaction curves of the two critical soil slope sections are shows in Fig.5.3. The result of maximum dry density (MDD) and optimum moisture content (OMC) are presented in Table 5.5.

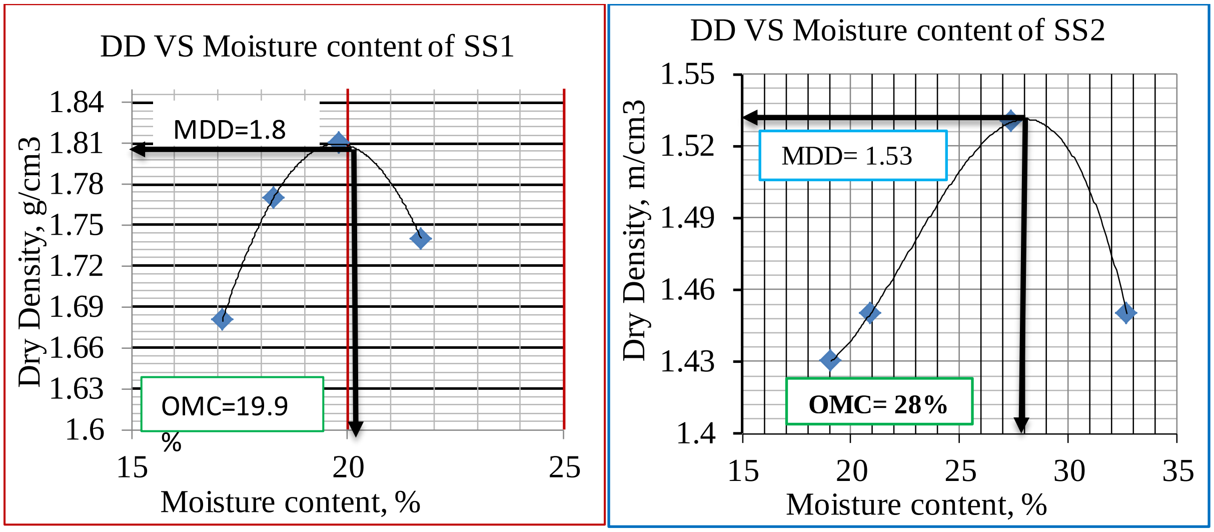

Figure5.3: Compaction curves of the soil critical soil slope section of the study area a) SS1 and b) SS2

Table5.5: Maximum dry density and optimum moisture content of the soil slope section at SSS1 and SSS2

Slope sections	Soil description	MDD, (g/cm3)	OMC (%)
SSS1	Well graded sand	1.81	19.9
SSS2	Well graded sand	1.53	28
SSS = Soil slope sections, MDD = maximum dry density, and OMC = Optimum moisture contents,			

5.1.7. Direct Shear Strength Tests

The direct shear test is one of the common strength tests for soils in which the shear strength parameters are determined to be used for slope stability analysis. In this study the shear strength parameter such as cohesion and angle of internal friction of the selected critical soil slope section has been determined from the direct shear tests as shown in Table 5.6. The result from direct shear test (table 5.6) indicates that the cohesion of soil slope section one (SSS1) and the soil slope section two (SSS2) are 30.38 KN/m2 and 32.41 KN/m2, respectively. While the internal friction angle of the soils from slope section one (SSS1) and the slope section two (SSS2) were found to have 29.56 ° and 21.57 ° respectively (Fig.5.4).

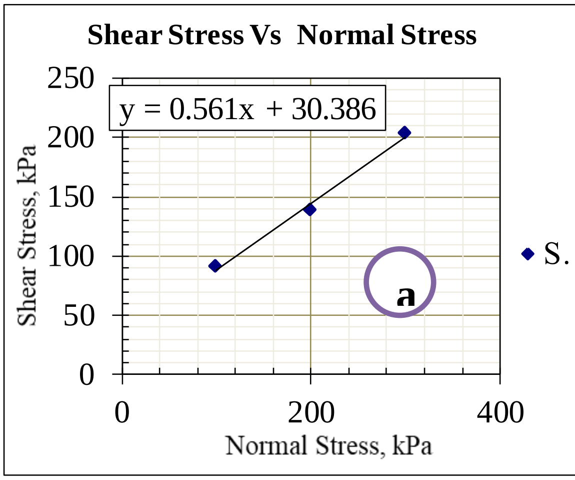

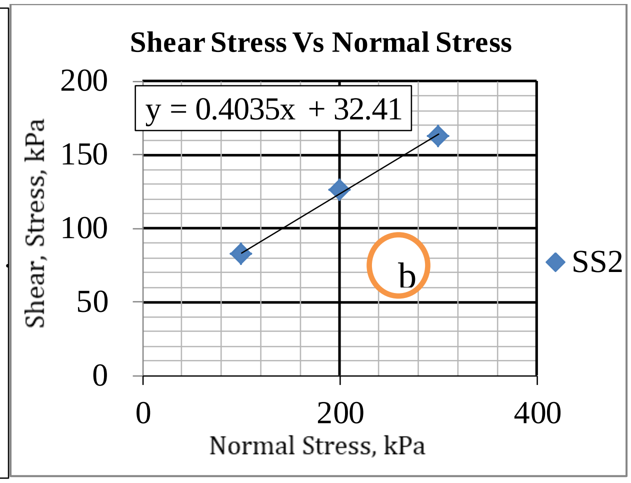

Figure5.4: Shear stress vs Normal stress of soil at a) SS1 and b) SS2

Table5.6: Shear strength parameters of soils for the soil slope section at SS1 and SS2

Slope section	Soil description	Shear strength parameter	
		Cohesion, (C) Kpa	Angle of internal friction (ϕ)
SSS1	Well graded sand	30.38	29.56⁰
SSS2	Well graded sand	32.41	21.57⁰
SSS = Soil slope section			

5.2. Classification of Soils Based on Unified Soil Classification (USC) System

The soils from selected critical slope section along the road section of the study area were classified by UCS system using gradation analyses and Atterberg limit test results (Table 5.7). According to the USC system, soil samples from SS1 and SS2 of the critical slope section along the road in the study area fall into the SW soil types (Fig.5.2) implying that both are sand soils. The detailed result and the UCS classification of the soils for the study area are presented in Table 5.7

Table5.7: Classifications of Soils based on USC Classification System

Slope section	Percent amount of particle size			Atterberg limit			USC Classifications
	Gravel	Sand	Fine materials (Silt and Clay %)	LL%	PL%	PI%	
SSS1	10.07	86.47	3.46	44.417	27.5	16.917	Well graded sand(SW)
SSS2	30.86	67.25	1.89	67.238	30.95	36.288	Well graded sand(SW)
SS= Soil slope sections, USC = Unified Soil Classifications, LL = Liquid limit, PL = plastic limit, and PI = Plasticity Index.							

5.3. Engineering Geological Characterization of the Rock mass

A detailed field assessment was conducted to identify the critical slope stability along the Arbarakete-Galamso road section and to describe the geological materials of the rocks and soils. Based on the detailed field assessment conducted, it was found that there are seven critical rock slope sections and two soil slope failures identified along the road section. The geological materials of the rocks and soils were described through visual observation, which helped in identifying the type of rocks, degree of weathering, and fracturing of rocks in different parts of the road section. These findings are crucial in determining the critical slope stability along the road section and will be helpful in developing appropriate measures to ensure the safety of road users.

5.3.1. Discontinuity Survey

Based on the discontinuity survey conducted according to the ISRM standard, important parameters were able to be obtained for analyzing the rock slope stability along the Arbarakete-Galamso road section of the study area. The survey covered joint orientation, joint spacing, joint filling, aperture, joint roughness, groundwater, and weathering condition of the rock slope. A total of seven critical rock slope sections were identified through the survey measurements. To provide a summary of the representative discontinuity survey measurements, Table 5.8 below have presented.

Table5.8: Summary of representative discontinuity parameters of critical rock slope sections.

Discontinuity parameter		Location of the critical slope sections						
		RSS1	RSS2	RSS3	RSS4	RSS5	RSS6	RSS7
Joint spacing(cm)		20-40	10-20	7-20	3-15	20-40	8-20	2-15
Condition of discontinuity	Persistence (m)	1-8	5-10	1-2	1-3	1-5	1-3	3-15
	Joint aperture(cm)	2-3	1-2	1-3	1	1	1- 4	1-2
	Filling materials	Soft gouges	No filling	No filling	Soft gouges	Fine materials	Soft gouges	open
	Roughness	rough	smooth	smooth	rough	rough	rough	rough
	Degree of Weathering	H.weat hered	S.weath ered	M.weath ered	H.weath ered	S.weather ed	H.weathe red	M.weath ered
GW. condition		dump	dump	dump	dump	dump	dump	dump
S = slightly weathered, M = Moderately weathered, H = Highly weathered and RSS = Rock Slope sections								

5.3.2. In-Situ Rock Strength Test

According to the study, the uniaxial compressive strength (UCS) of the intact rock at the critical slope section was determined using the Schmidt hammer strength test conducted in the fields (Barton & Choubey, 1977). This test was based on the (ASTM D5873, 2001) for the acquisition of rebound values. The average rebound value was converted into UCS of rocks using empirical equations (Eq.2.4), which were suggested by Barton and Choubey (1977). The lowest and highest strength of the rock was determined by the Schmidt hammer (L-type) ranges from 28.64 MPa to 60.37 MPa for slope sections RSS6 and RSS3 respectively as shown in Table 5.9.

Table5.9: Schmidt Rebound and UCS values from different critical slope sections.

Slope section	Schmidt hammer rebound value from each critical slope sections	Average of Rebound value for rock slopes	Av (R)	UCS (Mpa)	According to ISRM (1979)
RSS1	32,26,18,20,26,20,22,24,19,22	22.9	22.05	32.25	Moderate strength
	24,18,20,16,20,18,22,28,26,20	21.2			
RSS2	28,32,20,18,28,24,26,32,34,22	26.4	28.1	57.77	Medium strength
	25,30,26,44,32,30,32,29,22,28	29.8			
RSS3	26,29,32,20,28,24,30,35,28,33	29.5	30.9	60.37	Medium strength
	30,28,30,36,40,25,22,32,38,42	32.3			
RSS4	28,22,26,25,20,24,26,20,22,28	24.1	23.5	28.88	Moderate strength
	24,22,22,20,24,28,20,23,26,20	22.9			
RSS5	18,28,20,24,30,20,18,22,19,24	22.3	25.95	40.15	Moderate strength
	32,38,28,30,22,36,32,26,24,28	29.6			
RSS6	18,20,24,16,15,18,20,18,25,34	20.8	19.75	28.64	Moderate strength
	15,14,20,12,20,23,18,16,22,27	18.7			
RSS7	20,22,34,18,16,29,22,22,20,28	23.1	23	30.69	Moderate strength
	23,24,28,22,20,16,20,19,22,35	22.9			
	UCS – Uniaxial compressive strength, RSS- rock slope sections Av-Average of rebound values, R =Rebound value				

5.3.3. Rock Quality Designation (RQD)

As part of the present study, Rock Quality Designation was determined from the volumetric joint count (JV) on rock surfaces exposed along critical slope sections of the road in the study area according to Palmstrom's method (1982). After the measurements were taken from each critical slope section the volumetric joint account was calculated from the average spacing of joints for each critical slope section using equation (Eq.2.7). The resulting Rock quality designation index (RQD) values were summarized in Table 5.10. The joint count method revealed a minimum RQD value of 40.75% and a maximum value of 72.43% (Table 5.3). Based on Deere's classification (1988), the rock mass exposed to the road section of the study area was categorized as fair and good rock mass classes.

Table5.10: The Rock quality designation index determined from the volumetric joint count.

Slope section	JV (av)/1m*1m	RQD %	According to Deree (1988)
RSS1	20.74	43.26	Fair
RSS2	12.9	72.43	Good
RSS3	21.35	44.54	Fair
RSS4	22.5	40.75	Fair
RSS5	10.03	81.9	Good
RSS6	21.6	43.72	Fair
RSS7	20.5	47.35	Fair
RSS = Rock slope section and Jv, = volumetric joint account			

5.4. Laboratory Tests Results from the Rock Samples

The laboratory tests that are used to engineering characterization of rocks were normally conducted for classification purposes at each critical rock slope section along the road. For this study, laboratory analysis of rocks was undertaken to determine engineering characteristics rock such as point load tests, unit weight and density of rocks. In this study, a brief overview of these tests is presented as follows.

5.4.1. Point Load Tests

The uniaxial compressive strength of the intact rock was determined through point load strength tests. To classify the rock strength in the study area, a minimum of three to four irregular rock samples were obtained from each selected critical rock slope section, and the point load strength test was performed using ASTM D 5731-16 (1995) at Al-Asab Geotechnical laboratory. A total of twenty-six irregular rock samples were collected from the critical rock slope sections of the study area along road section. The average calculated point load strength was then converted to the appropriate uniaxial compressive strength (UCS) using equation 2.5. The calculated point load strength test results on separate rock samples obtained from each critical rock slope section (Table5.11) showed that the rock point load strength index ranges from 3.12MPa to 8.2MPa, with corresponding uniaxial compressive strengths of 74.88MPa to 196.8MPa. Based on the results of the point load strength tests on the rock samples, it can be concluded that the rock in the critical slope section of the study area have strength ranging from medium to high strength respectively (Deere & Miller, 1966).

Table5.11: Point load and uniaxial compressive strength test results of intact rocks

Slope sections	Sample ID	IS (50) Mpa	Ave, I S (50)	UCS (Mpa)	According to Deree and Miller 1966
RSS-1	RSS-11	2.8	3.5	84.2	Medium strength
	RSS-12	2.4			
	RSS-13	1.65			
	RSS-14	7.3			
RSS-2	RSS-21	9.4	8.2	196.8	High strength
	RSS-22	8.7			
	RSS-23	6.6			
RSS-3	RSS-31	8.1	6.9	164.6	High strength
	RSS-32	7.9			
	RSS-33	6.4			
	RSS-34	5.5			
RSS-4	RSS-41	4.9	4.4	105.6	Medium strength
	RSS-42	3.51			
	RSS-43	2.65			
	RSS-44	6.5			
RSS-5	RSS-51	5.7	5.9	141.6	High strength
	RSS-52	6.6			
	RSS-53	5.6			
RSS-6	RSS-61	3.9	3.12	74.88	Medium strength
	RSS-62	2.9			
	RSS-63	2.3			
	RSS-64	3.4			
RSS-7	RSS-71	7.5	4.15	99.9	Medium strength
	RSS-72	3.4			
	RSS-73	2.7			
	RSS-74	3.02			
	RSS = Rock Slope section, Ave- average, IS (50) corrected point load test, UCS- Uniaxial compressive strength of intact rocks				

5.4.2 Density and Unit Weight Rocks

In slope stability analyses, the unit weight of the rock is one of the input parameters. In this investigation, the density of rock was evaluated utilizing buoyancy techniques for irregular rock samples according to an ISRM (1978) standard. Accordingly, the representative rock samples were collected from seven critical rock slope sections of the study area and their corresponding unit weight was estimated. The results of Table 5.12 indicate that dry unit weights range from 21.8 to 30.4 KN/m3 and saturated unit weights range from 23.9 to 30.6 KN/m3.

Table5.12: Dry and saturated unit weights of rocks from laboratory tests

Slope sections	Rock units	Saturated unit weight γ_{sat} (kN/m3)	Dry unit weight γ_{d} (KN/m3)
RSS1	HW. upper basalt	26.6	25.7
RSS2	SW. upper basalt	30.6	30.4
RSS3	SW. upper basalt	27.3	27.1
RSS4	MW. Lower basalt	23.9	21.8
RSS5	SW. Lower basalt	26.7	26.0
RSS6	HW. Lower basalt	27.1	25.7
RSS7	MW. Lower basalt	25.2	23.6
	RSS= rock slope section		

5.5. Rock Mass Classifications

The classification of rock masses contains various inputs derived from intact rock and discontinuity properties both of which have a significant impact on the evaluation of the engineering behavior of rock masses. In this study, detailed measurements were taken on road cuts slope between Arbarekete and Badessa road section to collect data for rock mass classification using the Rock Mass Rating (RMR) and Geological Strength Index (GSI). As a result, a summary of these classifications was discussed as follows.

5.5.1. Rock Mass Rating

According to (Bieniawski, 1989), the rock mass rating (RMR) is used in a variety of rock engineering applications including mining, hydropower, tunneling projects and hillslope stability. Accordingly, the quality of the rock at the critical rock slope in the study area was determined using the (Bieniawski, 1989) basic rock mass rating system by determining five basic parameters such as Uniaxial compressive strength of intact rock (UCS), rock quality designation index (RQD), spacing of discontinuity, condition of discontinuity, and groundwater condition. In this study, the classification of rock masses was done based on the UCS result obtained from Schmidt hammer strength test and RQD values were determined from volumetric joint account methods in the field and the field evaluated rock mass classification parameters such as joint spacing, discontinuity condition, and groundwater condition were estimated and evaluated in the fields. The rating values were added for each parameter to categorize the rock mass of the study area based on Bieniawski, (1989). In seven critical slope sections, the RMR system ranges from 40 to 69, and the rocks are classified as fair (class C) to good (class B) rocks. It appears that the rock at slope sections RSS1, RSS2, RSS3, RSS4, RSS6 and RSS7 is Fair, whereas the rock at slope sections RSS5 is good. The detailed discontinuity parameters, including rating values and computed RMR are summarized in Table 5.13.

Table5.13: RMR values and classification of rocks in the critical slope sections (*Bieniawski, 1989*)

Slope sections	Rock types	Five basic RMR parameter rating value					RMR	Class	Description of Rock quality according to (Bieniawski, 1989)
		UCS	RQD	SP.	Con.	GWC			
RSS1	upper basalt	7	8	10	10	10	45	C	Fair rock
RSS2	upper basalt	12	13	8	10	10	53	C	Fair rock
RSS3	upper basalt	12	8	8	10	10	48	C	Fair rock
RSS4	Lower basalt	12	8	8	20	10	58	C	Fair rock
RSS5	Lower basalt	12	17	10	20	10	69	B	Good rock
RSS6	Lower basalt	7	8	8	10	10	43	C	Fair rock
RSS7	Lower basalt	7	8	6	10	10	40	C	Fair rock
UCS = Uniaxial compressive strength, RQD = Rock quality designation, SP = Spacing of discontinuity, Con = condition of discontinuity and GWC = ground water conditions									

5.5.2. Slope Mass Rating

The slope mass rating (SMR) is a modification to the rock mass rating that was first developed by Romana in 1985 (Dahiya, et al., 2022). To obtain SMR, adjustment factors derived from joint-slope relationship and method of excavation were added to the basic rock mass rating (RMR). Accordingly, the quality of the rock at the critical rock slope section in the study area was determined using the (Romana, 1985) rock mass rating values, adjustment factors values derived from joint-slope relationship and value derived from method of excavation. In this study, the classification of slope rock masses was done based on the RMR results calculated and presented in table 5.6 above, rate of adjustment factors values derived from joint-slope relationship(F_1, F_2, F_3) and rate value derived from method of excavation(F_4). The slope mass rating (SMR) values were calculated by using equation (Eq. 2.10) to categorize the rock mass of the study area based on (Romana, 1985). In seven critical slope sections, the SMR value ranges from 19 to 44, and the rocks are classified as very bad (class. No V) to normal (class. No III) rocks. It appears that the rock at slope sections RSS1, RSS4, RSS5, RSS6 and RSS7 are classified under bad rock quality; whereas the rock at slope sections RSS2 is normal and RSS3 is classified under very bad rock quality. The detailed adjustment factors and method of excavation, including their rating values and computed SMR are summarized in Table 5.14.

Table5.14**:** SMR values and classification of rocks in the critical slope sections **(**Romana, 1985**)**

Slope sections	Rock types	AF			ME	RMR	SMR Values	Class No.	Description of Rock quality	Stability
		F_1	F_2	F_3	F_4					
RSS1	Upper basalt	0.15	1	-60	0	45	36	IV	Bad	Unstable
RSS2	Upper basalt	0.15	1	-60	0	53	44	III	Normal	Partially stable
RSS3	Upper basalt	0.7	0.7	-60	0	48	19	V	Very Bad	Completely unstable
RSS4	Lower basalt	0.4	0.85	-60	0	58	38	IV	Bad	Unstable
RSS5	Lower basalt	0.7	1	-60	0	69	27	IV	Bad	Unstable
RSS6	Lower basalt	0.4	0.85	-50	0	43	26	IV	Bad	Unstable
RSS7	Lower basalt	0.15	1	-60	0	40	31	IV	Bad	Unstable
AF= adjustment factors, ME= method of excavation										

5.5.3. Geological Strength Index

The Geological Strength Index (GSI) is a geological engineering assessment of rock mass and one of the input elements used in rock data software to determine the shear strength and deformation characteristics of rocks. In this study, the geological strength index of the critical rock slope sections was estimated in the field by visual observation using the quantitative GSI chart suggested by Marinos and Hoek (2000) (Yang & Elmo, 2022). Accordingly, GSI value of the rock mass was evaluated based on the condition of discontinuity surfaces and structures in the rock masses and it was evaluated at surface outcrops slope face along the road. Additionally, field estimated GSI values were used to identify rock quality and as input parameters for finite element and limit equilibrium slope stability analysis. According to the GSI chart in appendix D by Hoek and Marinos (2000), GSI values were estimated in the field for seven critical rock slope sections.

Table5.15: The Geological strength index value of the critical rock slope section estimated in the field.

Slope sections	Rock units	Geological structure	GSI, a value estimated in the field	Surface conditions
RSS1	SW. Upper basalt	Very blocky	48	fair
RSS2	SW. Upper basalt	Blocky	65	good
RSS3	HW. Upper basalt	Blocky/Disturbed	32	Poor
RSS4	MW. Lower basalt	Very blocky	46	fair
RSS5	MW. Lower basalt	Blocky	67	good
RSS6	HW. Lower basalt	Blocky/Disturbed	35	poor
RSS7	MW. Lower basalt	Very blocky	45	fair
GSI = Geological strength index, RSS = Rock slope sections, SW= slightly weathered, HW = highly weathered and MW = moderately weathered.				

5.5.4. Rock Mass Strength and Deformation Parameters

5.5.4.1. Determination of Rock Mass Shear Strength Parameters

The shear strength of a rock mass is determined using the generalized Hoek Brown strength criterion in terms of major and minor principal stresses from the Rocdata software. The Rocdata 3.0 software (Rocscience, 2004) was used to determine the equivalent Mohr-Coulomb shear strength parameter (c and ϕ) based on the Hoek–Brown failure criterion see (Appendix I). The input parameters of Rocdata software include the Geological Strength Index (GSI), Uniaxial Compressive Strength of intact rocks (UCS), material constant of intact rock (mi), unit weight of rocks (γ), slope height, and Disturbance factor (D). In this study, the value of GSI was estimated from the field as tabulated in (Table 5.15). The UCS can be determined by performing insitu Schmidt hammer strength test on rocks summarized in Table 5.9. The material constant of intact rock (mi) was taken from the presented data and already built in the rock data software Rocscience, (2004) (Appendix K). The unit weight of rocks (γ) determined in the laboratory using buoyancy techniques as presented in (Table 5.12) was used in the analysis. The slope height can be estimated in the field by measuring the tape meter and the Disturbance factor (D) was a factor that depends on how much the rock mass has been disturbed by mechanical excavation and stress reduction. It ranges from zero to one for in situ rock masses that have not been disturbed to highly disturbed rock mass. In addition, the disturbance factor (D) is in the range of 0.7 to 1.0 for blasted rock slopes. The value of D used in this study was range from 0.7 to 1 which is already included in the Rocdata software. A summary of Rocdata software's parameters for determining rock mass shear strength is shown in Table 5.18.

Table5.16: Input parameters for determining the shear strength of rocks

Input parameter Rocdata software	Critical rock slope sections						
	RSS1	RSS2	RSS3	RSS4	RSS5	RSS6	RSS7
UCS, (Mpa)	32.25	57.77	60.37	28.88	40.15	28.64	30.69
GSI	48	65	32	46	47	35	45
Mi.	25	25	25	25	25	25	25
D	0.7	0.7	1	0.7	0.7	0.7	0.7
γ (KN/m3)	25.7	30.4	27.1	21.8	26	25.7	23.6
H (m)	38	45	23	25	35	26	25
Rock type	Upper basalt	Upper basalt	Upper basalt	Lower basalt	Lower basalt	Lower basalt	Lower basalt
RSS = Slope sections, UCS, = Uniaxial compressive strength of intact rocks, GSI = Geological strength index, mi = Rock material constant, D = disturbance factor, γ = is unit weight of rocks and H = height of slope.							

5.5.4.2 Determination of Rock mass Deformation Parameters

In this study, the deformation modulus and strength of the rock mass are the required inputs for numerical models to evaluate the rock slope stability analysis. In addition, one of the most essential rock characteristics utilized in numerical modeling of rock slope is Poisson's ratio (vrm) and intact modulus (Em). The modulus of deformation of rocks was determined using Rocdata software (Rocscience, 2004). However, the Poisson's ratio of the rock mass (vrm) was estimated from equation 3.13 using the relationship between the Poisson's ratio, Geological strength index (GSI) and material constant (mi) according to (Balazs, 2009). Detailed information on the deformation parameters of the rock mass at critical rock slope sections in the study area is presented in Table 5.17 below.

Table5.17: Summary of the deformation parameters of the rock mass in the study area

Slope sections	Rock units	Cohesion (Mpa)	Friction angle (ϕ)	Deformation modulus, Em (Mpa)	Poisson's ratio(V)
RSS1	HW. Upper basalt	0.264	28	3284.87	0.286
RSS2	SW. Upper basalt	0.892	32	11715.6	0.253
RSS3	SW. Upper basalt	0.181	49	1786.44	0.318
RSS4	MW. Lower basalt	0.15	44	2134.36	0.291
RSS5	MW. Lower basalt	0.269	40	3465.42	0.289
RSS6	HW. Lower basalt	0.155	45	1466.9	0.313
RSS7	MW. Lower basalt	0.213	50	2700.3	0.293

The engineering geological map was prepared through integration of data obtained from field survey characterization of rocks and laboratory tests and analysis of soils and rocks (Fig.5.5).

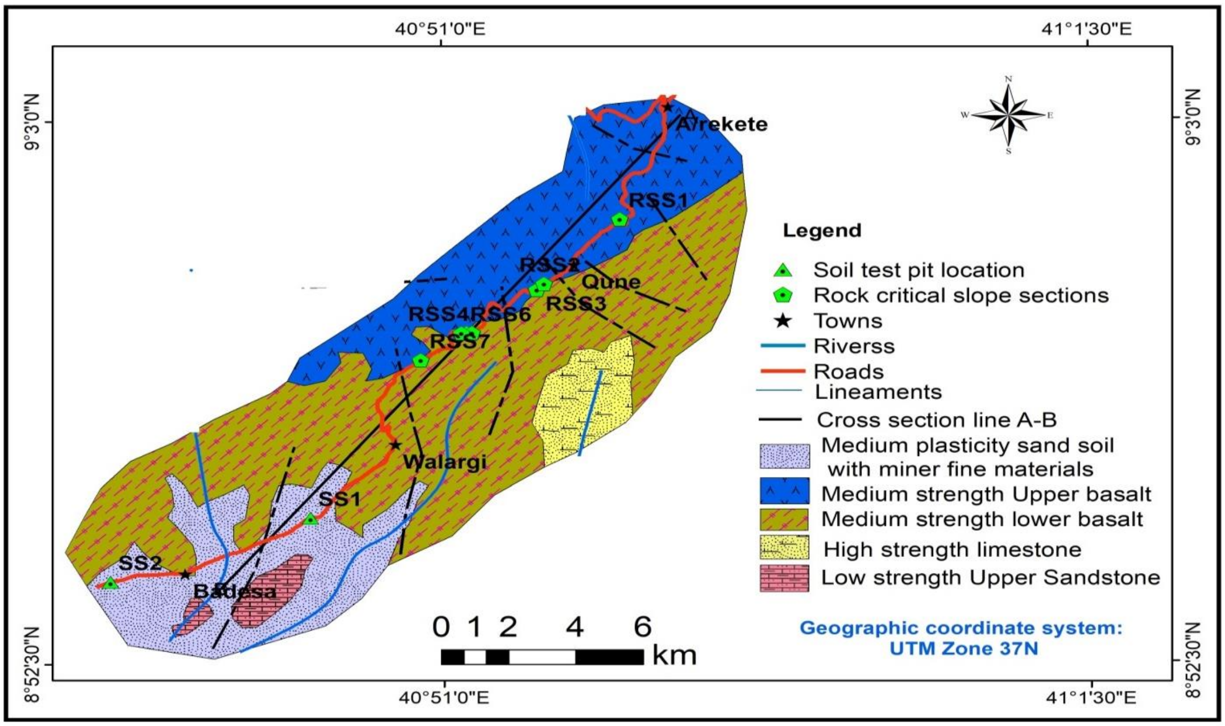

Figure5.5: Engineering geological map along the road section of the study area

5.6. Stability Analysis of Rock Slopes

The stability of rock slopes in the study area was analyzed using kinematic, limit equilibrium, and finite element methods.

5.6.1. Kinematic Slope Stability Analysis

For this study, the kinematic analysis was performed using Dips 6 software (Rocscience, 2004) to evaluate various mechanisms of slope failures such as a planar and wedge. The Dips software was used to process the data for the rock slope discontinuity which required the orientation of the discontinuities (dip and dip direction of joints), the slope face orientation (dip and dip direction of slope) and friction angle (Admassu & Shakoor, 2022; Barlow, et al., 2017). Dip and dip direction of joints and slope face orientation were determined in the field, although friction angle along the failure plane was determined using Rocdata software.

Table5.18: Input parameters used in Dips software for kinematic analysis.

Slope sections	Slope face orientation	Joint set orientations (Dip and Dip direction)			
	Slope D/DD, (º)	JS1, (º)	JS2, (º)	JS3, (º)	Friction angle, (º)
RSS1	70/230	60/260	75/140	56/180	28
RSS2	85/250	61/255	80/360	70/120	32
RSS5	70/270	56/320	50/250	----	40

The orientations of various joint sets from data obtained during the field survey were plotted on a lower hemisphere using a stereographic projection which is contoured to determine the various pole concentrations (Fig.5.6). According to the analysis, a wedge mode of failure was identified at the rock slope sections RSS1 and RSS2 by the intersection of two joints (Fig.5.6a and c). The wedge failure occurs at RSS1 where the slope face has 230º and the intersection of discontinuity sets (JS1 and JS3) and (JS2 and JS3) are falling within the critical zone. The former intersection line is plunging toward 203° with a plunge angle of 55°; whereas, the later intersection line is plunging toward 180° with a plunge angle of 50° in which these conditions increase the likelihood of wedge failure. In the same ways, the wedge failure occurs at RSS2 where the slope face has 250º and the intersection of discontinuity sets (JS1 and JS2) and (JS1 and JS3) are falling within the critical zone. Similarly, the former intersection line is plunging toward 308° with a plunge angle of 55°; whereas, the later intersection line is plunging toward 187° with a plunge angle of 40° in which these conditions increase the likelihood of wedge failure. The planar mode of failure was identified at slope location RSS2 and RSS5 (Fig.5.6b and d). According to the result of the analysis, planar type of failure which is potentially located at the RSS2 and RSS5 were vulnerable to planar failure due to respective discontinuity set JS1 in which the pole of the joint sets fail inside the daylight envelope. A detailed summary of the possible modes of failure at the critical slope section as well as the joint set responsible for mode failure is presented in Table 5.19. Finally, a deterministic method was used to conduct the stability analysis of the two modes of failure in order to calculate the factor of safety.

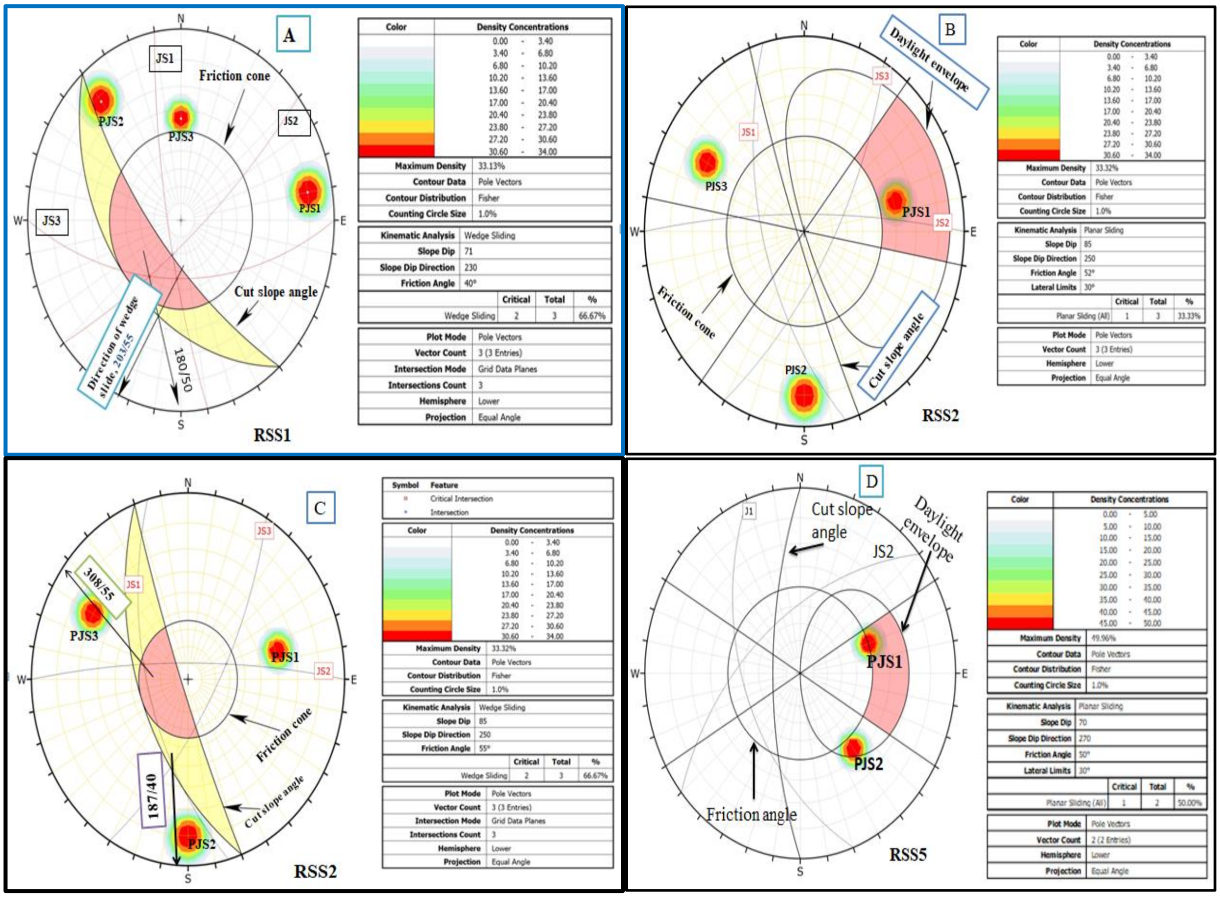

Figure5.6: Kinematic analyses for different modes of rock slope failure: Wedge failure at (a and c) and planar failure at (b and d), respectively.

Table5.19: Mode of failures from kinematic analysis of rock slope sections

Slope sections	Mode of failure from kinematic analysis rock slope sections
RSS1	Two Wedge failure, at the intersection points of joint JS1 and JS3 and at the intersection points of joint JS2 and JS3
RSS2	Two Wedge failure, at the intersection points of joint JS1 and JS2 and at the intersection points of joint JS1 and JS3
	Planar failure due to joint set JS1
RSS5	Planar failure due to joint set JS1
	RSS = Rock Slope sections, JS1 = joint set one. JS2 = Joint set two, JS3 = joint set three.

5.6.2. Slope Stability Analysis Using Deterministic Methods

According to the kinematic analysis results (Fig.5.6), probable planar rock slope failure occurs at slope sections RSS2 and RSS5, a wedge failure occur at slope section RSS1and RSS2. A factory of safety of slope stability assessment was conducted using Rocplane and Swedge software for planar and wedge modes of failure, respectively (Goodman, 1989; Park and West, 2001; Wyllie and Mah, 2004). The software was used to analyze and interpret the factor of safety for the structurally controlled critical rock slope under static dry, static saturated, dynamic dry, and dynamic saturated conditions. For this analysis Shear strength parameters (cohesion and friction angle) of rock mass for the three structural controlled critical selected rock slope sections were obtained from Barton-Bandis failure criteria using Rocdata 3 software (Rocscience, 2004) see appendix I and the unit weight of rock was obtained from the laboratory tests and summarized in Table 5.12. Furthermore, external loads such as horizontal seismic acceleration and groundwater conditions were considered during the stability analysis. In these sections the stability of slope subjected to the two modes of failures which were planar and Wegde after analyzing kinematic analysis results using the Rocplane and Swedge software (Rocscience, 2004).

5.6.2.1. Deterministic Snalysis of Planar Failures

The kinematic analysis results in (Fig.5.6b and d) revealed that at rock slope sections RSS2 and RSS5, planar mode of failure occurred due to their respective joint sets JS1 (PJ1) respectively. Deterministic analysis was used to construct the three-dimensional and side view graphs of the rock slope using the Rocplane software (Wang, et al., 2022). Accordingly, the factor of safety (FOS) for the planar mode of failure has been analyzed using Rocplane software (Rocscience, 2004). The input parameters used to determine the factor of safety using Rocplane software include slope geometry, the discontinuity set orientation and the shear strength parameters (cohesion and angle of internal friction), and the unit weight of rocks. The summary of input parameters used in Rocplane software for determination of FOS at critical rock slope sections with a planar mode of failure are tabulated in Table 5.20 below.

Table5.20: Input parameter used in Rocplane software for planar mode of failure

Slope sections	Input parameter for Rocplane software to determine factor of safety the planar failure										
	Slope geometry			Failure plane				Shear strength		Forces	
	Joint set	Dip, (º)	H (m)	Dip, (º)	Wv	γr (t/m3)	USA, (º)	ϕ, (º)	C(t/m2)	γw (t/m3)	α
RSS2	JS1	71	45	60	9	30.4	11	41	9.6	1	0.08
RSS5	JS1	70	35	56	9.5	26.0	10	31	4.4	1	0.08
Where γ = the unit weight of the rock, USA = the upper slope angle, ϕ = friction angle, c = cohesion, γw = water pressure, α = the seismic coefficient, H = the slope height and JS1= the joint set one, JS3 = joint set three and WV = the waviness of plane.											

The modeling of planar failures in Fig.5.7 and 5.8 demonstrated that planar failures are possible at rock slope section RSS2 and RSS5 due to the presence of their respective joint set JS1. The factor of safety analysis was performed on their respective joint set JS1 on rock slope section RSS2 and RSS5 (Fig.5.7 and 5.8) using the Rocplane software (Rocscience, 2004). Accordingly, the evaluated factor of safety for slope section RSS2 was larger than one in both static dry and dynamic dry conditions as shown in Fig.5.7, and less than one in both static saturated and dynamic saturated conditions. However, the evaluated factor of safety for joint JS1 of slope section RSS5 was less than one under all anticipated states. In slope stability analysis, a factor of safety of less than one showed that a slope is unstable (Tsige, et al., 2019; Shariati & Fereidooni, 2021). This implies that, the factor of safety for slope section RSS2 was less than one in both static saturated and dynamic saturated conditions. which indicated that the slope section RSS2 was marginally stable; whereas, on slope section RSS5 it was unstable for static dry, dynamic dry, static saturated and dynamic saturated conditions as shown in Fig. 5.7 and 5.8, respectively. As a result, suitable remedial measures are required for these specific slope sections to avoid the slope from failing on the road. The summary of the factor of safety analysis results and slope status at RSS2 and RSS5 under different anticipated conditions for the planar mode of failure is presented in Table 5.21.

Table5.21: Factor of safety and slope status under different condition for planar rock failure.

Slope sections	Joint sets	Factor of safety of planar failure formed on rock slope section at RSS2 and RSS5 at different conditions			
		Static dry (FOS)	Static saturated (FOS)	Dynamic dry (FOS)	Dynamic saturated (FOS)
RSS2	JS1	1.41	0.96	1.27	0.84
	Stability condition	Stable	Stable	Unstable	Unstable
RSS5	JS1	0.95	0.56	0.85	0.47
	Stability condition	Unstable	Unstable	Unstable	Unstable

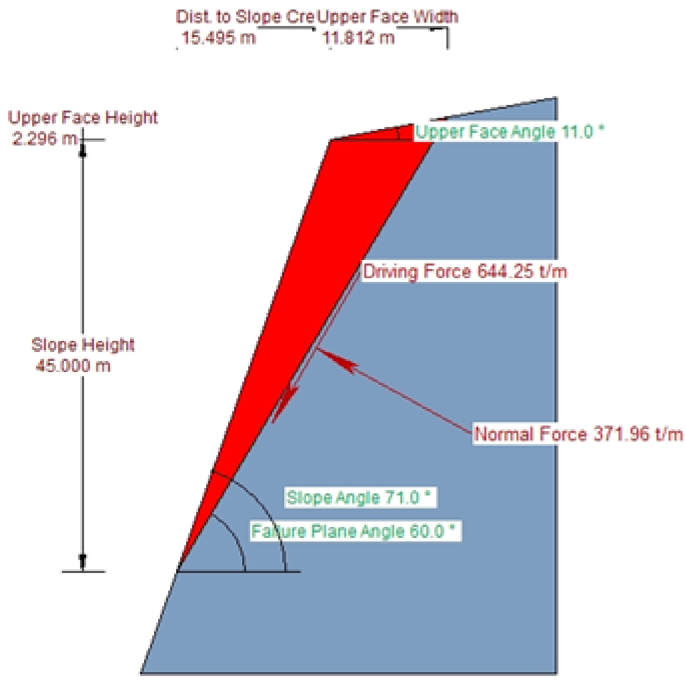

Static dry

Factor of Safety	1.41
Driving Force	644.25t/m
Resisting Force	906.53t/m
Wedge Weight	743.92t/m
Wedge Volume	247.97m^3/m
Shear Strength	847.62t/m^2
Normal Force	371.96t/m
Plane Waviness	9.0°

RSS2

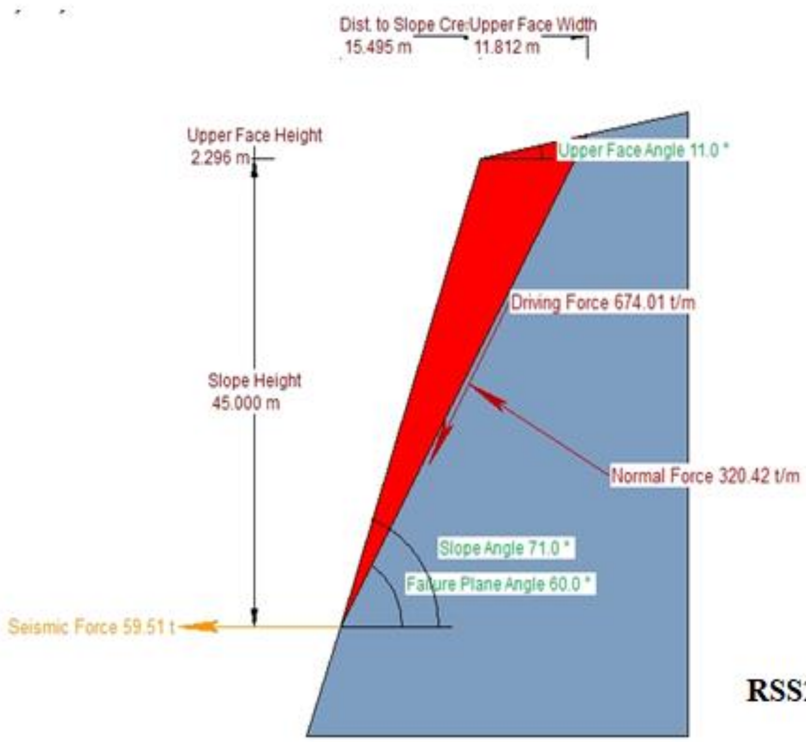

Dynamic dry

Factor of Safety	1.27
Driving Force	674.01t/m
Resisting Force	853.57t/m
Wedge Weight	743.92t/m
Wedge Volume	247.97m^3/m
Shear Strength	802.82t/m^2
Normal Force	320.42t/m
Seismic Force	59.51t
Plane Waviness	9.0°

RSS2

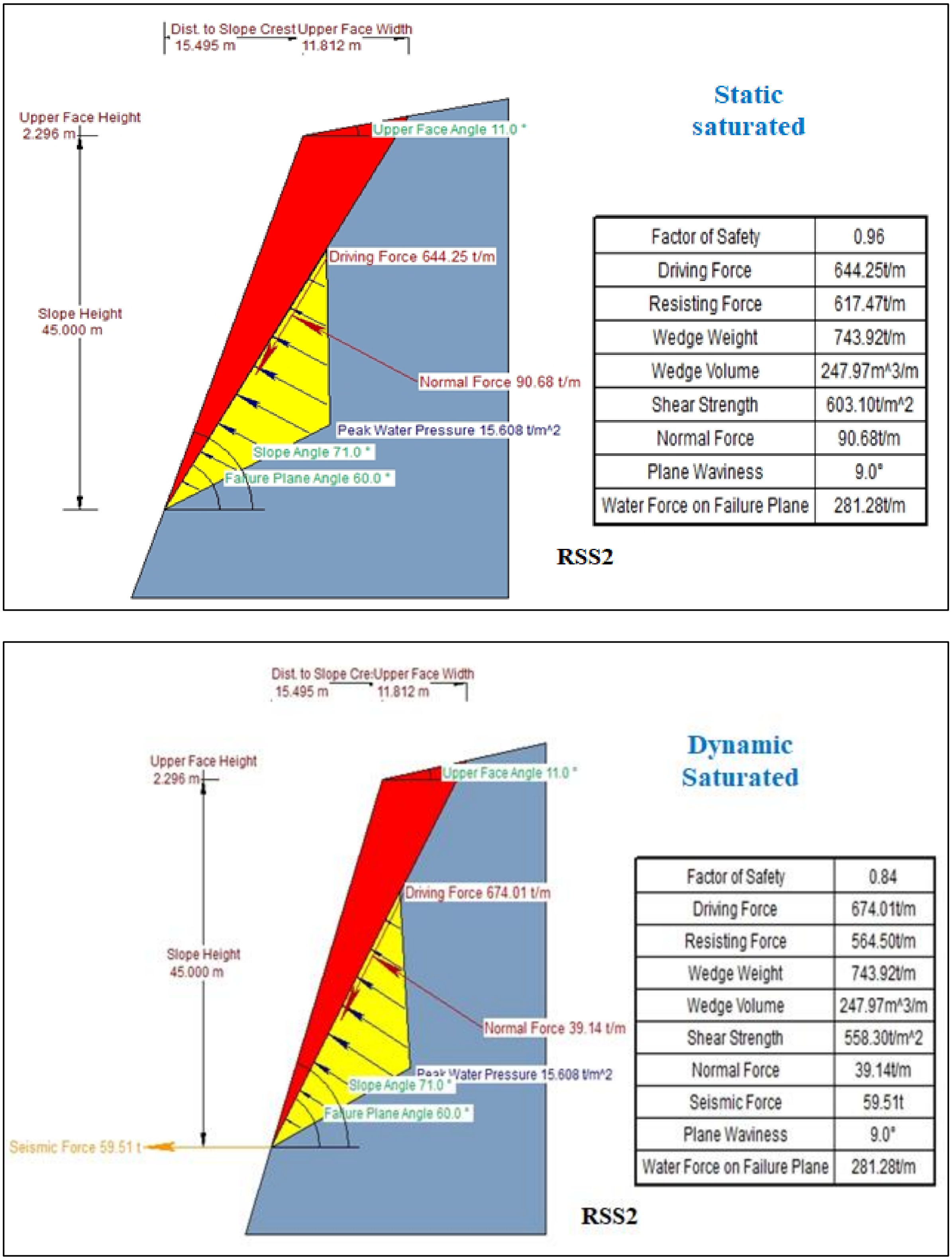

Figure5.7: Slope stability analysis of planar failure by Rocplane software on the rock slope section two (RSS2) and forces acting on failure plane JS1 under different conditions.

Static dry

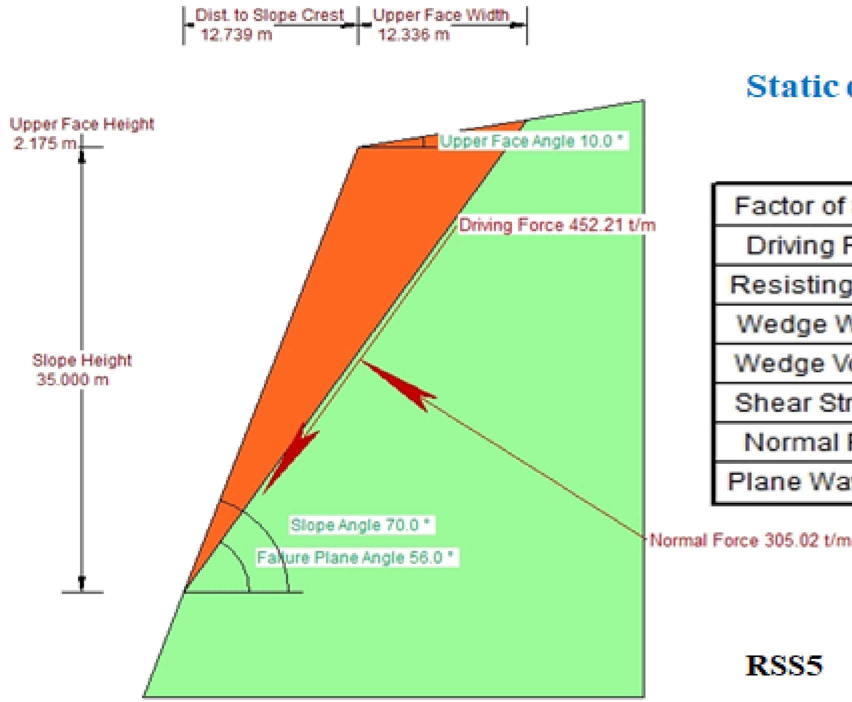

Factor of Safety	0.95
Driving Force	452.21t/m
Resisting Force	431.62t/m
Wedge Weight	545.47t/m
Wedge Volume	202.03m^3/m
Shear Strength	380.58t/m^2
Normal Force	305.02t/m
Plane Waviness	9.5°

RSS5

Factor of Safety	0.85
Driving Force	476.62t/m
Resisting Force	403.83t/m
Wedge Weight	545.47t/m
Wedge Volume	202.03m^3/m
Shear Strength	358.84t/m^2
Normal Force	268.85t/m
Seismic Force	43.64t
Plane Waviness	9.5°

Dynamic dry

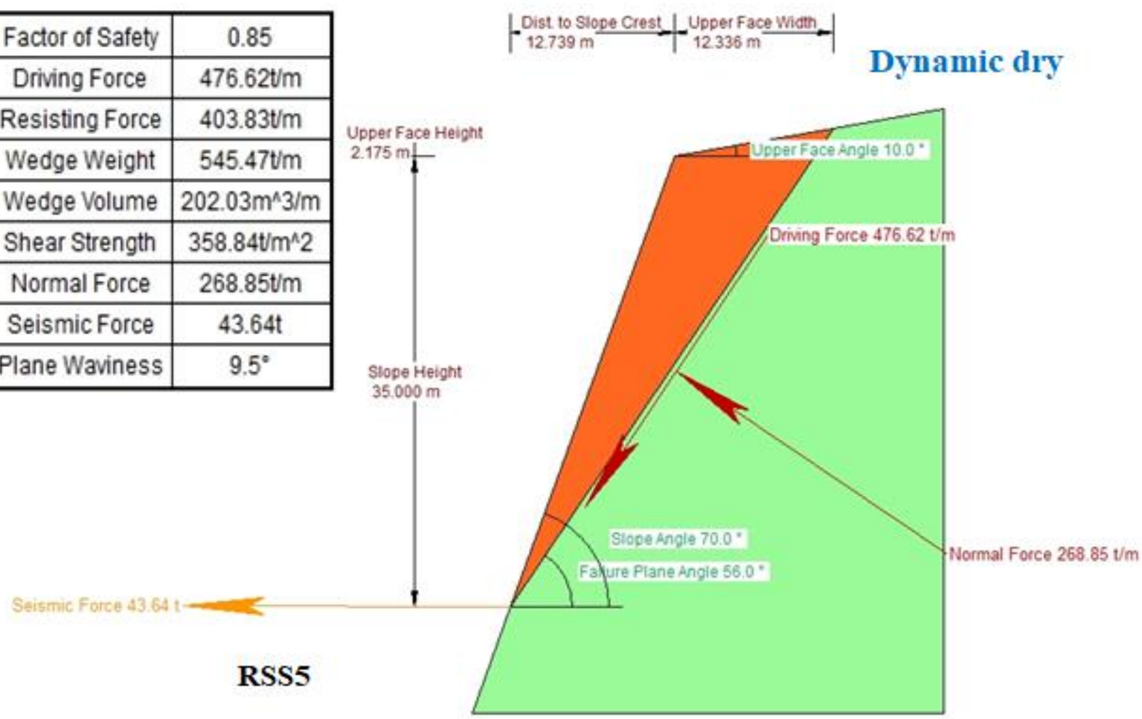

RSS5

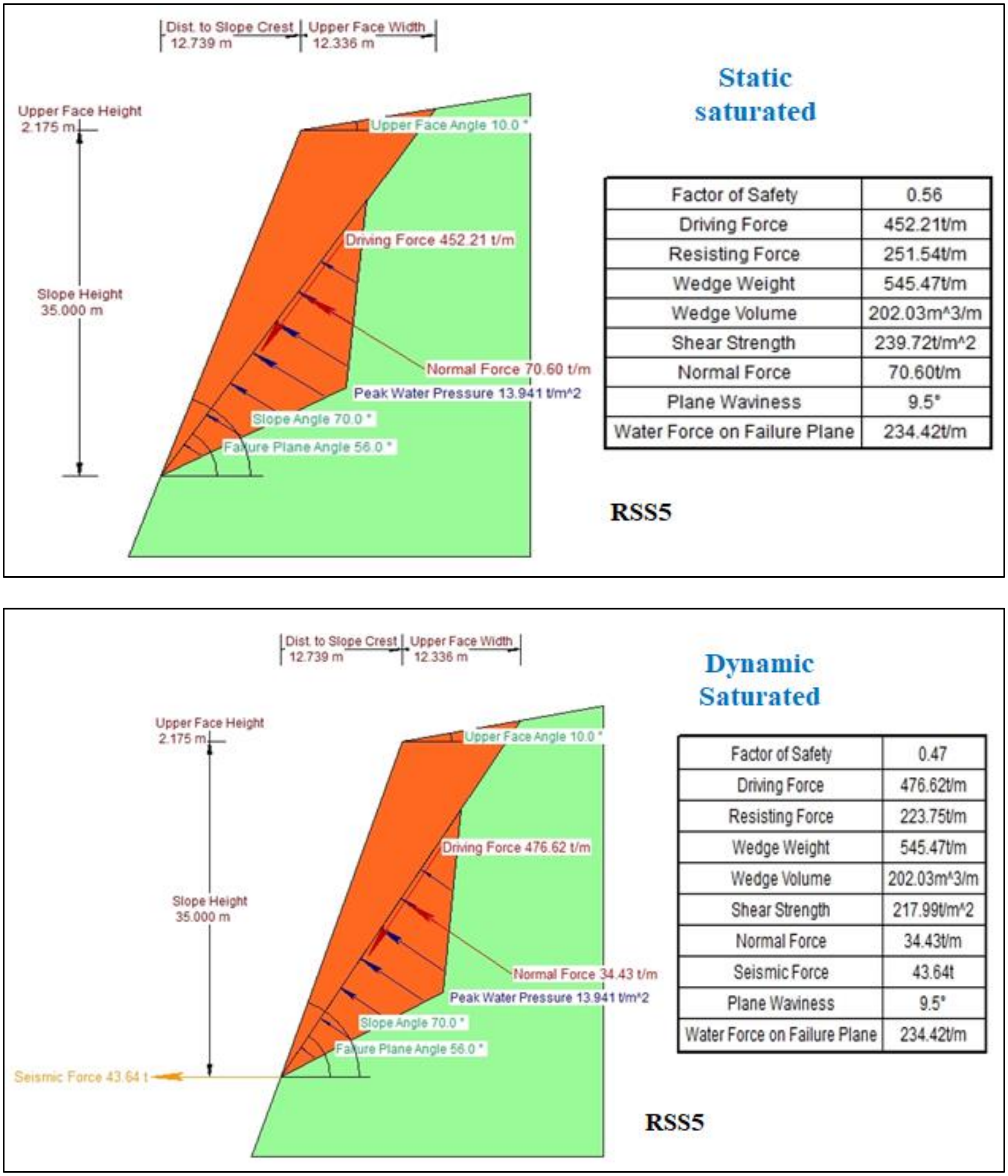

Figure5.8: Slope stability analysis of planar failure by Rocplane software on the rock slope section five (RSS5) and forces acting on failure plane JS1 at different conditions.

5.6.2.2. Sensitivity Analysis for Rock Planar Failures

According to the results of the sensitivity analysis for the planar mode of failure at slope section RSS2 due to joint sets JS1, slope angle has a greater effect on slope stability of slope rather than other parameters such as cohesion, unit weight, upper face angle, friction angle along the failure of the plane, slope angle, slope height and water percent filled as indicated the graph of factory of safety versus percent change (Fig.5.9a). However, the sensitivity analyses result for a planar mode of rock slope failure formed at slope section RSS5 due to joint set JS1 (Fig.5.9b) demonstrated that angle of failure plane has a greater impact on the stability of slope rather than other parameters such as friction angle along failure plane, water percent filled, failure plane angle, slope height and cohesion along failure plane as indicated on graph of factor of safety versus the percent change (Fig.5.9b).

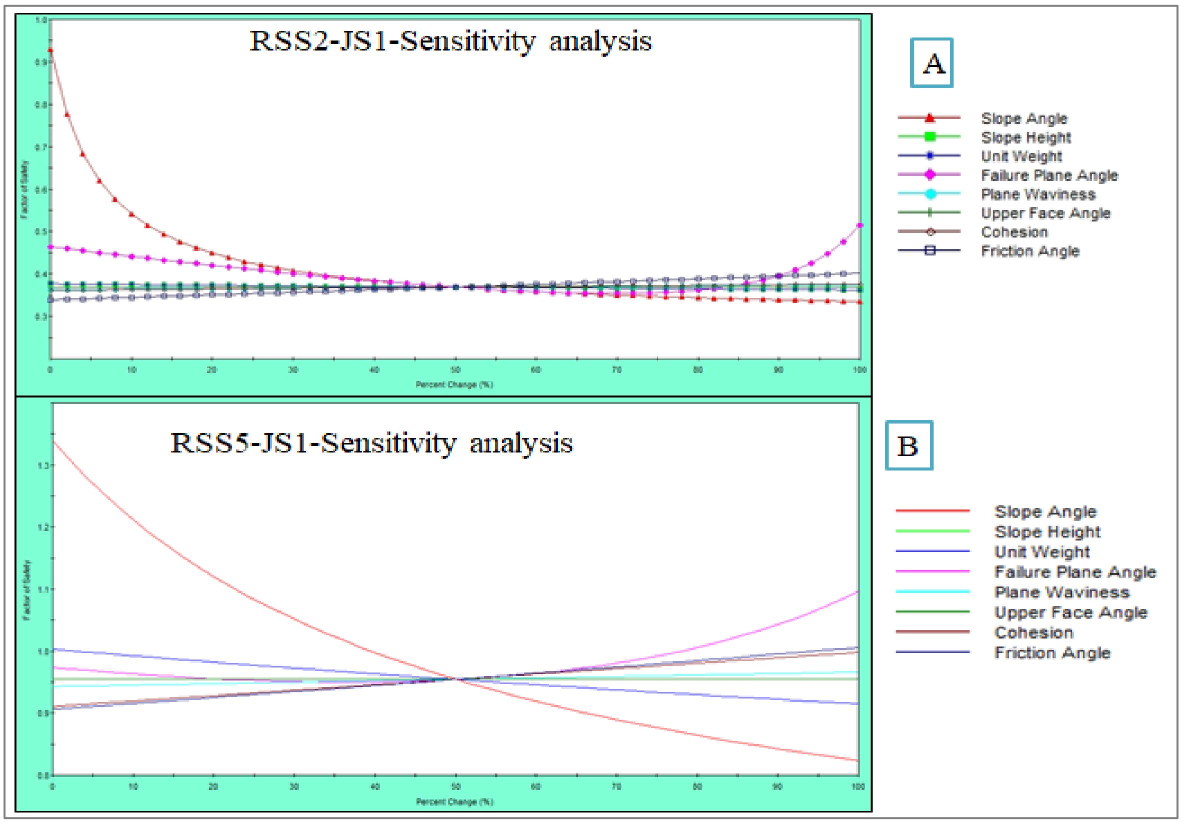

Figure5.9: Sensitivity analysis results of the rock planar failure at a) RSS2 and b) RSS5

5.6.2.3. Deterministic Analysis of Wedge Failures

Kinematic analysis of the intersection of the joint sets (JS1and JS3) and (JS2 and JS3) (Fig5.7a) indicates that the wedge failures occurred at rock slope section RSS1, according to graphical modeling. Similarly, kinematic analysis of the intersection of the joint sets (JS1and JS2) and (JS and JS3) (Fig5.6c) indicates that the wedge failures occurred at rock slope section RSS2. Based on kinematic analysis, Swedge software (Swedge 4.0 Rocscience, 2004) was used to evaluate the stability of rock slopes with wedge modes of failure, which uses deterministic method stability analysis (Budetta, 2020). The factor of safety (FOS) of the wedge mode of failure has been analyzed using Swedge software (Swedge4, Rocscience, 2004) for the critical rock slope section RSS1 and RSS2. The input parameters used to determine the factor of safety by Swedge software (Rocscience, 2004) were slope geometry, the discontinuity set orientation and the shear strength parameters of the discontinuity sets (cohesion and angle of internal friction) were evaluated by Rocdata software and unit weight of rocks was obtained from the laboratory tests. A summary of the input parameters for Swedge software to determine FOS at critical rock slope sections with wedge failure mode is presented below, in Table 5.22.

Table5.22: Input parameters used in Swedge software for wedge mode of failures

Slope section		Input parameter of Swedge software for determining factor of safety wedge failure										
		Joint sets orientation		Shear strength of joint sets.		Slope geometry				γw (t/m3)	γ (t/m 3)	α (g)
	Joint sets	Dip, (º)	D/D, (º)	C, (t/m2)	ϕ, (º)	D, (º)	D/D, (º)	USA, (º)	H(m)			
RSS1	JS1	80	260	5.5	41	71	230	10	38	1	25.7	0.08
	JS3	56	180	4.7	39.4					1		0.08
RSS2	JS1	60	255	9.6	44.5	85	250	11	45	1	30.4	0.08
	JS3	70	140	12	45.8					1		0.08

D/D = Dip direction, C = the cohesion, ϕ = friction angle, D = dip, USA= the Upper slope angle, γw = the unit weight of water, γ = the unit weight of rocks, H, = height of slope, α =the seismic coefficients, JS1 = the joint set one and JS2 = the Joint set two

In this study, the stability of rock slope RSS1 and RSS2 was analyzed using deterministic analysis by Swedge software (Rocscience, 2004) at their respective joint sets (JS1and JS3) to determine the factor of safety at different conditions. According to the analysis results, the factor of safety of rock for the potential failure plane at slope section RSS1 is 1.56 and 1.34 under static dry and dynamic dry conditions, respectively. Similarly, the factor of safety of rock slope section (RSS2) is 1.85 and 1.52 under static dry and dynamic dry conditions, respectively. This indicates that the rock slope section (RSS1 and RSS2) were stable for both static dry and dynamic dry conditions. However, both have a factor of safety less than one in static saturated and dynamic saturated conditions in the presence of seismic energy and water pressure in the rock joints which reduces the shear strength of the rock and increases the probability of rock slope failure. Generally, the factor of safety analysis results using Swedge software at RSS1 and RSS2 under different anticipated conditions and its stability were summarized in Table 5.23 as follows bellow.

Table5.23: The factor of safety and the slope stability at different conditions for wedge rock failure

Slope sections	Loading condition	Factor of safety	Stability condition
RSS1	Static dry	1.56	Stable
	Static saturated	0.99	Unstable
	Dynamic dry	1.34	Stable
	Dynamic saturated	0.91	Unstable
RSS2	Static dry	1.85	Stable
	Static saturated	0.52	Unstable
	Dynamic dry	1.52	Stable
	Dynamic saturated	0.49	Unstable

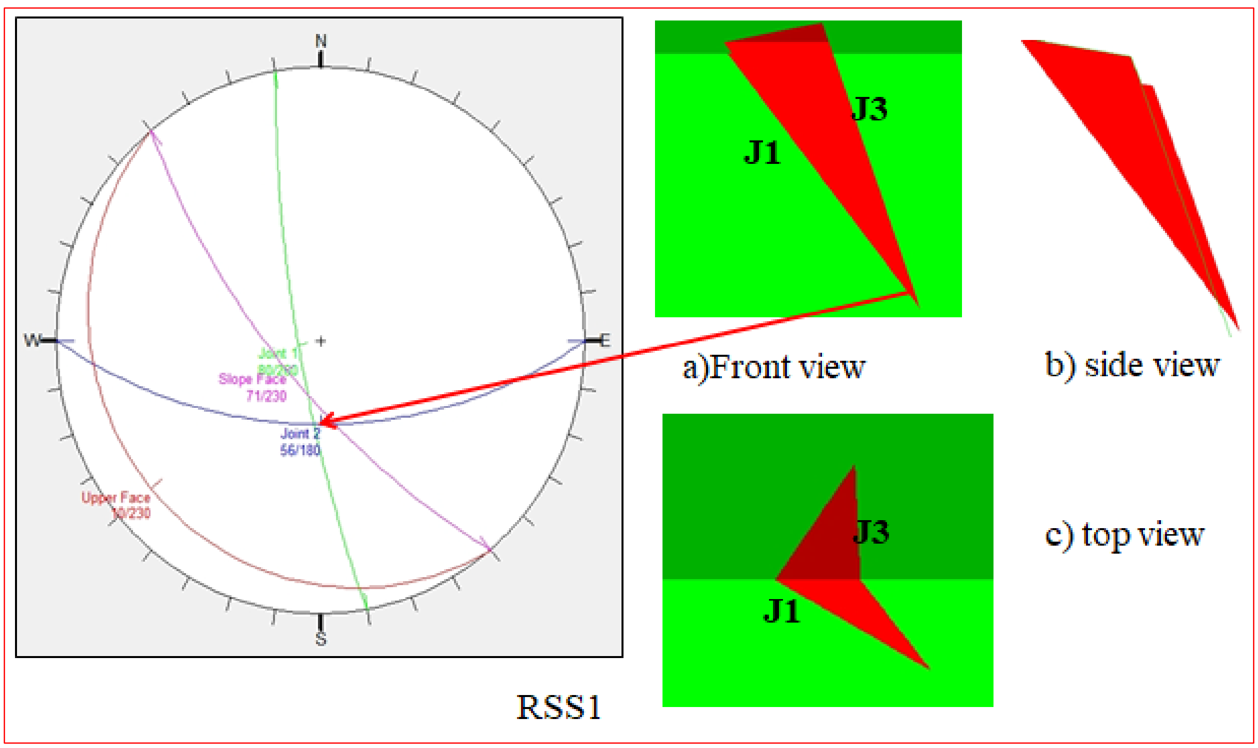

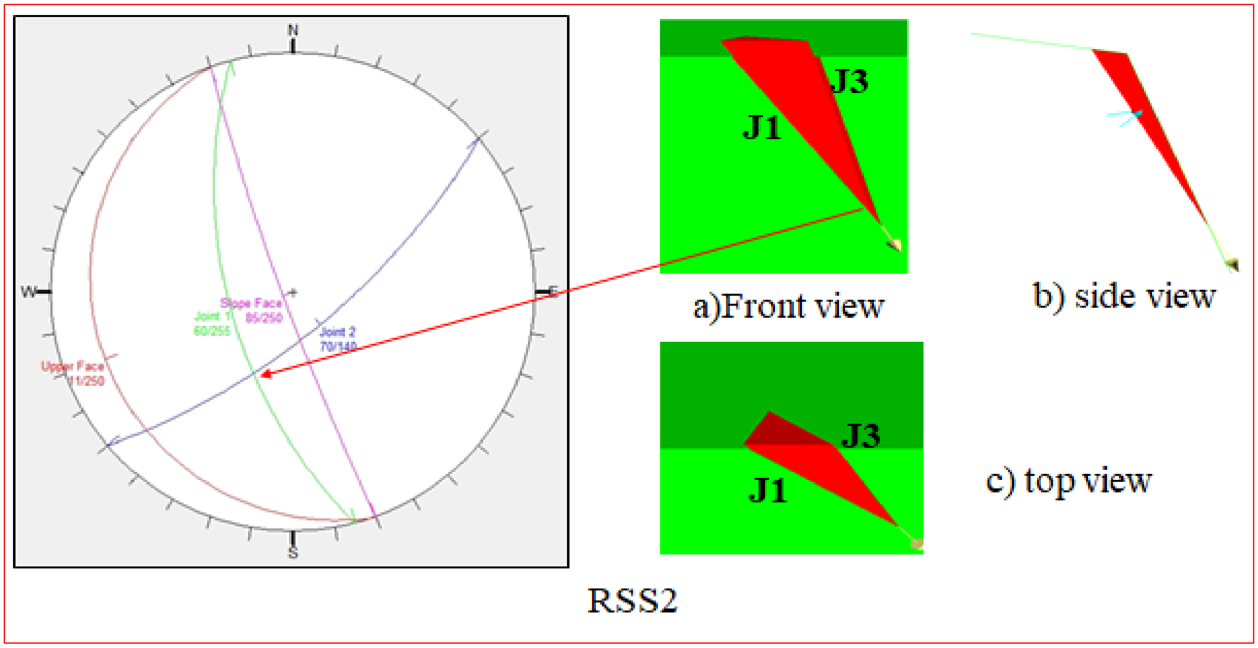

Figure5.10: Stereographic projection and Wedge failure at rock slope RSS1 and RSS2

5.6.3. Slope Stability Analysis of Rocks Using Limit Equilibrium Method

For this study slope stability analysis of the four critical slope sections was performed using the limit equilibrium approach in terms of Factor of Safety (FOS) by employing the General Limit Equilibrium (GLEM) or Morgenstern-Price method. The stability analysis of these four critical slope sections was evaluated by determining the factor of safety under various conditions. The analysis was done using slide 6 software (Rocscience, 2004) within the Mohr-Coulomb model. The input parameters used in this software are material properties such as cohesion, angle of internal friction, and unit weight of rocks. For this study shear strength parameters (cohesion and friction angle) of rock mass for the four critical selected slope sections were obtained from Hoek-Brown failure criteria using Rocdata3 software (Rocscience, 2004) see appendix I and the unit weight of rock was obtained from the laboratory tests which can be summarized in Table5.5. Furthermore, external loads such as horizontal seismic acceleration and groundwater conditions were taken into account during the stability analysis. The study area is found in a high seismic zone and the horizontal acceleration from seismic loading with a magnitude average (α) of 0.08g taken from EBCS 8 (1995) was used for dynamic dry and dynamic saturated conditions.

Table5.24: Input parameters for limit equilibrium slope stability analysis of rocks

Slope sections	Materials	Strength Model	Input parameter				Seismic horizontal acceleration (α) g
			Cohesion (Mpa)	friction angle, (°)	Unit weight (KN/m3)		
					γdry	γsat	
RSS3	HW.Basalt	Mohr-coulomb	0.181	49	27.1	27.3	0.08
RSS4	MW.Basalt		0.15	44	21.8	23.9	0.08
RSS6	HW.Basalt		0.155	45	25.7	27.1	0.08
RSS7	MW.Basalt		0.213	50	23.6	25.2	0.08
RSS = rock slope sections, MW = Moderately weathered basalt, SW = slightly weathered basalt and HW = highly weathered basalt							

The slope stability analysis factor of safety for non-structurally controlled four rock slope sections were determined using slide software through the Mohr-Coulomb model.

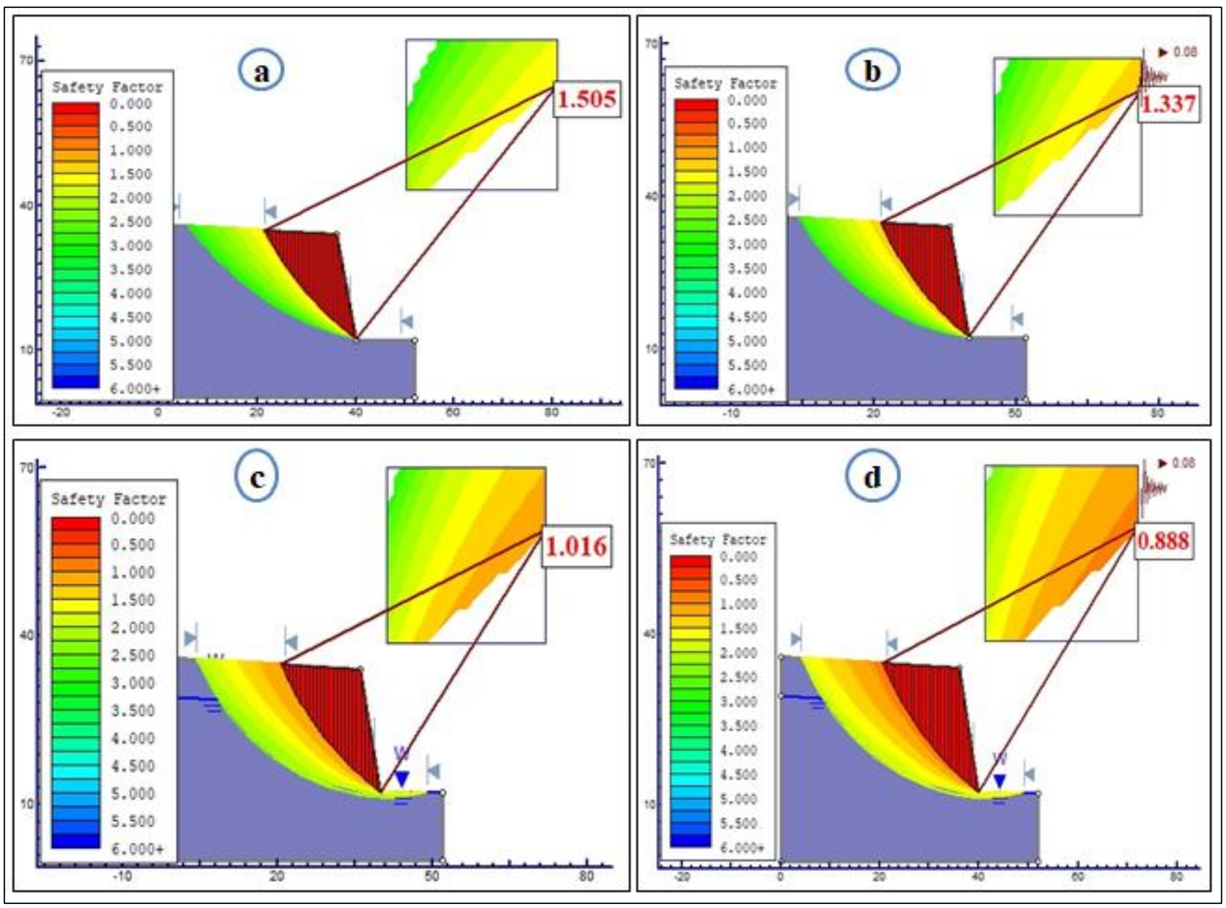

Figure5.11: Slope stability analysis results using Limit equilibrium method for rock slope section RSS3 under a) static dry condition, b) Dynamic dry condition, c) Static saturated condition and d) dynamic saturated conditions.

The minimum factor of safety and critical slip surface of the rock at critical slope section RSS3 is determined using the General limit equilibrium methods/spencer by considering various conditions as indicated in Figures 5.11. Accordingly, the analyses result at the critical rock slope section RSS3 revealed that the factor of safety under static dry condition is 1.505 as shown in (Figs.5.11a); while, under dynamic dry, static saturated and dynamic saturated conditions factor of safety is 1.337, 1.016 and 0.888 as shown in figs.5.11 (c), (b) and (d) respectively. This indicated that the rocks at critical slope section RSS3 was stable under static dry, dynamic dry, and static saturated; whereas, it was unstable under dynamic saturated conditions. In addition, a factor of safety analyzed under saturated slope conditions is relatively small compared to static dry slope conditions. This clearly shows the impact of groundwater on slope stability (Kabeta, et al., 2020).

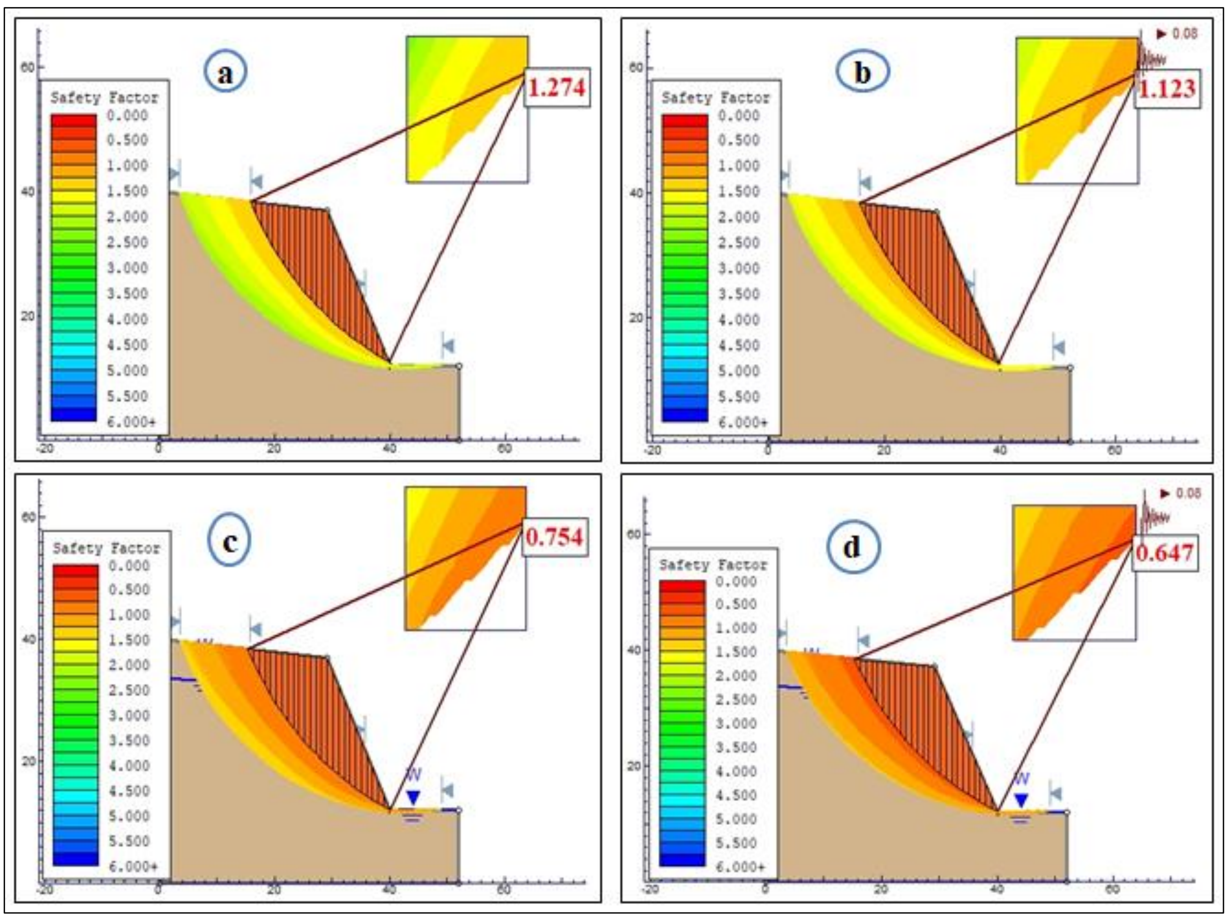

Figure5.12: Slope stability analysis result using Limit equilibrium method for rock slope section RSS4 under a) static dry condition, b) Dynamic dry condition, c) Static saturated condition and d) dynamic saturated conditions.

Based on the above analysis results, the minimum factor of safety and critical slip surface of the rock at critical slope section RSS4 is determined using the General limit equilibrium/spencer methods by considering various conditions as indicated in Figures 5.12. Accordingly, the analyses result at the critical rock slope section RSS4 revealed that the factor of safety under static dry and dynamic dry conditions is 1.274 and 1.123 as shown in Figs.5.12 (a) and (b) respectively. Similarly, the factory of safety under static saturated and dynamic saturated condition is 0.754 and 0.647 as shown in Figs.5.12 (c) and (d) respectively. This indicated that the rocks at critical slope section RSS4 was stable under static dry and dynamic dry condition; whereas, it was unstable under static and dynamic saturated conditions.. In addition, a factor of safety analyzed under saturated slope conditions is relatively small compared to dry slope conditions. This clearly shows the impact of groundwater on slope stability (Kabeta, et al., 2020).

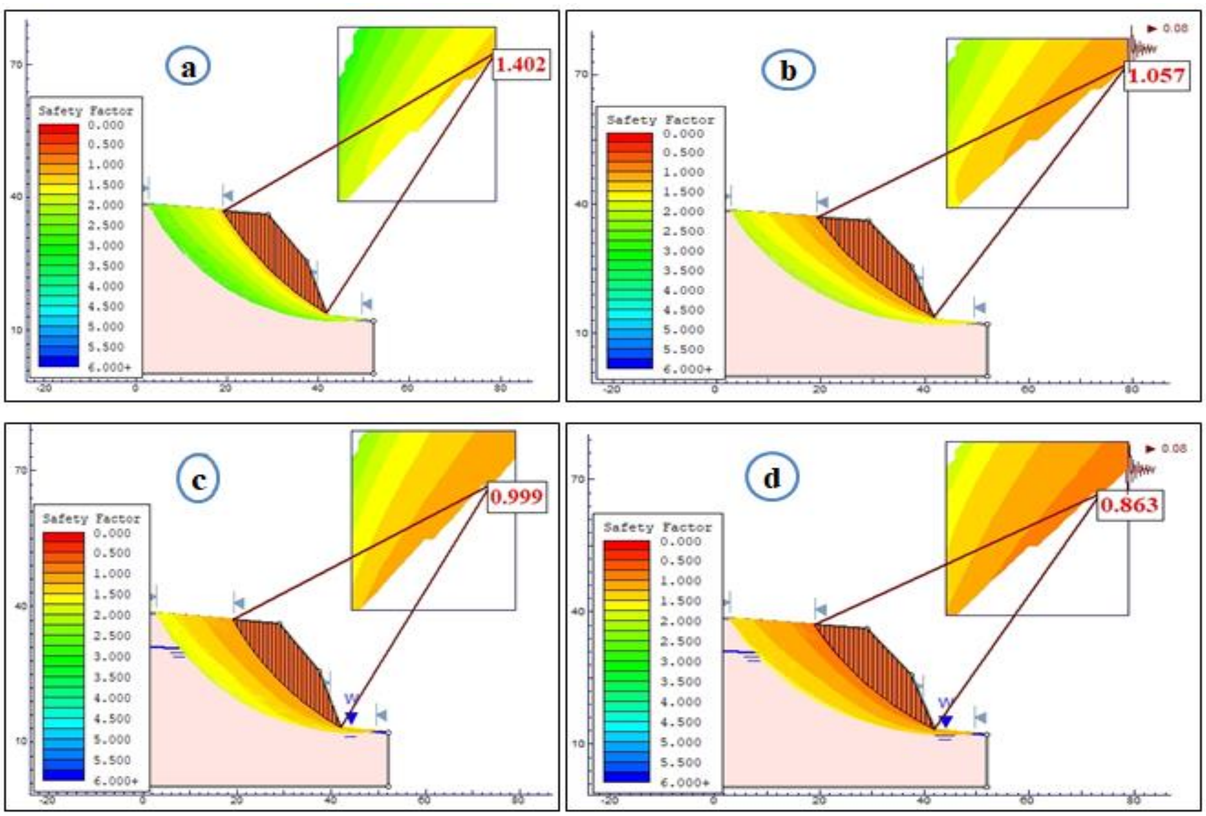

Figure5.13: Slope stability analysis result using Limit equilibrium method for rock slope section RSS6 under a) static dry condition, b) Dynamic dry condition, c) Static saturated condition and d) dynamic saturated conditions.

According to the above analysis results, the minimum factor of safety and critical slip surface of the rock at critical slope section RSS6 is determined using the General limit equilibrium/spencer methods by considering various conditions as indicated in Figures 5.13. Accordingly, the analyses result at the critical rock slope section RSS6 revealed that the factor of safety under static dry and dynamic dry condition is 1.402 and 1.057 as shown in Figs.5.13 (a) and (b); while, under static saturated and dynamic saturated conditions factor of safety is 0.999 and 0.863 as shown in Figs.5.13 (c) and (d) respectively. This indicated that the rocks at critical slope section RSS6 was stable under static dry and dynamic dry condition; whereas, it was unstable under static saturated and dynamic saturated conditions.

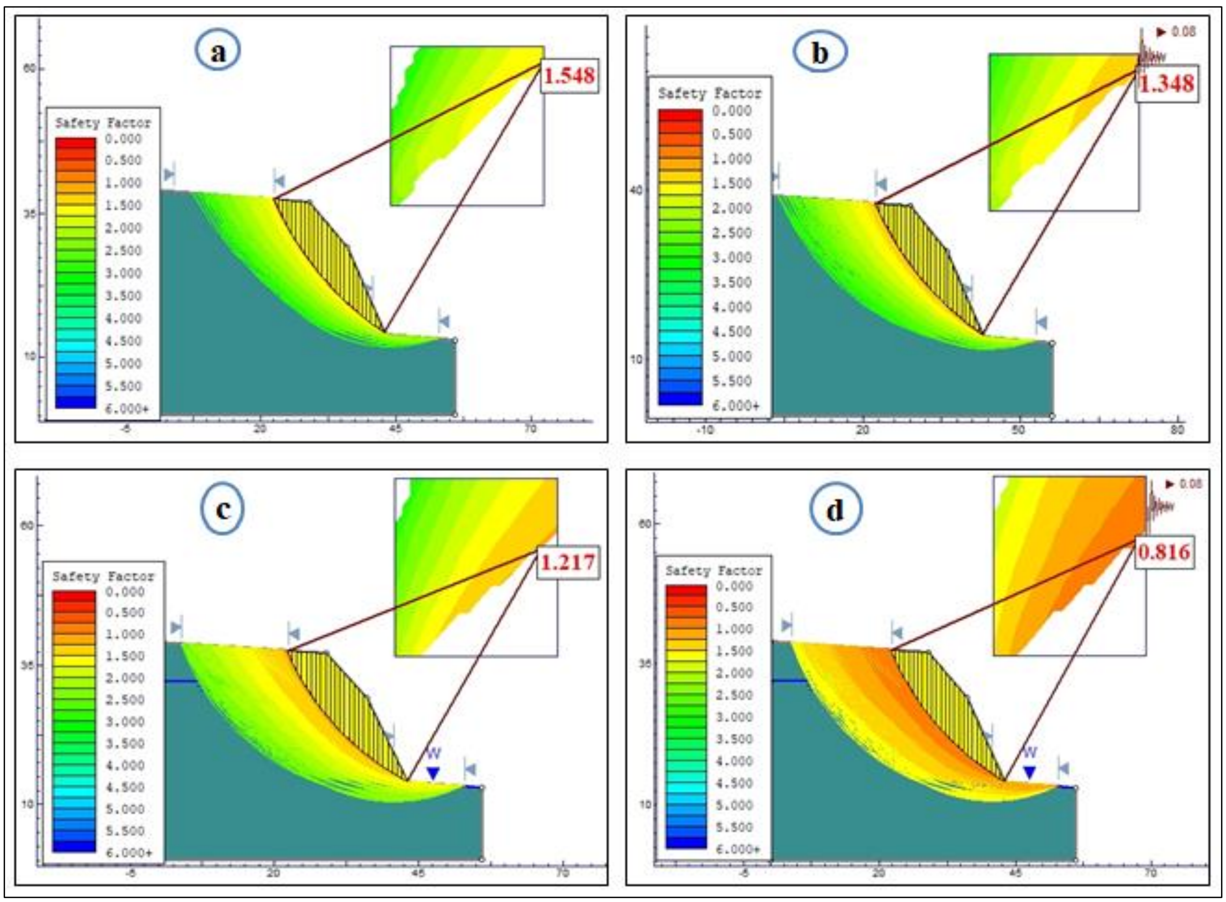

Figure5.14: Slope stability analysis result using Limit equilibrium method for rock slope section RSS7 under a) static dry condition, b) Dynamic dry condition, c) Static saturated condition and d) dynamic saturated conditions.

According to the above analysis results, the factory of safety for rock slope section RSS7 using limit equilibrium analysis is 1.548, 1.348 and 1.217 under static dry, dynamic dry and static saturated conditions respectively, as illustrated in Figs 5.14 (a), (b) and (c) respectively. This demonstrates that under the three conditions the rock at critical slope section RSS7 is stable as the result of the factor of safety greater one (Christian, 2004; Shariati and Fereidooni, 2021). However, the factor of safety that was determined under dynamic saturated condition is 0.816 as shown in Fig.5.14 (d). This implies that the rock slope section RSS7 is unstable under dynamic saturated conditions. From dynamic dry to dynamic saturated conditions the effect of seismic activity on slope stability shows significant variation. In addition, when the static dry condition is compared with the static saturated condition, the factor of safety is very low for rock slope section RSS7 (Fig.5.14). This implies the effect of groundwater on slope stability is very high (Kabeta, et al., 2020).The summary of factors of safety evaluated using the general limit equilibrium/spencer method under static dry, static saturated, dynamic dry and dynamic saturated conditions of four rock slope section are shown in Table 5.25.

Table5.25: Summary of the minimum factor of safety and slope status for each slope sections

Slope sections	Method	Loading condition	Factor of safety (FOS)	Slope stability condition
RSS3	GLEM/ Spencer	Static dry	1.505	Stable
		Static saturated	1.016	Stable
		Dynamic dry	1.337	Stable
		Dynamic saturated	0.888	Unstable
RSS4	GLEM/ Spencer	Static dry	1.274	Stable
		Static saturated	0.754	Unstable
		Dynamic dry	1.123	Stable
		Dynamic saturated	0.647	Unstable
RSS6	GLEM/ Spencer	Static dry	1.402	Stable
		Static saturated	0.999	Unstable
		Dynamic dry	1.057	Stable
		Dynamic saturated	0.863	Unstable
RSS7	GLEM/ Spencer	Static dry	1.548	Stable
		Static saturated	1.217	Stable
		Dynamic dry	1.348	Stable
		Dynamic saturated	0.816	Unstable
	GLEM = General Limit Equilibrium method			

5.6.4. Rock Slope Stability Analysis Using Finite Element Method

For this study, the rock slope stability analysis of critical selected slope sections was performed by the finite element method. The finite element analysis was performed using the Phase2 software (Rocscience, 2004) and the slope stability condition can be express in the term of the Strength Reduction factor (SRF) value. The critical shear strength reduction factor (SRF) which is equivalent to the factor of safety (FOS) was calculated using a finite-element-based numerical simulation in the Phase2 software program (Aswathi, et al., 2017). For this study the critical rock selected slope section the factory of safety was estimated by limit equilibrium and finite element methods using the same material properties, slope angle, slope geometry and boundary condition. In addition, the input parameters utilized in this method are the same with that used in the limit equilibrium method, the exception of Young's modulus (Erm), Poisson's ratio (v) and dilatancy angle of the rocks. In this study, the Young's modulus (Erm) of rock mass was calculated using Rocdata software according to Hoek (2006), and the Poisson ratio (v) of rock slope materials was determined based on appropriate literature (Balazs, 2009). Finite element slope stability analysis was performed in this study in order to determine the critical strength reduction factor or FOS of the rock slope's static dry condition, static saturated condition, dynamic dry condition, and dynamic saturated condition. The input parameters used in stability analysis using finite element method (FEM) was presented in Table 5.26 below.

Table5.26: Input parameters for finite element stability analysis to compute critical strength reduction factor.

Slope section	Materials	Strength Model	C (Mpa)	ϕ,(º)	Erm (Mpa)	Ψ(º)	Unit weight (KN/m3)		V	α (g)
							γdry	γsat		
RSS3	HW.Basalt	Mohr-coulomb	0.181	49	1786.44	6.13	27.1	27.3	0.318	0.08
RSS4	MW.Basalt		0.15	44	2134.36	5.5	21.8	23.9	0.291	0.08
RSS6	HW.Basalt		0.155	45	1466.9	5.6	25.7	27.1	0.313	0.08
RSS7	MW.basalt		0.213	50	2700.3	6.3	23.6	25.2	0.293	0.08

RSS = Rock slope section, C = cohesion, ϕ = angle of internal friction, Erm= deformation modulus, γ = Unit weight of rocks, V = Poisson ratio and α = seismic horizontal acceleration, Ψ = Dilatancy angle of rocks, MW = moderately weathered, SW =Slightly weathered, Hw = highly weathered lower basalts.

Stability analysis of non-structurally controlled four critical rock slope sections on critical strength reduction factor (SRF) was determined using phase2 software through the Mohr-Coulomb model as shown below.

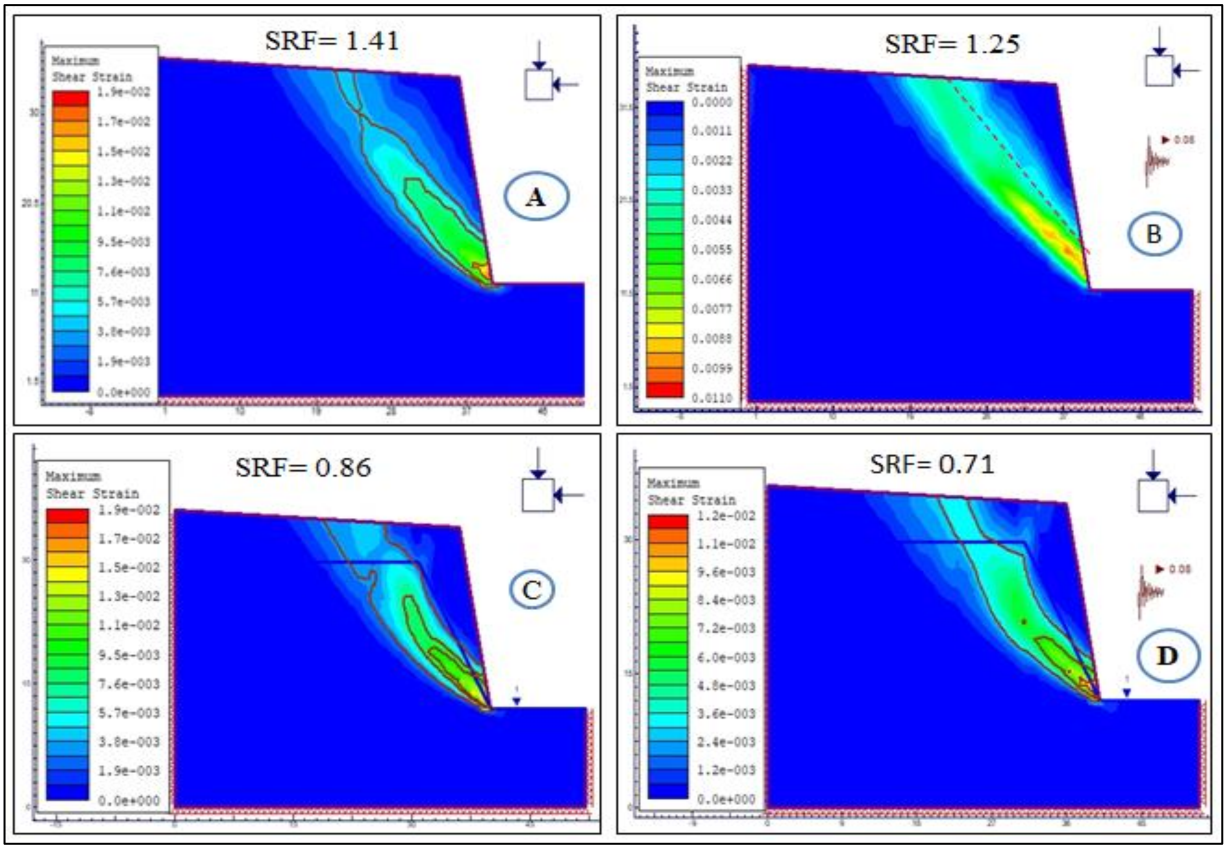

Figure5.15: Slope stability analysis finite element method for rock slope section RSS3 under a) static dry, b) Dynamic dry, c) Static saturated and d) dynamic saturated conditions.

According to the analysis results, the strength reduction factor of the rock slope section RSS3 is 1.41 and 1.25 under static dry and dynamic dry conditions as shown in Figs.5.15 (a) and (b) respectively. This demonstrates that in both static and dynamic dry conditions the rock at critical slope section RSS3 is stable as the result of the factor of safety greater one (Christian, 2004; Shariati and Fereidooni, 2021). However, the strength reduction factor of rock slope section (RSS3) was 0.86 under static saturated conditions and 0.71 under dynamic saturated conditions as shown in Figs.5.15 (c) and (d), respectively. The results showed that the critical SRF or FOS for static saturated and dynamic saturated conditions is less than one, indicating that the slope is unstable (Chirstian, 2004; Shariati and Fereidooni, 2021). Furthermore, when we compare the result of the strength reduction factor under different anticipated conditions for this slope section, the strength reduction was decreased by 11.34 % when we move from static dry to dynamic dry, by 39% from static dry to static saturated and by 49.64% from static dry to dynamic saturated condition. This demonstrates that pore water pressure has a greater degree of influence on destabilizing these slope sections than seismic activity (Kabeta, et al., 2020).

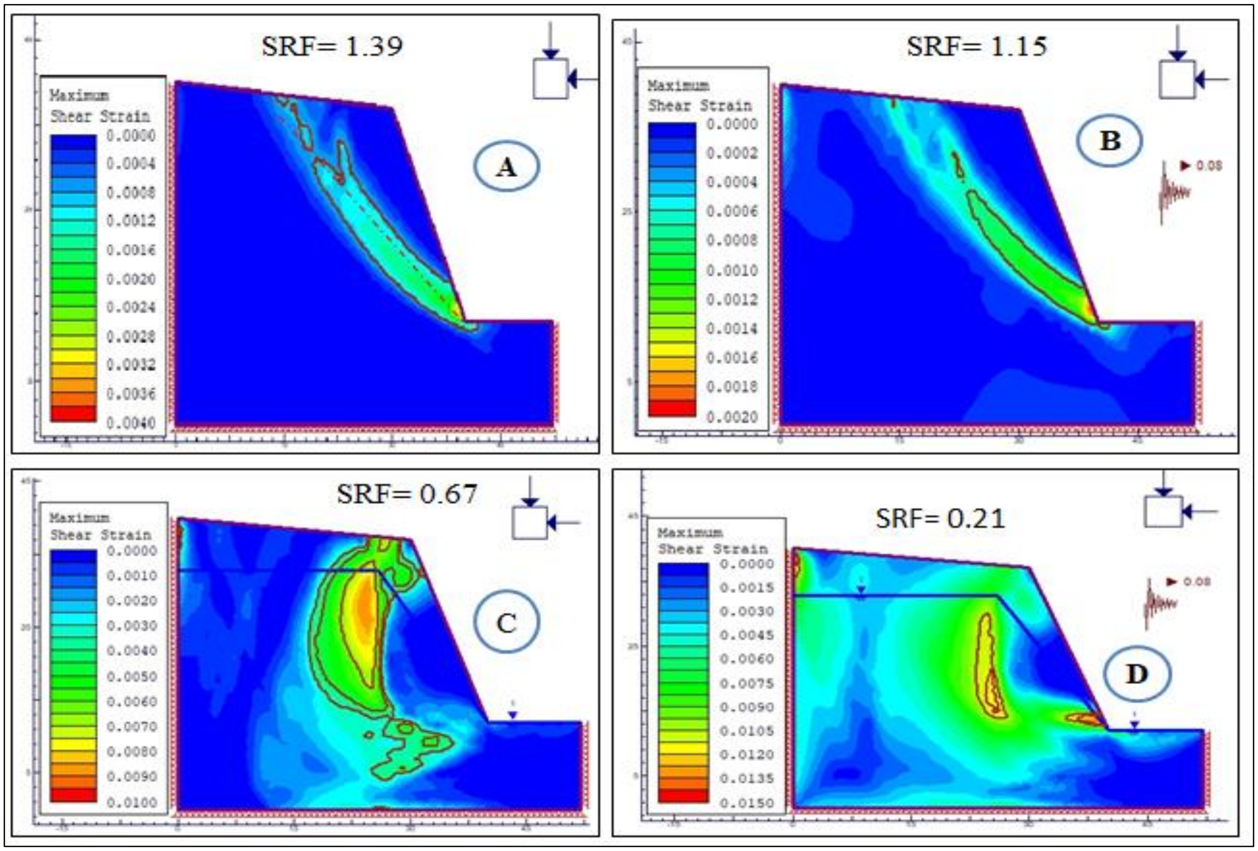

Figure5.16: Slope stability analysis finite element method for rock slope section RSS4 under a) static dry, b) Dynamic dry, c) Static saturated and d) dynamic saturated conditions.

According to the analysis results, the strength reduction factor of the rock slope section RSS4 is 1.39 and 1.15 under static dry and dynamic dry conditions as shown in Figs.5.16 (a) and (b) respectively. There is a possibility that the slope may fall under influence of triggering events such as excessive rain and seismic activity. This demonstrates that in both static and dynamic dry conditions the rock at critical slope section RSS4 is stable as the result of the factor of safety greater one (Christian, 2004; Shariati and Fereidooni, 2021). However, the strength reduction factor of rock slope section (RSS4) is 0.67 under static saturated conditions and 0.21 under dynamic saturated conditions as shown in Figs.5.16 (c) and (d), respectively. The results showed that the critical SRF or FOS for static saturated and dynamic saturated conditions is less than one, indicating that the slope is unstable (Chirstian, 2004; Shariati and Fereidooni, 2021). The results indicated that pore water pressure plays a greater role in destabilizing slope sections than horizontal seismic acceleration. Furthermore, when we compare the result of the strength reduction factor under different anticipated conditions for this slope section, the strength reduction was decreased by 17.26 % when we move from static dry to dynamic dry, by 51.79% from static dry to static saturated and by 84.89% from static dry to dynamic saturated condition.

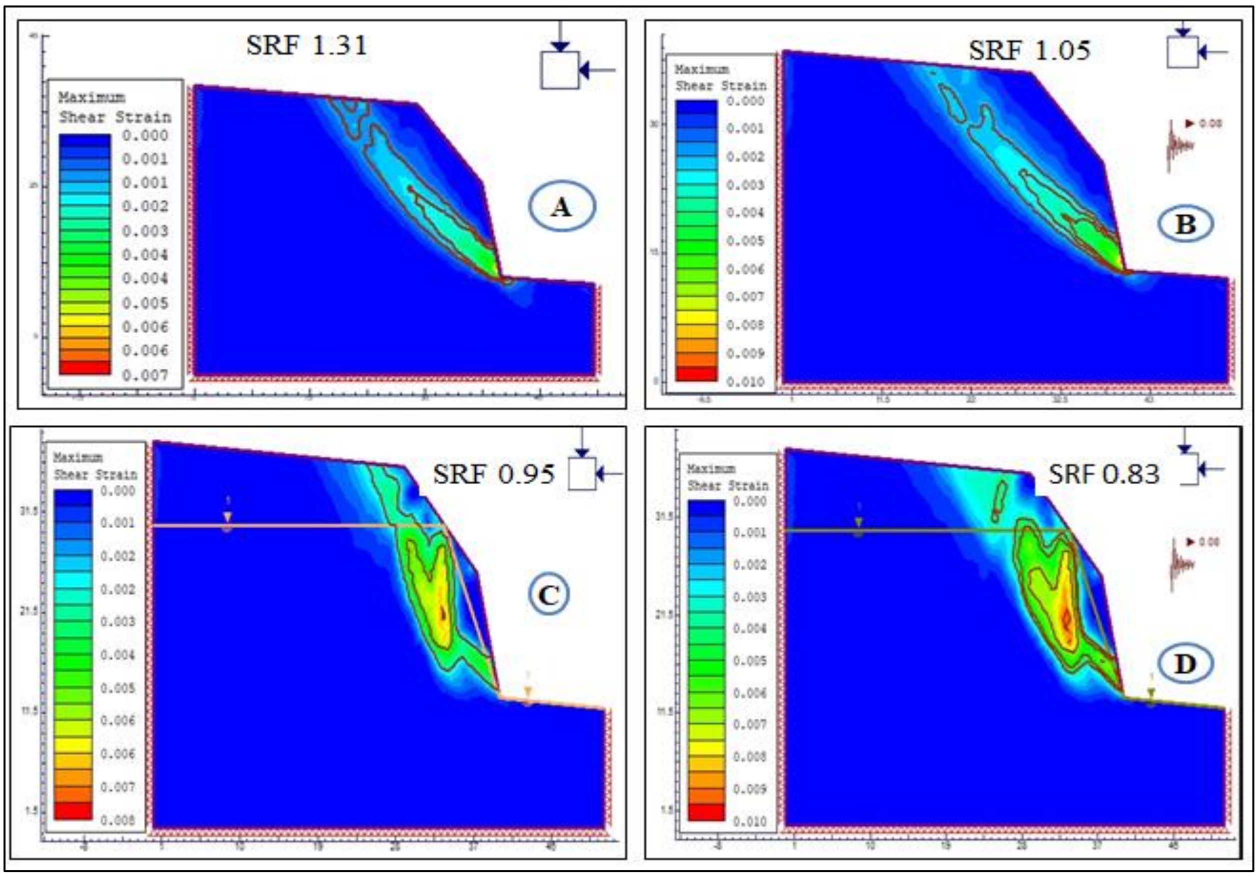

Figure5.17: Slope stability analysis finite element method for rock slope section RSS6 under a) static dry, b) Dynamic dry, c) Static saturated and d) dynamic saturated conditions.

The minimum factor of safety or strength reduction factor determined from FEM analysis of the rock slope section RSS6 is 1.31 and 1.05 for static dry and dynamic dry conditions respectively as shown in Figs. 5.17 (a) and (b) respectively. The critical SRF or FOS results for the slope at static dry and dynamic dry conditions is greater than one indicating that the slope is stable. However, the strength reduction factor of rock slope section (RSS6) is 0.95 under static saturated conditions and 0.83 under dynamic saturated conditions as shown in

Figs.5.17 (c) and (d), respectively. The results showed that the critical SRF or FOS for static saturated and dynamic saturated conditions is less than one, indicating that the slope is unstable (Chirstian, 2004; Shariati and Fereidooni, 2021). When we compare the results of the strength reduction factor under different conditions, it is decreased by 19.84% when we move from static dry to dynamic dry, by 27.48% from static dry to static saturated and by 36.64% from static dry to dynamic saturated conditions. This demonstrates that pore water pressure has a greater degree of influence on destabilizing these slope sections than seismic activity (Kabeta, et al., 2020). The results indicated that pore water pressure plays a greater role in destabilizing slope sections than horizontal seismic acceleration.

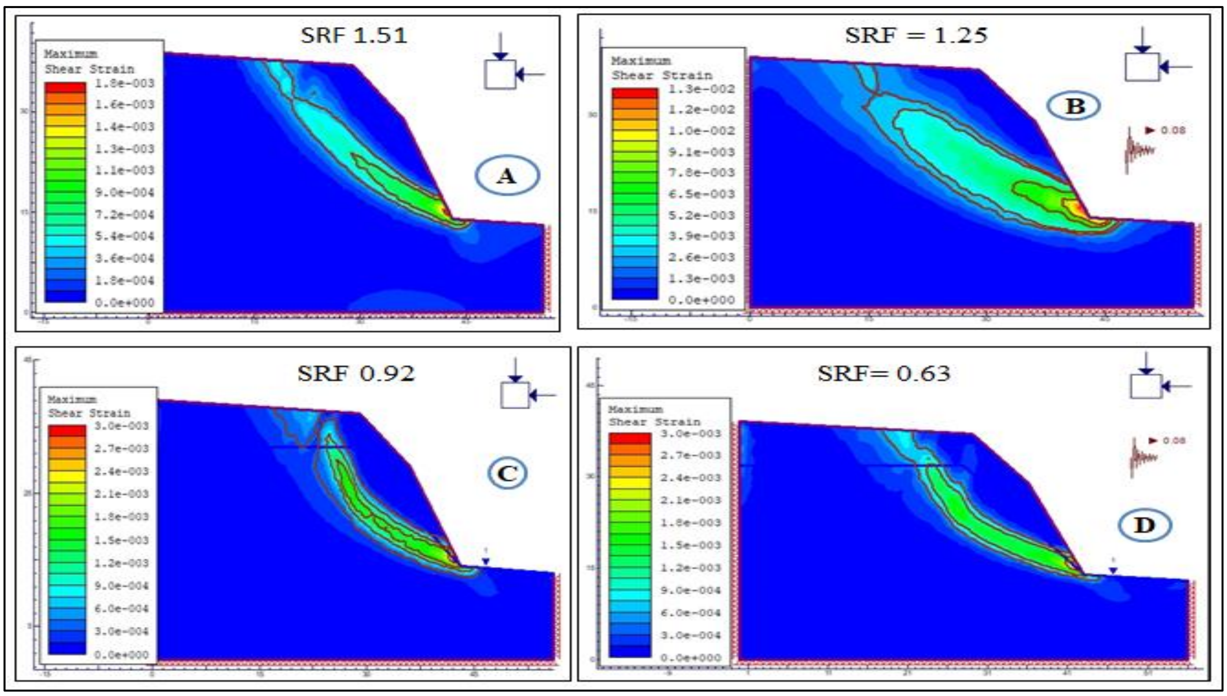

Figure5. 18: Slope stability analysis finite element method for rock slope section RSS7 under a) static dry, b) Dynamic dry, c) Static saturated and d) dynamic saturated conditions.

According to the analysis results above, the minimum factor of safety or strength reduction factor determined from FEM analysis of the rock slope section RSS7 is 1.51 and 1.25 for static dry and dynamic dry conditions, respectively as shown in Figs. 5.18 (a) and (b). The critical SRF or FOS results for the slope at static dry and dynamic dry conditions is greater than one indicating that the slope is stable. In addition, the analyses results showed that the critical SRF of RSS7 is 0.92 and 0.63 during static saturated and dynamic saturated conditions, respectively as shown in Figs.5.18 (c) and (d). The results showed that the SRF or FOS for static saturated and dynamic saturated conditions is less than one, indicating that the rock slope section RSS7 is unstable under static and dynamic saturated conditions (Chirstian, 2004; Shariati and Fereidooni, 2021). When we compare the results of the strength reduction factor under different conditions, it is decreased by 17.22% when we move from static dry to dynamic dry, by 39% from static dry to static saturated and by 49.6% from dynamic dry to dynamic saturated conditions. This indicated that the effect of pore water pressure plays a greater role in destabilizing these slope sections as compared to horizontal seismic acceleration. The effect of horizontal seismic acceleration on the factor of safety is very small. The summary of the strength reduction factor (SRF) analyzed using FEM under static dry, static saturated, dynamic dry and dynamic saturated of four rock slope conditions was presented in Table 5.27 below

Table5.27: Critical SRF and slope stability under different conditions of rock slope sections

Slope sections	Method	Loading condition	Factor of safety (FOS)	Slope stability condition
RSS3	Strength Reduction method	Static dry	1.41	Stable
		Static saturated	0.86	Unstable
		Dynamic dry	1.25	Stable
		Dynamic saturated	0.71	Unstable
RSS4	Strength Reduction method	Static dry	1.39	Stable
		Static saturated	0.67	Unstable
		Dynamic dry	1.15	Stable
		Dynamic saturated	0.21	Unstable
RSS6	Strength Reduction method	Static dry	1.31	Stable
		Static saturated	0.95	Unstable
		Dynamic dry	1.05	Stable
		Dynamic saturated	0.83	Unstable
RSS7	Strength Reduction method	Static dry	1.51	Stable
		Static saturated	0.92	Unstable
		Dynamic dry	1.25	Stable
		Dynamic saturated	0.63	Unstable

5.7. Slope Stability Analysis of Soils

For this study, the factory of safety for the two soil slope sections were estimated under limit equilibrium and finite element methods using the same material properties, slope angle, and slope geometry. The analysis was carried out to identify whether the slope is stable or unstable. The factor of safety (FOS) was analyzed and interpreted using the limit equilibrium and finite element methods for failure surface in soil slope under static dry, static saturated, dynamic dry and dynamic saturated conditions.

5.7.1 Slope Stability Analysis of Soils Using Limit Equilibrium Method

Slope stability analyses of two soil slope sections were conducted using the general limit equilibrium (GLE) or Morgenstern-Price method. In slope stability analysis using General Limit Equilibrium (GLE) or Morgenstern-Price method determining the critical potential slip surface is an essential measure on obtaining a minimum factor of safety in each slope section utilizing slide software (Abramson et al., 2002; Singh et al., 2016). In addition, in the Rocscience Slide software, the general limit equilibrium approaches satisfy all the equilibrium conditions (Ferdlund et al., 1981). Soil slope portion SS1 has approximately 26 meters of height, 55 meters of length, and approaches the road at nearly a 60-degree angle. Similarly, the soil slope section SS2 has approximately 28 m height and nearly dips at 40 degrees towards to the road. Both soil slope sections have a circular mode of failure as identified in the field. The critical soil slope sections SS1 and SS2 were composed of homogeneous material as determined by field observations based on physical characteristics and laboratory analysis such as grain size and Atterberg limit test results. According to the results of the laboratory test of the soil slope section the SS1 is silty sand and SS2 is clayey sand. It shows that the soil slope section composed sand soil. The determination of slope geometry, shear strength parameters (angle of internal friction and cohesion) and soil unit weight is very important, because they are the input parameters of soil slope stability analysis. The internal friction angle, cohesion, and unit weight of soils of slopes SS1 and SS2 are determined from laboratory test and summarized in Table 5.27. In this study, the General Limit Equilibrium Methods (GLE M) was used to determine the factor of safety for two different slope sections with varying geometry and material properties under static dry, static saturated, dynamic dry and dynamic saturated slope conditions. The summary of input parameters for the two selected soil slope sections is shown in (Table 5.28).

Table5.28: The input parameter for soil slope stability analysis

Slope section	material	Unit weight (KN/m3)		Cohesions (KN/m2)	Angle of internal friction (degree)
		γdry	γsat		
SS1	Well graded sand	8.9	11.3	30.4	29.56
SS2	Well graded sand	12	13.5	32.41	21.57
SS = soil slope section, γdry = dry unit weight and γsat = saturated unit weight of soils.					

For this study during analysis using the above input parameters in Table5.27 presented the factor of safety (FOS), and slip surface was determined and interpreted for static dry, static saturated, dynamic dry and dynamic saturated conditions using General limit equilibrium or Morgensternprice methods of LEM. The safety factor evaluation was performed under static dry conditions, representing the stability status without considering the effect of earthquake load and presumed to be dry during the dry season in the study area. In addition, the safety factor evaluation was performed under dynamic saturated conditions, which means the slope was subjected to seismic horizontal acceleration (α=0.08g) of the study area and presumed to be saturated during heavy rainfall in the study area (Lamessa and Meten, 2021).

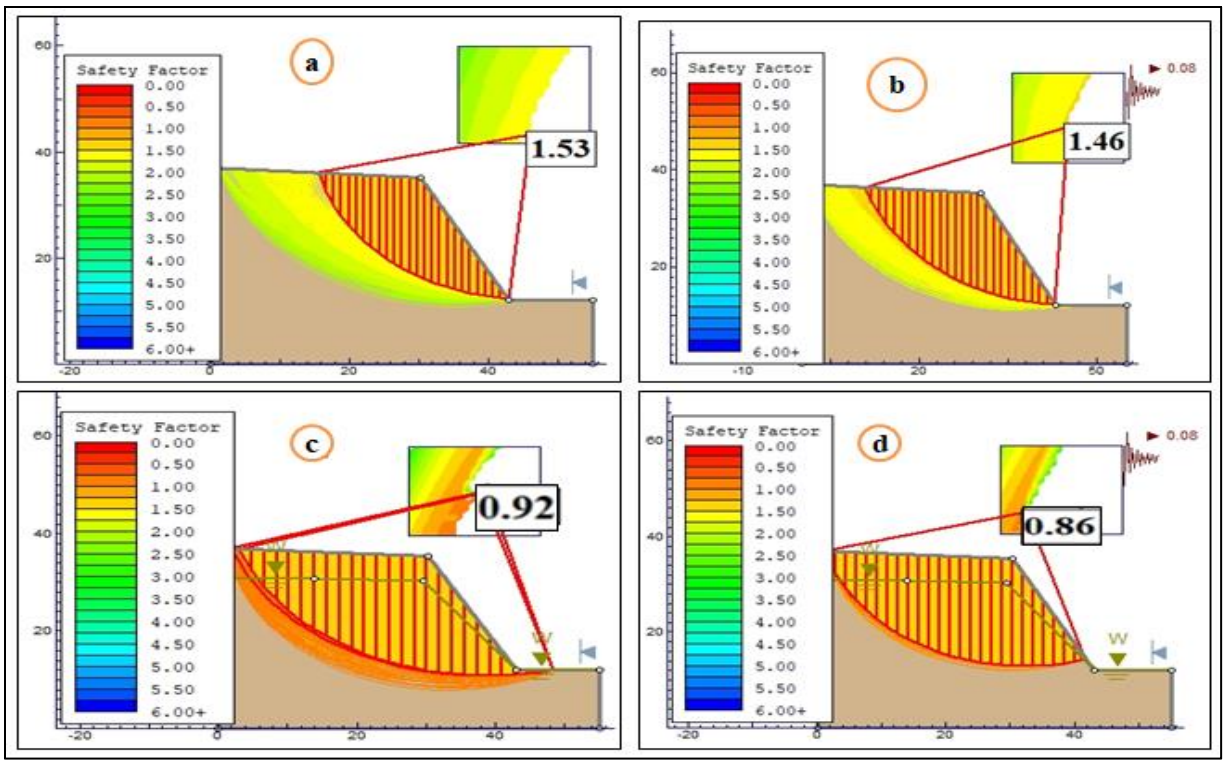

Figure5.19: Slope stability analysis by Limit equilibrium method for soil slope section SS1 at a) static dry, b) dynamic dry, c) static saturated and d) dynamic saturated conditions

The above analysis indicates that in static and dynamic dry conditions, slope section SS1 has a factor of safety of 1.53 and 1.46, respectively (Fig.5.19a and b). The results showed that the soil slope section SS1 is stable under static and dynamic dry conditions. However, the factor of safety that was determined under static saturated and dynamic saturated conditions of the SS1 is 0.92 and 0.86 respectively as shown on (Fig.5.19c and d). This indicates to the unstable slope section under static saturated and dynamic saturated condition. This was due to the ground water can affect slope stability by increasing pore water pressure, by increasing weight on a slope when the soil mass is fully saturated, decreasing effective stress and result in loss of shear strength parameter.

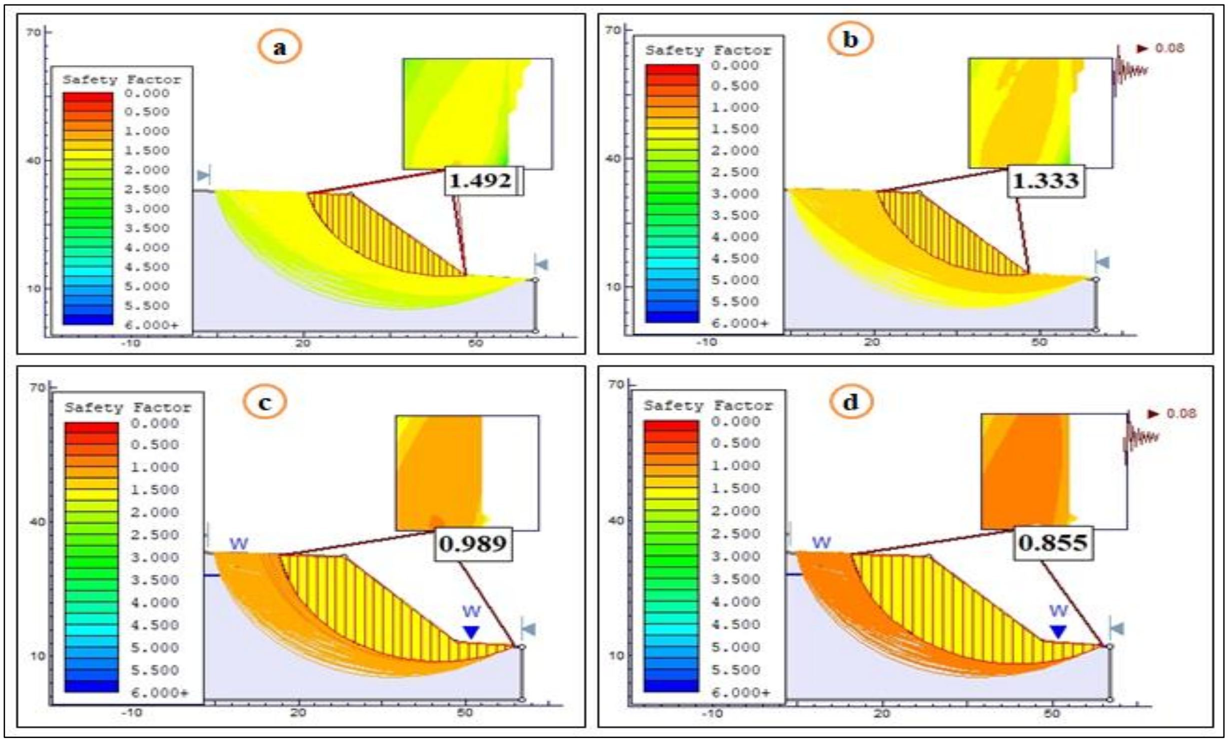

Figure5.20: Slope stability analysis by Limit equilibrium method for soil slope section SS2 at a) static dry, b) dynamic dry, c) static saturated and d) dynamic saturated conditions

According to the analysis results above, the factor of safety of soil slope section (SS2) is 1.492 and 1.333 under static and dynamic dry conditions as shown on (Figs.5.20a and b) respectively. This shows that soil slope section SS2 was stable in both static and dynamic dry conditions. However, the factor of safety that was determined under static saturated and dynamic saturated conditions of the SS2 is 0.989 and 0.855 respectively (Figs.5.20c and d). This indicates that the soil slope section SS2 is unstable when saturated and unstable when under static saturated and dynamic saturated conditions. The effect of seismic activity on slope stability changes less significantly from dynamic dry to dynamic saturated conditions. In addition, a factor of safety computed for SS2 under saturated slope conditions is relatively small compared to static dry slope conditions. This indicates that the rise in the groundwater table during the high rainfall season has more significant impact on the slope instability. The summary of factors of safety determined using the general limit equilibrium method (GLEM), spencer and Bishop simplified methods under static dry, static saturated, dynamic dry and dynamic saturated slope conditions was presented in Table 5.29.

Table5.29: Factor of safety and slope status under different anticipated condition of soil slope section SS1 and SS2.

Slope sections	Loading condition	FOS by different methods			Slope stability conditions
		GLEM	Spencer	Bishop simplified	
SS1	Static dry	1.52	1.53	1.50	Stable
	Static saturated	0.89	0.90	0.86	Unstable
	Dynamic dry	1.46	1.46	1.42	Stable
	Dynamic saturated	1.08	1.09	0.92	Stable/Unstable
SS2	Static dry	1.48	1.49	1.49	Stable
	Static saturated	0.98	0.98	0.98	Unstable
	Dynamic dry	1.33	1.33	1.33	Stable
	Dynamic saturated	0.87	0.87	0.85	Unstable
FOS= factor of safety, GLEM = General limit equilibrium method, SS = Soil slope					

5.7.2. Slope Stability Analysis of Soil Using Finite Element method

The factor of safety (FOS) was analyzed and interpreted using the finite element method for failure surface in soil slope under static dry, static saturated, dynamic dry and dynamic saturated conditions. The input parameters for the two soil slope sections which are used in finite element modeling include cohesion, internal friction angle, the unit weight of soil, Poisson‘s ratio (ν), dilatancy angles (ψ) and elastic modulus. The internal friction angle, cohesion, and unit weight of the two soils slope sections (SS1 and SS2) are determined from laboratory tests. The elastic modulus of a soil (Es) and Poisson’s ration (v) that is used for numerical modeling were determined from the correlation and recommendation of literature (TESHAGER, 2019). The Poisson’s ration (v) was calculated using eq.3.15 (Bowles, 1996) and the deformation modulus was calculated from equation 3.17 (Das, 2002).

Table5.30: Input parameters for soil slope stability analysis using finite element method

Slope materials	materials	Unit weight (KN/m2)		C (Mpa)	ϕ(°)	Ψ (°)	v	Es (KN/m2)
		$_{\gamma}$dry	$_{\gamma}$sat					
SS1	Well graded sand	8.9	11.3	30.4	29.56	0	0.17	9600
SS2	Well graded sand	12	13.5	32.41	21.57	0	0.05	13200
$_{\gamma}$dry = dry unit weight of soil, $_{\gamma}$sat = the saturated unit weight of soil, C = cohesion, ϕ = angle of internal friction, ψ = dilatancy angle, v = Poisson’s ratio and Es = young modulus								

The safety factors for the selected critical soil slope sections (SS1and SS2) were determined in Phase2 software (Rocscience, 2004) using the Mohr-Coulomb model and discussed as stated bellows.

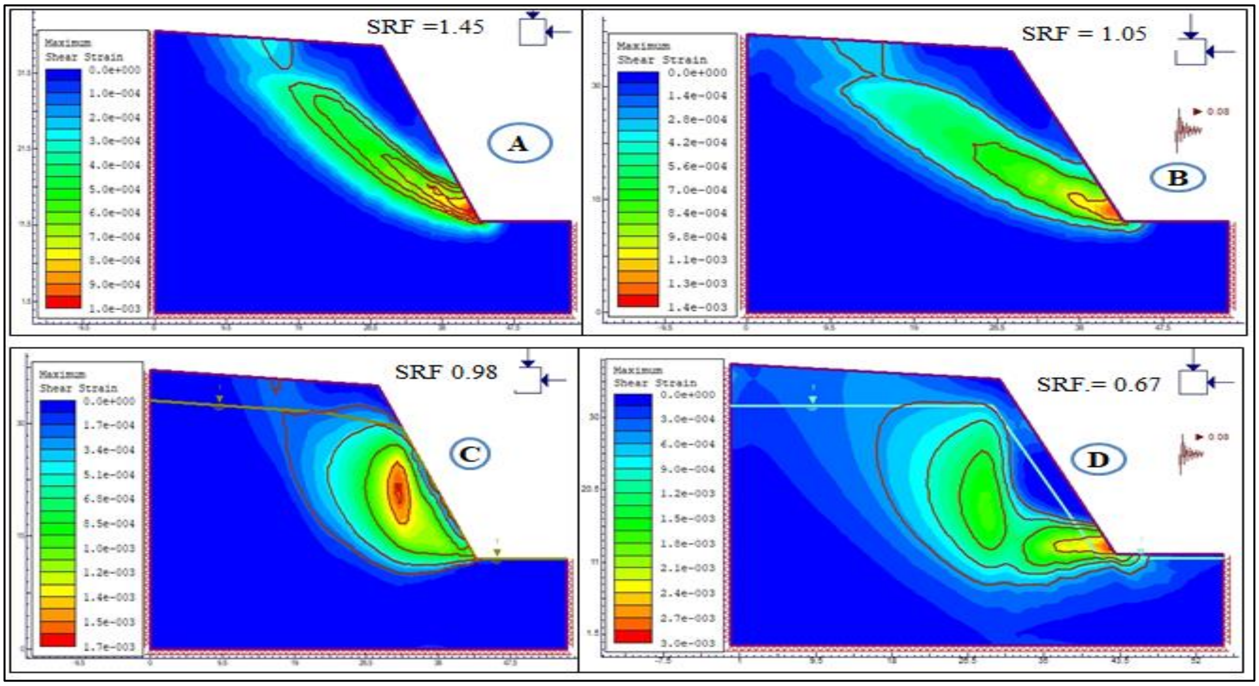

Figure5.21: Factor of safety for slope soil section SS1 using phase2 software under a) static dry, b) dynamic dry, c) static saturated and d) dynamic saturated conditions.

According to the above analysis results the safety factor of soil at slope section SS1 is 1.45 and 1.05 under static and dynamic dry conditions (Figs.5.21a and b) respectively. This shows that soil slope section SS1 was stable in both conditions. However, the factor of safety that was determined under static saturated and dynamic saturated conditions of the soil slope section SS1 is 0.98 and 0.67 and less than one as shown on (Figs.5.21c and d) respectively. This indicates that the soil at critical slope section SS1 is unstable under static saturated and dynamic saturated conditions. When we compare the result of the strength reduction factor at different conditions the strength reduction factor decreased 27.6% from static dry to dynamic dry, 32.4% from static dry to static saturated and 36.2% from dynamic dry to dynamic saturated conditions. This demonstrating that pore water pressure has a greater effect on destabilizing these slope sections than seismic activity.

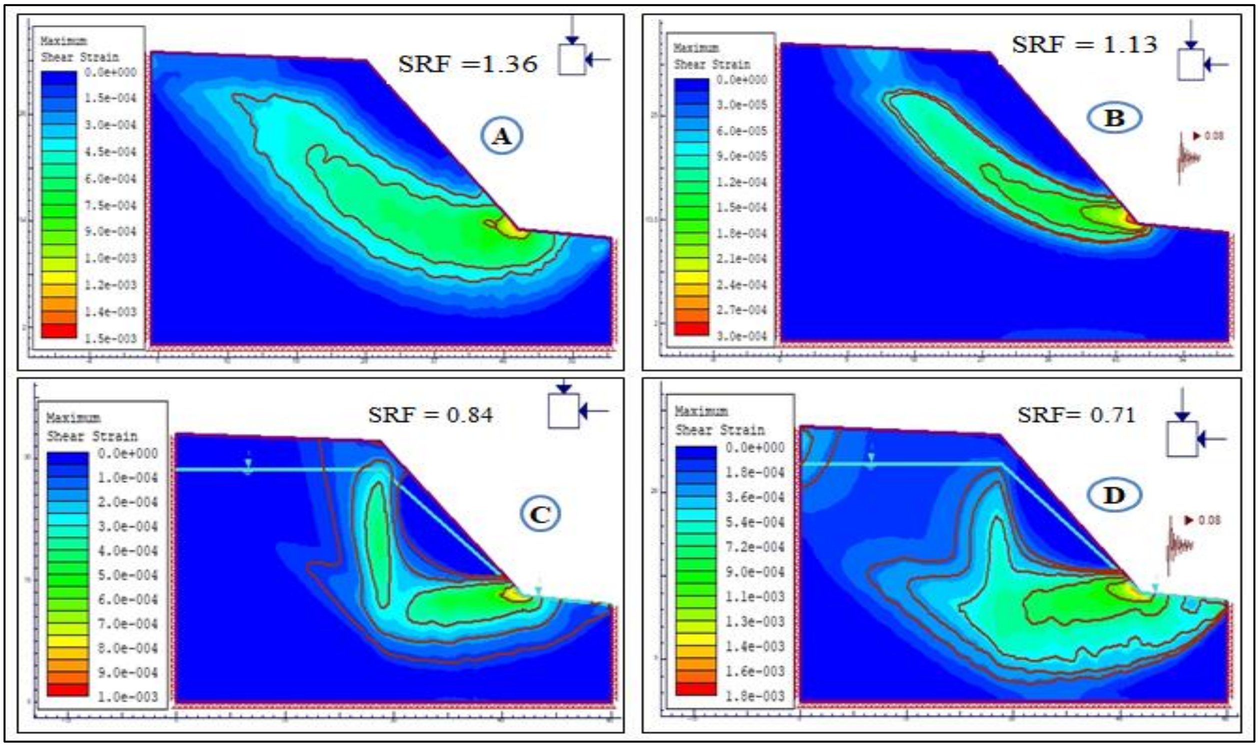

Figure5.22: Factor of safety for slope soil section SS2 using phase2 software under a) static dry, b) dynamic dry, c) static saturated and d) dynamic saturated conditions.

From the above analysis result, the minimum factors of safety or strength reduction factor determined from the FEM analyses of the soil slope section SS2 is 1.36 and 1.13 for static dry and dynamic dry condition as shown in (Figs.5.22a and b). This indicates that the soil slope section SS2 was stable in both static and dynamic dry conditions. However, the strength reduction factor that was determined under static saturated and dynamic saturated conditions of the soil slope section SS2 is 0.84 and 0.71 as shown in (Figs.5.22c and d). This revealed that when the slope is supposed to be static saturated and dynamic saturated, the critical SRF or FOS is less than one, indicating that the slope was unstable (Shariati & Fereidooni, 2021). When we compare the result of the strength reduction factor under different anticipated conditions the strength reduction factor decreased by 16.9% from static dry to dynamic dry, by 38.2% from static dry to static saturated and by 37.2% from dynamic dry to dynamic saturate conditions. The factor of safety is decreasing that indicates pore water pressure has a significant impact on the slope stability since it affects the shear strength of the materials (Kabeta, et al., 2020).

Table5.31: Factor of safety and slope status under different anticipated condition of soil slope section SS1 and SS2.

Slope sections	Method	Loading condition	The factor of safety (FOS)	Slope stability conditions
SS1	Strength reduction method	Static dry	1.45	Stable
		Static saturated	0.98	Unstable
		Dynamic dry	1.05	Stable
		Dynamic saturated	0.67	Unstable
SS2	Strength reduction method	Static dry	136	Stable
		Static saturated	0.84	Unstable
		Dynamic dry	1.13	Stable
		Dynamic saturated	0.71	Unstable

5.8 Comparison of FEM and LEM Results

In this study, the comparison of limit equilibrium and finite element methods was made by using the result of factor of safety for both rock and soil slope obtained from the slide and phase 2 software. The factor of safety obtained using slide software was found to be slightly higher than that of phase 2 of finite element methods. However, the result obtained using phase 2 provides more detailed information about the stress, strain, deformation, and displacements at any point in the slope section. Additionally, FEM gives information about the deformations at working stress levels and can monitor progressive failure including overall shear failure. Hence, the result obtained from phase 2 is more reliable than that of slide software. It should be noted that the limit equilibrium slide based software gives only uniform factor of safety along the failure surface and doesn't consider the stress-strain relationship of the materials. The factor safety (FOS) and strength reduction factor (SRF) results from FEM and LEM analyses are shown in Fig. 5.23.

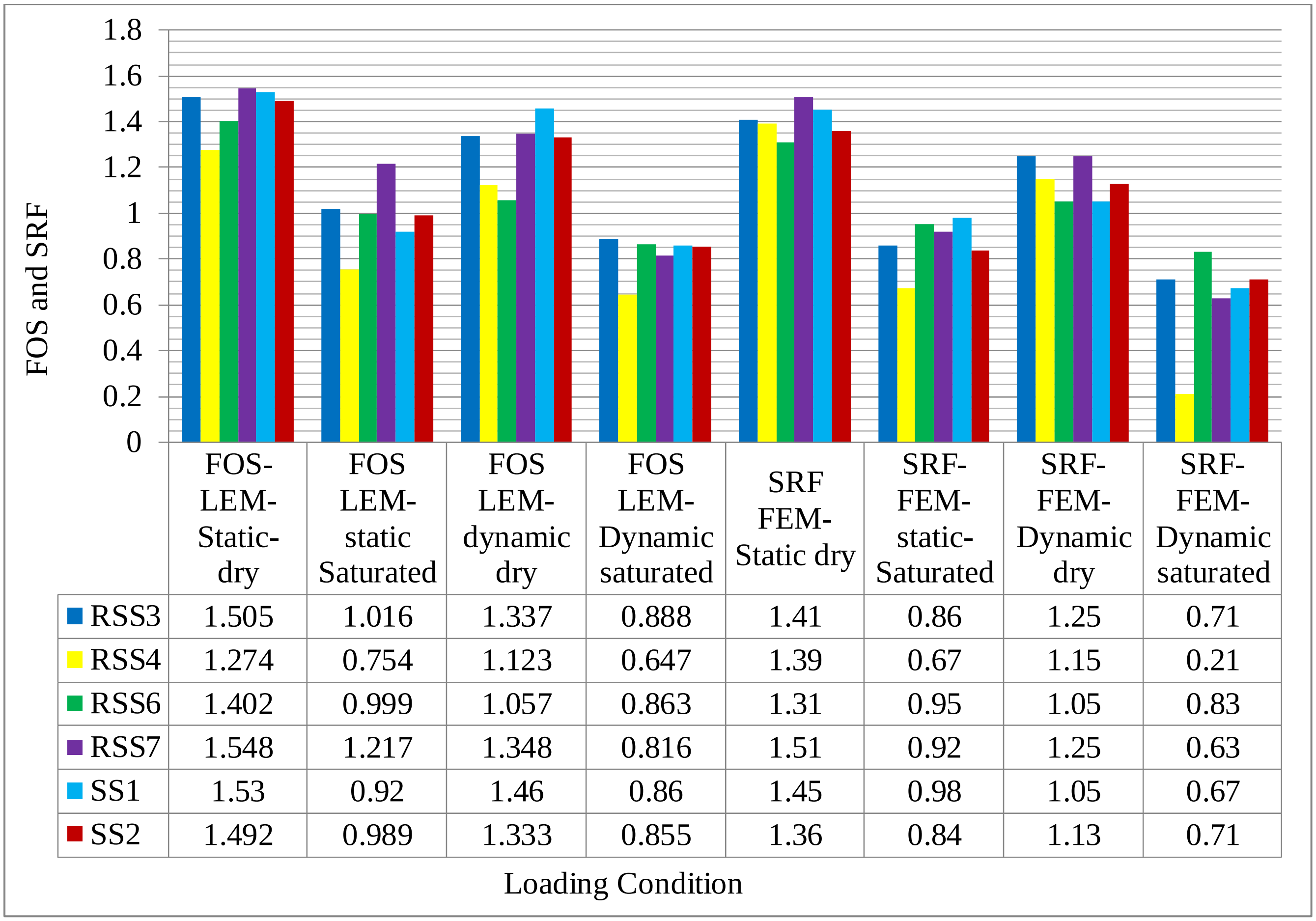

	FOS-LEM-Static-dry	FOS LEM-static Saturated	FOS LEM-dynamic dry	FOS LEM-Dynamic saturated	SRF FEM-Static dry	SRF-FEM-static-Saturated	SRF-FEM-Dynamic dry	SRF-FEM-Dynamic saturated
RSS3	1.505	1.016	1.337	0.888	1.41	0.86	1.25	0.71
RSS4	1.274	0.754	1.123	0.647	1.39	0.67	1.15	0.21
RSS6	1.402	0.999	1.057	0.863	1.31	0.95	1.05	0.83
RSS7	1.548	1.217	1.348	0.816	1.51	0.92	1.25	0.63
SS1	1.53	0.92	1.46	0.86	1.45	0.98	1.05	0.67
SS2	1.492	0.989	1.333	0.855	1.36	0.84	1.13	0.71

Figure5.23: Factor of safety comparison with LEM and FEM at different conditions.

5.9 Remedial Measures

In this study, appropriate remedial measures were recommended based on the actual stability condition of the slope, determined through numerical evaluation and field investigation. According to Popescu (2001), slope failure remedial measures are generally categorized into four groups: modification of slope geometry, providing drainage, engineering retaining structures, and internal soil reinforcement. For these study area, it is recommended to implement the following measures to maintain stability in the critical slope sections: **Modification of slope geometry:** This can involve reshaping the slope by adjusting its angle or creating terraces to reduce the overall slope height and enhance stability.

Providing drainage: Effective drainage systems should be implemented to manage surface and subsurface water. This can include surface drainage channels, subsurface drains, and erosion control measures to prevent water accumulation and minimize the risk of slope failure.

Engineering retaining structures: Depending on the slope conditions, retaining structures such as retaining walls or gabion walls should be required to provide additional support and stability to the slope. Internal soil reinforcement: Measures such as soil nailing, ground anchors, or geosynthetic reinforcements can be employed to strengthen the soil within the slope and improve its stability. By implementing these recommended measures, the stability of the critical slope sections in the study area can be effectively maintained, reducing the risk of slope failure and ensuring the safety of the area.

5.9.1 Modification of Slope Geometry

The study area slope is moderately steep to very steep which causes an increase in tangential gravity force due to maximum value of shear stress there by favors slope instability. The geometry of the slope is one of the most important parameters which effects of its stability from the landslide of the study area (Anbalagan, 1992; Raghuvanshi et al., 2014; Shiferaw, 2021). For this study, according to the analysis results the slope height and slope angle are critical elements influencing the stability conditions of the studied slopes. Considering these factors, mitigation measures to reduce their instability were suggested. Slope stability assessment for remedial works was conducted using LEM method with the applications slide software (slide 6 Rocscience 2004). The slope was assessed for its stability in term of factor of safety (FOS). The remedial measures for slope modification geometry were proposed such as the effect of slope height, slope angle and benching slope was evaluated using slide 6 software (Popescu, 2001). The slope geometry can be changed by reducing a slope angle, slope height and removing material from the landslide of the study area (Anbalagan, 1992; Raghuvanshi, et al., 2014; Shiferaw, 2021).

5.9.1.1. Reducing of Slope Angle and Slope Height

The stability of slopes is affected by slope angle and height as discussed in various studies (Shiferaw, 2021; Chatterjee and Krishna, 2019; Kale et al., 2021; Anbalagan, 1992; Raghuvanshi et al, 2014). The numerical models were conducted for different slope heights and angles, and the results indicate that decreasing slope angle and height tend to increase the factor of safety. It is important to note that there is an inverse relationship between slope angle/height and factor of safety. The evaluation results were generated using slide 6 software (Rocscience, 2004) and presented in Figures 5.24 and 5.25.

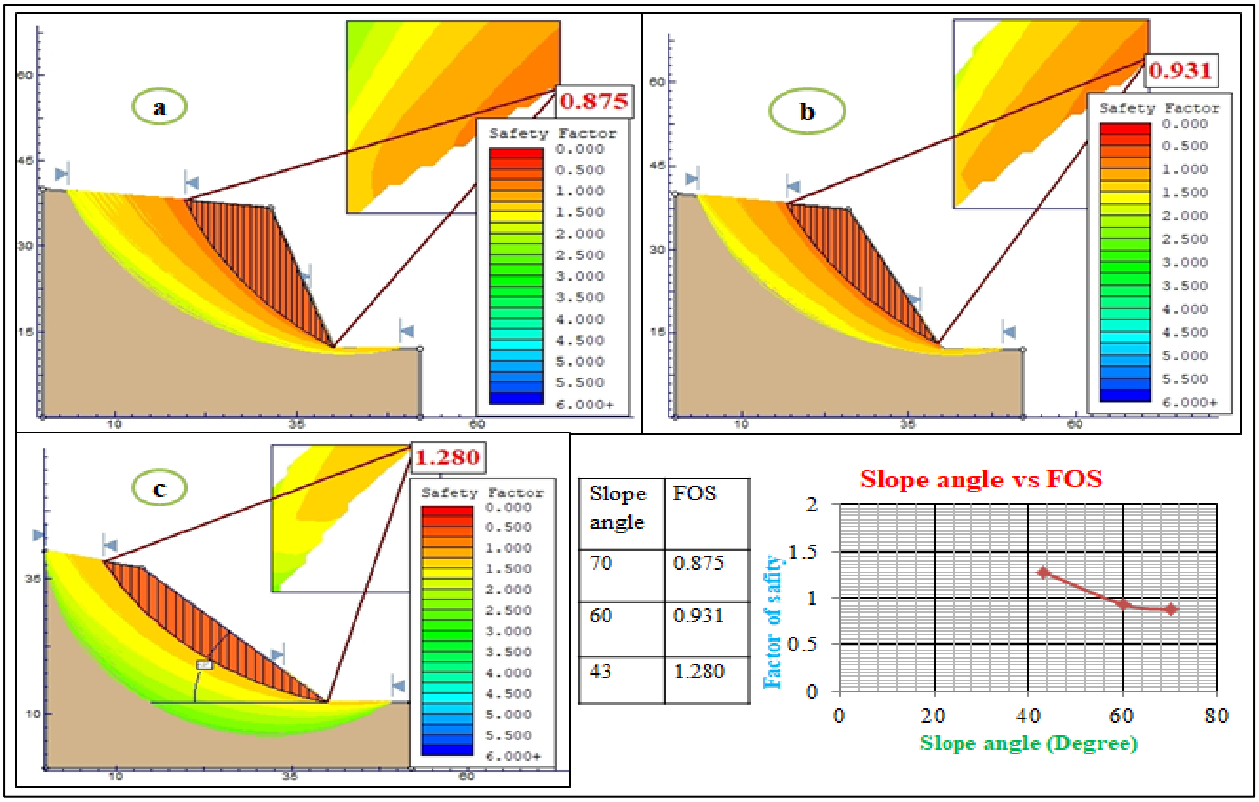

Slope angle	FOS
70	0.875
60	0.931
43	1.280

Figure5.24**:** Effect of slope angle on factor of safety of slope analysis using slide software, a) at 70º, b) at 60º and c) at 43º

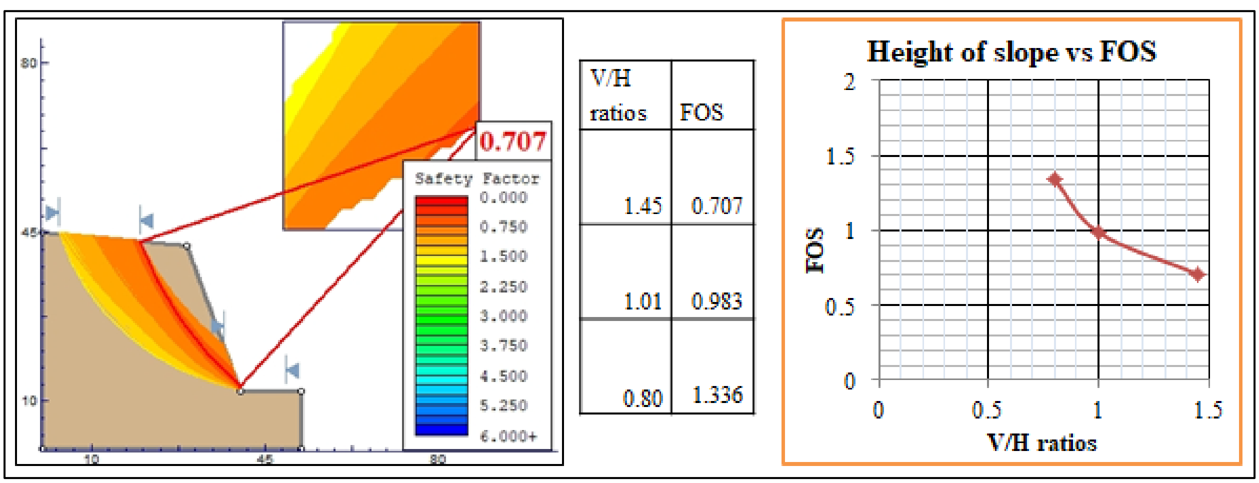

V/H ratios	FOS
1.45	0.707
1.01	0.983
0.80	1.336

Figure5.25**:** Effect of slope height on factor of safety of slope stability analysis using slide software.

5.9.1.2. Benching the Slope

Through the utilization of benching, a single steep slope can be transformed into multiple lower ones (Abramson, 2002). This technique is especially useful in changing a very steep slope into a gentler one on a single slope profile. In this study, the focus was on unstable rock slope section two (RSS2) and the effect of benching on slope cut, with the factor of safety analyzed using slide 6 software (Rocscience, 2004) under the static dry condition. As a result, the effect of slope bench on the safety factor was determined for one, two, and three bench numbers. Fig.5.26 demonstrates the slide software analysis results which was plotted and presented.

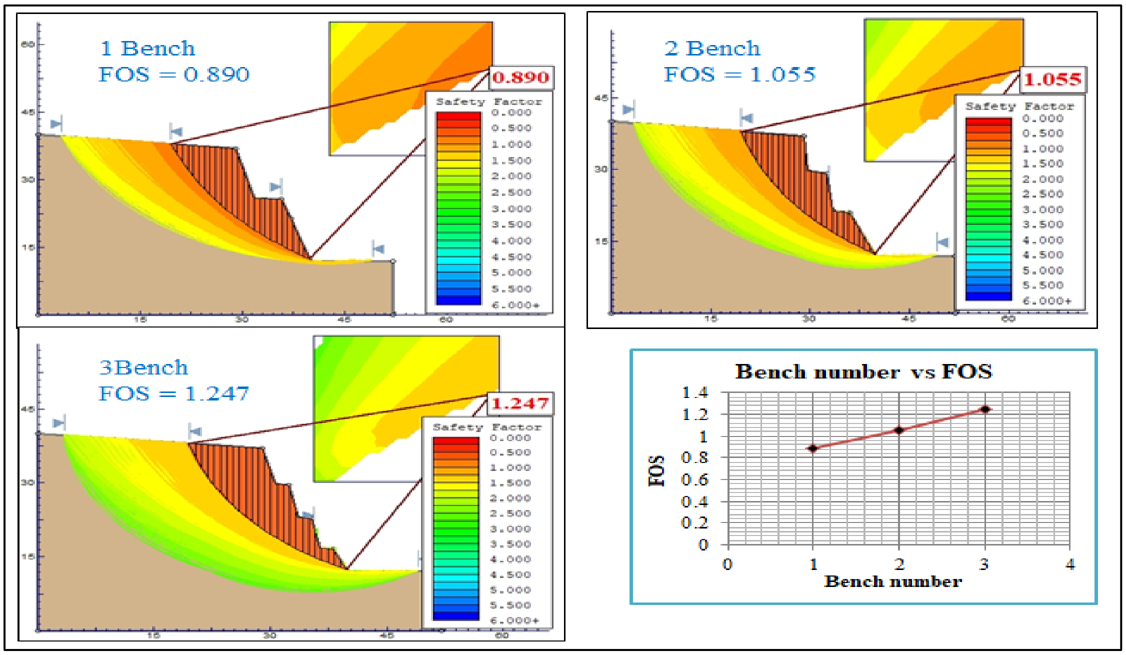

Figure5.26**:** Effect of benching slope face on factor of safety for slope stabilization using slide software.

The results of this analysis, as shown in Fig.5.26, demonstrate that the factor of safety increases as the number of benches increases. This highlights the strong and direct relationship between the bench number in slope and the factor of safety, indicating that increasing benching can be important for slope stabilizations. Ultimately, the slope was found to be most stabilized when 2 and 3 benches were performed, with an increase in bench number leading to improved performance in stabilizations.

5.9.2. Providing Drainage

To address the active landslide problems, it is crucial to implement effective remedial measures, such as providing drainage for both surface and subsurface water (Panigrahi, 2021). The absence of drainage in the studied area makes it susceptible to erosion and instability during heavy rainfall. To mitigate these issues, it is recommended to install surface drainage along the top side of the slide area, running from east to west. This will help divert excess water away from the slope, reducing the potential for erosion and instability.

Additionally, limiting runoff is essential to reduce the continuity of slope failure in selected critical soil slope sections across the road. Implementing measures such as terracing, contour trenches, or retention ponds can help control and manage runoff, preventing it from accumulating and further destabilizing the slope. By providing effective drainage systems and managing runoff, the risk of erosion and slope failure can be significantly reduced, ensuring the stability and safety of the road and surrounding areas.

5.9.3. Providing Engineering Retaining Structures

It's important to manage soil movement along the slope for safety reasons. One way to do this is by building gabion on one side of the slope. Additionally, supplying embankments along the failed slope can help create a stable slope at critical soil slope sections. To further mitigate risks, several retaining structures such as gravity retaining walls, reinforced earth retaining structures, rock slope face retention nets, and rock fall stopping systems are recommended. Protective rock measures against erosion can also be applied to the slope rock to reduce the probability of rock failures onto the road. While some rock slope sections in the study area are stable, others may require the removal of loose blocks to prevent future rock falling or sliding. To prevent this from happening, retention measures such as engineered ditches, wide shoulders, berms, steel barriers, and net should be provided along with retaining walls.

CHAPTER SIX

6. CONCLUSION AND RECOMMENDATION

6.1 CONCLUSION

In conclusion, the present study successfully utilized various methods to assess the stability of slopes along the road corridor from Arbarakete to Badessa town in the southeastern plateau of Ethiopia. Through reconnaissance studies and extensive field surveys critical rock and soil slope sections prone to failure were identified. Extensive field work, laboratory tests, and in-situ measurements provided valuable data on the geological and slope conditions. The kinematic analysis, deterministic methods, limit equilibrium, and finite element methods were employed to analyze slope stability under different loading conditions. The results indicated that the critical slope sections have been evaluated and their stability assessed. This information will play a crucial role in ensuring the safe and effective management of the road corridor.

Based on the comprehensive data acquisition and analysis methods used in this study, several key findings can be concluded:

- The study area exhibits heavily fractured and weathered rock masses, with seven critical rock slopes and two critical soil slope sections identified.
- The rock qualities, determined by RQD values and rock mass rating, ranged from fair to good. Based on the in-situ tests, it was determined that most of the rocks along the road sections have medium to high strength basalt rock units. The kinematic analysis identified two modes of failure mechanisms: planar mode at slope sections RSS2 and RSS5, and wedge mode at slope sections RSS1 and RSS2, which confirmed the observed failure modes in the field.
- Kinematic analysis confirmed two modes of failure mechanisms: planar mode at slope sections RSS2 and RSS5, and wedge mode at slope sections RSS1 and RSS2. The observed failures in the field were consistent with the results of the kinematic analysis.
- Deterministic stability analyses using rocplane and swedge software were conducted for the planar and wedge modes of rock slope failure. The results indicated that for the planar mode, the factor of safety at RSS2 was greater than one under static dry and

dynamic dry conditions, but less than one under static saturated and dynamic saturated conditions. At RSS5, the factor of safety was less than one under all anticipated conditions. However, for the wedge mode, the factor of safety at RSS1 and RSS2 was greater than one under static dry and dynamic dry conditions, but less than one under static saturated and dynamic saturated conditions.

- Consequentially, finite element and limit equilibrium stability analyses methods were performed on four non-structural critical rock slope sections. The results showed that RSS3 and RSS6 were stable under static dry conditions but unstable under all other conditions by both methods. RSS4 was unstable under all anticipated conditions and under both saturated conditions by LEM and FEM, respectively.
- RSS7 was stable under both dry conditions and unstable under both saturated conditions by LEM and stable under all anticipated conditions except under dynamic saturated condition by FEM.
- Additionally, the study conducted gradation analyses and Atterberg limit tests on the soils in the slope sections. The results indicated that the soils have medium to high plasticity index and a high liquid limit. The moisture content tests revealed a range of 11.5% to 20.7% for the soils in the study area.
- Furthermore, the analysis of soil slope sections using both the Limit Equilibrium Method (LEM) and Finite Element Method (FEM) showed that the soil slopes were stable under static dry and dynamic dry conditions, but unstable under static saturated and dynamic saturated conditions.
- Comparing the factors of safety (FOS) obtained from slide software and phase2 software; it was found that LEM provided a slightly higher FOS. The analysis also revealed that the FEM approach provides more comprehensive information on the failure surface, including stress, strain, deformation, and displacement at any point in a slope section.
- Finally, the remedial measures analysis identified that flattening the slope angle, lowering the slope height, and benching the slope section have a significant influence on slope stability.

Overall, the findings of this study provide comprehensive and accurate information on the engineering geological and slope stability conditions of the study area, enabling informed decision-making and appropriate measures to mitigate potential slope failures along the road corridor.

6.2. Recommendation

Based on the outcome and findings of the present study, the following recommendations were forwarded.

- Based on the present study, it has been concluded that certain rock slope sections in the study area are only partially unstable under certain conditions, while others are unstable under all anticipated conditions. To mitigate further failures and stabilize the slope, it is recommended to implement shotcrete, rock bolts, and retaining walls with anchors.
- Combining two or three methods with engineering and economic considerations is highly recommended. Reshaping bench and slope geometry is also recommended to mitigate instability problems caused by the slope height and slope angle.
- It is important to note that sensitivity analysis for the wedge mode of rock slope failures was not conducted due to limitations in the Swedge software. Therefore, using software that can complete the studies and perform sensitivity analysis for the wedge mode of rock slope failures is highly recommended.
- Further geotechnical investigations, geophysical surveys, and topographic surveys should be performed to better evaluate the influence of critical factors for slope instability. Additionally, a well-designed drainage system is necessary for the area, as it is highly affected by poor drainage due to its undulated landscape.
- Further study is required to identify the effect of surface and groundwater on stability condition; particularly the study area is highly susceptible to slope failure during the rainy season.

REFERENCES

ASTM D 5731-16. (1995). index of rocks.ASTM standard test method for determination of point load strength. *American society for testing and materials, 04.08*, 142-148.

ASTM D2216. (1998). Content of Soil and Rock by Mass Standard Test Method for Laboratory Determination of Water (Moisture), Conshohocken, 19428.

Abbate, A., Longoni, L., Ivanov, V. I., & Papini, M. (2019). Wildfire impacts on slope stability triggering in mountain areas. *Geosciences, 9*(10), 417.

Abbate, E., Bruni, & Sagri, M. (2015). Geology of Ethiopia: A Review and Geomorphological Perspectives. *In P. Billi (Ed.), Landscapes and Landforms of Ethiopia* , 33–64.

Abramson, L. W., Lee, T. S., Sharma, S., & Boyce, G. M. (2002). *Slope stability and stabilization methods.* John Wiley & Sons.

Admassu, Y., & Shakoor, A. (2022). DIPANALYST: A computer program for quantitative kinematic analysis of rock slope failures. Computers & geosciences. *54*, 196-202.

Ahmed, M. F., Sher, F., & Mehmood, E. (2023). Evaluation of landslide hazards potential at Dasu dam site and its reservoir area. *Environmental Earth Sciences. Environmental Earth Sciences,, 82*(7), 183.

ALEMU, T. (2010). ETHIOPIAN GEOSCIENCES & MINERAL ENGINEERING ASSOCIATION (EGMEA).

Alhamdi, M. K., & Albusoda, B. S. (2021). A Review on Deep mixing method for soil improvement). *In IOP Conference Series: Materials Science and Engineering, 105*(1), 012110.

Ambassa, Z., & Amba, J. C. (2022). Towards an Advanced New Emerging Method of Determination of Mohr–Coulomb Parameters of Soils from at the Oedometric Test: Case Study-Lateritic Soils of Cameroon. *Mathematical Problems in Engineering, 2022*.

Asmare, D., & Hailemariam, T. (2021). Assessment of rock slope stability using slope stability probability classification (SSPC) system, around AlemKetema, North Shoa, Ethiopia. *Scientific African, 12*, e00730.

ASTM D5873. (2001). Standard test method for determination of rock hardness by rebound hammer method.

ASTM D 4318. (1998). Standard Test Method for Liquid Limit, Plastic Limit and Plasticity Index of soils. *American society for testing and materials, Conshohocken* , 19428 .

ASTM D 854. (1998). Standard Test Method for Specific Gravity of Soils. *American society fortesting and materials, Conshohocken*, PA;19428.

Aswathi , C. K., Jana, A., Dey, A., & Sreedeep, S. (2017). Stability assessment of a heavily jointed rock slope using limit equilibrium and finite element methods. *In Indian Geotechnical Conference, 6*.

Awang, H., Salmanfarsi, A. F., Misbahuddin, A. Z., & Ali, M. I. (2021). Slope stability analysis of rock mass using Rock Mass Rating and Slope Mass Rating. *In IOP Conference Series: Earth and Environmental Science, 682*(1), 012015.

Aydan, O. (2016). Large rock slope failures induced by recent earthquakes. *Rock Mechanics and Rock Engineering, 49*(6), 2503-2524.

Azarafza, M., Akgün, H., Ghazifard, A., Asghari-Kaljahi, E., Rahnamarad, J., & Derakhsh, R. (2021). Discontinuous rock slope stability analysis by limit equilibrium approaches–a review . *International Journal of Digital Earth, 14*(12), 1918-1942.

Balazs, V. (2009). A Possible Method for Estimating the Poisson's Rate Values of the Rock Masses. *Acta Geod. Geoph. Hung, 44*(3), 313–322.

Bao, C., Zhan, L., Xia, Y., Huang, Y., & Zhao, Z. (2022). Development Trend and Stability Analysis of Creep Landslide With Obvious Slip Zone Under Rainfall-Taking Xinchang Xiashan Basalt Slope as an Example. *Frontiers in Earth Science, 9*. doi:808086

Barlow, J., Gilham, J., & Ibarra Cofrã, I. (2017). Kinematic analysis of sea cliff stability using UAV photogrammetryg. *International Journal of Remote Sensing, 38*(8-10), 2464-2479.

Barton, N., & Choubey, V. (1977). The shear strength of rock joints in theory and practice. *Rock mechanics, 10*(1), 1-54.

Barton, N., Wang, C., & Yong, R. (2023). Advances in joint roughness coefficient (JRC) and its engineering applications. *Journal of Rock Mechanics and Geotechnical Engineering*.

BAYOU, N. B. (2020). EVALUATION OF SLOPE STABILITY CONDITIONS BY NUMERICAL ANALYSIS, A CASE OF OTOLO-SAWLA ASPHALT ROAD PROJECT, SOUTHERN PART OF ETHIOPIA (Doctoral dissertation).

Bekele, A., Boccalettii, M., Dainelli, P., & Getaneh, I. (1992). Fracture pattern of the Main Ethiopian Rift Area. *Structural map from lansat imagery and field observations (1:500,000) Consiglio Nazionale Delle Ricerche*.

Bekele, A., & Meten, M. (2022). Modeling rock slope stability using kinematic, limit equilibrium and finite-element methods along Mertule Maryam–Mekane Selam road, central Ethiopia. *Modeling Earth Systems and Environment*, 1-27.

Belew, A. Z., Tenagashaw, D. Y., Ayeie, W. T., & Andualem, T. (2022). Coupled Analysis ofSeepage and Slope Stability: a Case Study of Ribb Embankment Dam, Ethiopia. *Water Conservation Science and Engineering*, 1-22.

Bieniawski, Z. (1989). .. Engineering rock mass classifications: a complete manual for engineers and geologists in mining. *civil, and petroleum engineering: NewYork, xii*, 251.

Bocaletti, M. (1999). The Ethiopian Rift System. *Acta Vulcanological: Journal of the National Volcanic Group of Italy, 2*(1).

Bosellini, A., Russo, A., & Schroeder, R. (1999). Stratigraphic evidence for an Early Aptian sea-level fluctuation: the Graua Limestone of southeastern Ethiopia. *Cretaceous research, 20*, 783-791.

Bowa, V. M., & Samson, A. (2022). Slope Stability Analyses Subjected to Slide Head Toppling Failure Mechanisms.

Bowles, J. E. (1996). Foundation Analysis and Design. *5th Edition, The McGraw-Hill Companies, Inc., New York*.

Broch, E., & Franklin, J. A. (1972). The point-load strength test. *International Journal of Rock Mechanics and Mining Sciences, 9*(6), 669–676.

Budetta, P. (2020). Some remarks on the use of deterministic and probabilistic approaches in the evaluation of rock slope stability. *Geosciences, 10*(5), 163.

Cala, M., & Flisiak, J. (2020). Slope stability analysis with FLAC and limit equilibrium methods). *In FLAC and Numerical Modeling in Geomechanics-2001*, 111-114.

Caroles, L. (2023). Probabilistic Seismic Hazard Analysis on Pavement Failure Restoration; Case Study of Sorong–Makbon Road. Sustainability. *15*(7), 5994.

Carter, T. G., & Marinos, V. (2020). Putting geological focus back into rock engineering design. *Rock Mechanics and Rock Engineering, 53*(10), 4487-4508.

Casagrande, A. (1932). Research of Atterberg Limits of Soils Public Roads. *13*(8), 121-213.

Chango, Z., Huang, F., Huang, J., Jiang, S. H., Zhou, C., & Zhu, L. (2021). Experimental study of the failure mode and mechanism of loess fill slopes induced by rainfall. *Engineering Geology, 280*.

Chen, H., Qin, S., Xue, L., & Xu, C. (2021). Why the Xintan landslide was not triggered by the heaviest historical rainfall: Mechanism and review. *Engineering Geology, 294*, 106379.

Chen, J., Du, C., Qingzhao, Z., Guo, X., Xue, J., & Jang, B. (2022). *A Case Study of Two Failures of a High Cut-slope in the Northeastern Area of Sichuan.* China.

Cuomo, S., Di Perna, A., & Martinelli, M. (2021). Modelling the spatio-temporal evolution of a rainfall-induced retrogressive landslide in an unsaturated slope . *Engineering Geology, 294*.

Dadi, O. M., & Chala, E. T. (2022). Stability Analysis of Rock-Socketed Piles on Inclined Slope: Case Study on Conveyor Belt Foundations of Dangote Cement, Ethiopia.

Das, B. M. (2002). Soil Mechanics Laboratory Manual. *Oxford University Press, New York, 6th Edition*, 8-9.

Deere, D. U., & Miller, R. P. (1966). Engineering classification and index properties for intact rocks. *Tech Report*. *Air Force Weapons Lab*, 65-116.

Dietze, M., Bel, R., Ozturk, U., Cook, K. L., Andermann, C., & Beer, A. R. (2022). .More than heavy rain turning into fast-flowing water–a landscape perspective on the 2021 Eifel floods. *Natural Hazards and Earth System Sciences*, *22*(6), 1845-1856.

Dips 6.0, & Rocscience. (2004). Retrieved from http://www.rocscience.com/software/dips

Diro, G. A., Kabeta, W. F., & Teshager, D. K. (2020). Assessments of Geotechnical Conditions and Slope Stability Analysis: Case Study in Gedo town, Ethiopia. *Int*. *J*. *Sci*. *Res*. *Eng*. *Trends*, *6*(3), 1250-1258.

Edelbro. C. (2004). Evaluation of rock mass strength criteria (Doctoral dissertation, Luleå tekniska universitet).

El Jazouli, A., Barakat, A., & Khellouk, R. (2022). Geotechnical studies for Landslide susceptibility in the high basin of the Oum Er Rbia river (Morocco). *Geology, Ecology, and Landscapes, 6*(1), 40-47.

Elmo, D., & Stead, D. (2020). Disrupting rock engineering concepts: is there such a thing as a rock mass digital twin and are machines capable of learning rock mechanics?. *In Slope Stability 2020: Proceedings of the 2020 International Symposium on Slope Stability in Open Pit Mining and Civil Engineering*, pp. 565-576.

Fikadu, M. G. (2021). JIMMA INSTITUTE OF TECHNOLOGY (JIT) DEPARTMENT OF CIVIL AND ENVIRONMENTAL ENGINEERING GEOTECHNICAL ENGINEERING STREAM (Doctoral dissertation, Jimma University).

Gallage, C., Abeykoon, T., & Uchimura, T. (2021). Instrumented model slopes to investigate the effects of slope inclination on rainfall-induced landslides. *Soils and foundations, 61*(1), 160-174.

Gao, W., Yang, H., Hu, R. W., & Hu, R. (2022). Soil–rock mixture slope stability analysis bymicrotremor survey and discrete element method. *Bulletin of Engineering Geology and the Environment, 81*(3), 1-17.

Gemeda, D. O., Korecha, D., & Garedew, W. (2021). Evidences of climate change presences in the wettest parts of southwest Ethiopia. *Heliyon, 7*(9).

Getachew, N., & Meten , M. (2021). Weights of evidence modeling for landslide susceptibility mapping of Kabi-Gebro locality, Gundomeskel area, Central Ethiopia. *Geoenvironmental Disasters, 8*(1), 1-22.

Gidday, B. G., Ayothiraman, R., Ramaiah, B. J., & Ramana, G. V. (2023). Physical and numerical modeling of rainfall triggered shallow landslides in central highlands, Ethiopia. *Bulletin of Engineering Geology and the Environment, 82*(7), 239.

Goodman, R. E. (1989). Introduction to rock mechanics y. *New York: Wile, (Vol.2)*.

Gottron, D., & Henk, A. (2021). Upscaling of fractured rock mass properties–An example comparing discrete fracture network (DFN) modeling and empirical relations based on engineering rock mass classifications. *Engineering Geology, 294*, 106382.

Gutierrez-Martin, A. (2020). A GIS-physically-based emergency methodology for predicting rainfall-induced shallow landslide zonation. *Geomorphology, 359*, 107121.

Hack, R., Price, D., & N. , R. (2003). a new approach to rock slope stability – a probability classification (SSPC). *Bull Eng. Geol. Env. 62:*, 167–184.

Haile Fekadu, G., Melese, D. T., & Woldesenbet, T. T. (2022). Landslide susceptibility assessment using GIS on rock-soil slope along zabidar mountain road corridors, Ethiopia. *Geopersia, 12*(2), 201-222.

Hamza, T., & Raghuvanshi, T. K. (2017). GIS based landslide hazard evaluation andzonation–a case from Jeldu District, central Ethiopia. *Journal of KingSaudVUniversity-Science, 29*(2).

Havaej, M., & Stead, D. (2016). Investigating the role of kinematics and damage in the failure of rock slopes. *Computers and Geotechnics, 78*, 181-193.

Hayat, M. A., Ur Rehman, A., Ali, D., Saleem, A., & Mustafa, N. (2019). Developing Empirical Models for Uniaxial Compressive Strength Prediction by Using Non-Destructive TestResults. *Journal of Mining Science, 55*, 883-892.

He, Y., Cai, Z., Wang, F., Guo, C., Xiang, B., & He. (2023). Numerical investigation on slope stability influenced by seismic load and discontinuity with a continuous-discontinuous method. *Bulletin of Engineering Geology and the Environment, 82*(3), 70.

Hoek , E., Carranza-Torres , C., & Corkum , B. (2002). Hoek-Brown failure criterion-2002 edition. *Proc. of NARMS-Tac 1(1):267–273 index tests , 54* (5), 721–733.

Hossain, M., Islam, M. A., Badhon, F. F., & Imtiaz, T. (2021). Hydrometer Analysis. *Properties and Behavior of Soil-Online Lab Manual.*

Hussian, S., Mohammad, N., Ur Rehman, Z., Khan, N. M., Shahzada, K., Ali, S., & Sherin, Z. (2020). Review of the geological strength index (GSI) as an empirical classification and rock mass property estimation tool: origination, modifications, applications, and limitations. *Advances in Civil Engineering, 2020*, 1-18.

Ibrahim, M. B., Salisu, S. A., Musa, A. A., Abussalam, B., & Hamza, S. M. (2022). Framework for the identification of shallow ground movement in modified slopes (an expert opinion). *In IOP Conference Series: Earth and Environmental Science , 106*(1), 12055.

Ismail, A., Safuan, A. R., Sa'ari, R., Mustaffa, M., Abdullah, R. A., Kassim, A., & Kalatehjari, R. (2022). Application of combined terrestrial laser scanning and unmanned aerial vehicle digital photogrammetry method in high rock slope stability: A case study.*Measurement,195*, 1112343.

ISRM. (2014). International Society of Rock Mechanics. Suggested Methods for Determining Tensile Strength of Rock Materials. *International Journal of Rock Mechanics and Mining Sciences, Geomechanics Abstract, 15*(3), 99- 103.

Jain, V., Singh, A., Sinha, R., & Tandon, S. K. (2020). Evolution of modern river systems: an assessment of 'landscape memory'in Indian river systems. *Episodes Journal of International Geoscience, 43*(1), 535-551.

Kabeta, W. F., Diro, G. A., & Teshager, D. K. (2020). Assessments of Geotechnical Conditions and Slope Stability Analysis. *International Journal of Scientific Research, 6*(3), 10.

Kamal, A. M., Hossain, F., Rahman, M. Z., Ahmed, B., & Sammonds, P. (2022). Geological and soil engineering properties of shallow landslides occurring in the Kutupalong Rohingya Camp in Cox's Bazar, Bangladesh. *Landslides, 19*(2), 465-478.

Kazmi, D., Qasim, S., Harahap, I. S., Baharom, S., Mehmood, M., Siddiqui, F. I., & Imran, M. (2017). Slope remediation techniques and overview of landslide risk management. *Civil engineering journal, 3*(3), 180-189.

Kazmin, V. (1972). Geology of Ethiopia; explanatory note to the Geological map of Ethiopia, 1:2,000,000. *EIGS, Addis Ababa*.

Khanna, R., & Dubey, R. K. (2021). Comparative assessment of slope stability along road-cuts through rock slope classification systems in Kullu Himalayas, Himachal Pradesh,India. *Bulletin of Engineering Geology and the Environment, 80*(2), 993–1017.

Komadja, G. C., Pradhan, S. P., Oluwasegun, A. D., Roul, A. R., Stanislas, T. T., Laïbi, R. A., . . . Onwualu, A. P. (2021). Geotechnical and geological investigation ofslope stability of a section of road cut debris-slopes along NH-7, Uttarakhand, India. *Results in Engineering, 10*. doi: 100227

Kumar, M. S., & Raj Kumar, M. (2022). Factors Affecting Slope Stability of an Opencast Mine: A Brief Study. *Int. J. Innov. Sci. Res. Technol., 7*, 878-882.

Laimer, H. J. (2021). Engineering geomorphology: A novel professional profile to face applied challenges in earth surface dynamics in mid-Europe. *Earth Surface Processes and Landforms, 46*(11), 2127-2135.

Luna, P., Dakoulas, P., Zheng, W., Çetin, K. O., Perlea, M., Kung, G. T., & Barani, S. (2010). General Report—Session 4.

Mebrahtu, T. K., Heinze, T., Wohnlich, S., & Alber, M. (2022). Slope stability analysis of deep-seated landslides using limit equilibrium and finite element methods in Debre Sina area, Ethiopia. *Bulletin of Engineering Geology and the Environment, 81*(10).

Mengesha, T., Tadiwos, C., & Workneh, H. (1996). Explanation to the Geological Map of Ethiopia, 1:2,000,000 scale, Second Edition, Bull. No. 3, EIGS, Addis Ababa.

Moreno-Maroto, J. M., & Alonso-Azcarate, J. (2022). Evaluation of the USDA soil texture triangle through Atterberg limits and an alternative classification system. *Applied Clay Science, 229*, 106689.

Omar, M. (.–U. (2017). Omar, M . *Empirical correlations for predicting strength properties of rocks–United Arab Emirates., 11*(3), 248-261.

Palin, R. M., Santosh, M., Cao, W., Li, S. S., Hernandez-Uribe, D., & Parsons, A. (2020). Secular change and the onset of plate tectonics on Earth. *.Earth-Science Reviews, 207*, 103-172.

Panchal, S., & Shrivastava, A. K. (2022). Landslide hazard assessment using analytic hierarchy process (AHP): A case study of National Highway 5 in India. *Ain Shams Engineering Journal, 13*(3), 10-26.

Pandit, K., Singh, M., Sharma, S., Sandhu, H. A., & Sahoo, J. (2021). Back-Analysis of a Debris Slopethrough Numerical Methods and Field Observations of Slope Displacements. *Indian Geotechnical Journal, 51*(4), 811-828.

Panigrahi, R. K. (2021). Different Sets of Remediation for Mitigation of Landslides in Hilly Terrains of India. *In Stability of Slopes and Underground Excavations: Proceedings of Indian Geotechnical Conference 2020, 3*, 133-144.

Pantelidis, L. (2010). Rock slope stability assessment through rock mass classification systems. *International Journal of Rock Mechanics and Mining Sciences, 46*(2), 315-325.

Pauli, A., Kraus, M. A., & Siebert, G. (2021). Experimental and numerical investigations on glass fragments: shear-frame testing and calibration of Mohr–Coulomb plasticity model. *Glass Structures & Engineering, 6*, 65-87.

Price, D. G. (2009). *Engineering geology principles and practice.* Berlin Heidelberg: Springer-Verlag.

Qin, C., & Zhou, J. (2023). On the seismic stability of soil slopes containing dual weak layers: True failure load assessment by finite-element limit-analysis. *Acta Geotechnical, 18*(6), 3153-3175.

Raghuvanshi, T. K. (2017). Plane failure in rock slopes–A review on stability analysis techniques. *Journal of King Saud University-Science*.

Rahman, S. S., Siddiqua, S., & Cherian, C. (2022). Sustainable applications of textile waste fiber in the construction and geotechnical industries: A retrospect. *Cleaner Engineering and Technology, 6*, 100420.

Rocscience. (2004). RocPlane2.0. Retrieved from http://www.rocscience.com/software/rocplaneRocscience,2004

Romana M. (1985). New adjustment ratings for application of Bieniawski classification to slopes.

Proc. Int. Symp. on the Role of Rock Mechanics: 49-53.

Roul, A. R., Pradhan, S. P., & Mohanty, D. P. (2021). Investigation to slope instability along railway cut slopes in Eastern Ghats mountain range, India: A comparative study based on slope mass rating, finite element modelling and probabilistic methods.

Savi, S., Comiti, F., & Strecker, M. R. (2021). Pronounced increase in slope instability linked to global warming: A case study from the eastern European Alps. *Earth Surface Processes and Landforms, 46*(7), 1328-1347.

Shao, Q., Matthai, S., Driesner, T., & Gross, L. (2021). Predicting plume spreading during CO 2 geo-sequestration: benchmarking a new hybrid finite element–finite volume compositional simulator with asynchronous time marching. *Computational Geosciences, 25*, 299-323.

Shariati, M., & Fereidooni, D. (2021). Rock slope stability evaluation using kinematic and kinetic methods along the Kamyaran-Marivan road, west of Iran. *Journal of MountainScience, 18*(3), 779–793.

Siddique, T., Pradhan, S. P., Vishal, V., & Mondal, .. (2019). Stability assessment of Himalayan road cut slopes along National Highway 58, India. *Environmental Earth Sciences, 76*, 1-18.

Singh, H. O., Ansari, T. A., Singh, T. N., & Singh, K. H. (2020). Analytical and numerical stability analysis of road cut slopes in Garhwal Himalaya, India. *Geotechnical and Geological Engineering, 38*, 4811-4829.

Singh, J., Pradhan, S. P., Singh, M., & Yuan, B. (2022). Modified block shape characterization method for classification of fractured rock: A python-based GUI tool. *Computers & Geosciences, 164*,

Sousa, R. L., Menezes, J. E., Ribeiro e Sousa, L., Kartam, K., Chamine, H. I., & Samra, C. A. (2022). Slope failures during the construction stage at Musandam independent power plant, Oman. *Arabian Journal of Geosciences, 15*(1), 1-19.

Stewart, J., Liu, A., & Choi, Y. (2003). Amplification factors for spectral acceleration in tectonically active regions. *Bull. Seism. Soc. Am, 93* (1), 332-352.

Sudani, P., & Patil, K. A. (2022). Geo-Mechanical Behaviorof Toe Excavated Land Slope.

Tadesse, K. (2007). Integrated geophysical data processing and interpretation of crustal structure in Ethiopia with emphasis on the Ogaden Basin and adjacent areas. *The University of Texas at El Paso*.

Taye, M., Sahlu, D., Zaitchik, B. F., & Neka, M. (2020). Evaluation of satellite rainfall estimates for meteorological drought analysis over the upper Blue Nile basin, Ethiopia. *Geosciences, 10*(9), 352.

Tefera , M., Tadiwos , C., & Workineh , H. (1996). Explanation of the geological map of Ethiopia,scale 1:2,000,000. *Ethiopian Institute of Geological Surveys Bull. No.3 A.Ababa University, Ethiopia*, *54*(3).

Tesfaye, M., Regassa, B., & Garo, T. (2023). Rock slope stability modeling using kinematic and limit equilibrium methods along Woliso to Wonchi lake road, central Ethiopia. *Modeling Earth Systems and Environment*, 1-17.

TESHAGER, D. K. (2019). NUMERICAL SIMULATION OF STATIC PILE LOAD TEST ON STRATIFIED SOIL DEPOSITS (Doctoral dissertation, ADDIS ABABA SCIENCE AND TECHNOLOGY UNIVERSITY).

Tsige, D., Senadheera, S., & Talema, A. (2019). Stability analysis of plant-root-reinforced shallow slopes along mountainous road corridors based on numerical modeling. Geosciences. *10*(1), 19.

Ullah, S., Khanb, M. U., & Rehmana, G. A. (2020). A brief review of the slope stability analysis methods. *Geological Behavior (GBR)*, *4*(2), 73-77.

Vanneschi, C., Rindinella, A., & Salvini, R. (2022). Hazard Assessment of Rocky Slopes: An Integrated Photogrammetry–GIS Approach Including Fracture Density and Probability of Failure Data. *Remote Sensing*, *14*(6), 1438.

Wang, L., Wu, C., Gu, X., Liu, H., Mei, L., & Zhang, W. (2020). Probabilistic stability analysis of earth dam slope under transient seepage using multivariate adaptive regression splines. *Bulletin of Engineering Geology and the Environment*, *29*, 2763-2775.

Wang, T., LuoQ., Li, Z., Zhang, W., Chen, W., & Wang, L. (2022). System safety assessment with efficient probabilistic stability analysis of engineered slopes along a new rail line. *Bulletin of Engineering Geology and the Environment*, *81*(1), 68.

Wanstreet, P. (2007). Finite element analysis of slope stability. *West Virginia University*.

Wolter, A. (2020). A REVIEW OF METHODS USED TO INVESTIGATE STRUCTURAL CONTROL ON SLOPE INSTABILITY. *Alpine and Mediterranean Quaternary*, *33*(2), 139-147.

Wyllie, D., & Mah, C. (2014). *Rock slope engineering civil and mining, 4th edition*. spon press, new york.

Yang, B., Mitelman, A., Elmo, D., & Stead, D. (2022). Why the future of rock mass classification systems requires revisiting their empirical past. *Quarterly Journal of Engineering Geology and Hydrogeology*, *55*(1), 2021-039.

Yang, D., & Elmo, D. (2022). Why Engineers Should Not Attempt to Quantify GSI. *Geosciences*, *12*(11), 417.

APPENDIXS

Appendix A: The location of the critical rocks and soil slope sections of the study area.

Slope section's location	Sample Code	Northing	Easting	Elevation(m)	Rock types
	RSS1	9° 1'4.28"N	40°53'52.95"E	2373	HW. upper basalt
	RSS2	8°59'49.45"N	40°52'38.85"E	2485	SW. upper basalt
	RSS3	8°59'42.75"N	40°52'31.95"E	2485	SW. upper basalt
	RSS4	8°58'52.85"N	40°51'28.33"E	2283	MW. Lower basalt
	RSS5	8°58'52.82"N	40°51'23.07"E	2275	SW. Lower basalt
	RSS6	8°58'52.49"N	40°51'18.09"E	2260	HW. Lower basalt
	RSS7	8°58'21.59"N	40°50'38.33"E	2172	MW. Lower basalt
SW= slightly weathered, MW= Moderately weathered, and HW = highly weathered					

Slope section's location	Sample Code	Northing	Easting	Elevation (m)	Sampling method
	SS1	8°55'19.35"N	40°48'50.06"E	1761	Disturbed sample from natural soil deposit depth of 1m.
	SS2	8°54'5.96"N	40°45'34.93"E	1700	Disturbed sample from natural soil deposit depth of 1m.
SS= Soil slope section					

Appendix B: Classification of UCS of rocks according to Deere and Miller (1966).

Unconfined compressive strength (UCS) (MPa)	Description of strength
Over 224	Very High strength
112-224	High strength
56-112	Medium strength
28-56	Low strength
Less than 28	Very low strength

Appendix C: Classification of UCS of rock according to the International Society for Rock Mechanics (ISRM) Standard

Unconfined compressive strength (UCS) (MPa)	Description of strength
>250	Very High strength
100-250	High strength
50-100	Medium strength
25-50	Moderate strength
5-25	low strength
<5	very low strength

Appendix D: Geological strength index (GSI) Values estimated in the field based on the weathering condition of discontinuity surface, rock mass structure and interlocking of rock blocks in successive site visit as proposed by chart for GSI, Hoek and Marinos, 2000.

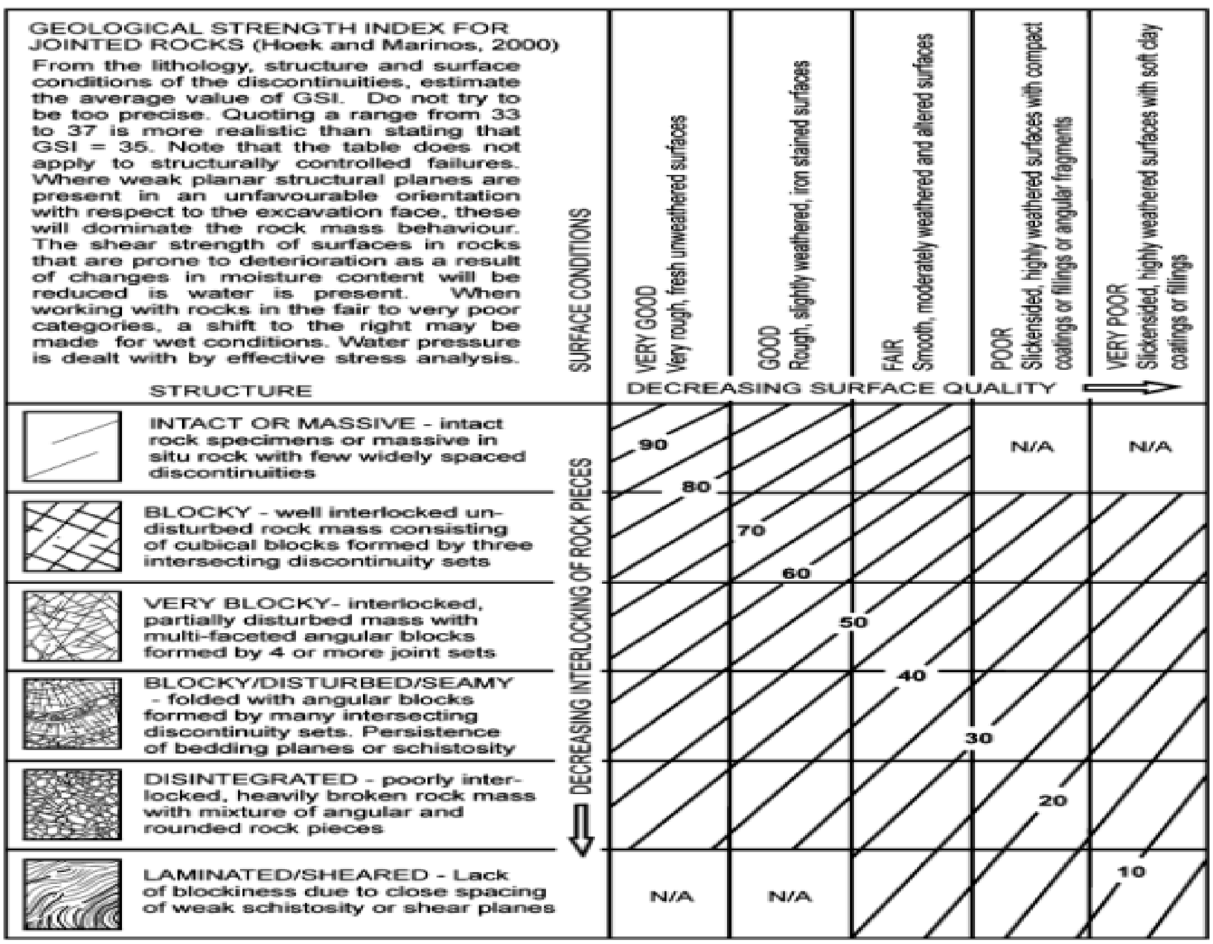

Appendix E: Dry unit weight of rock sample collected from field in laboratory results

Slope sections	Sample Code	m_d	ΔV	$\rho d = Md/\Delta V$ g/cm3	$\gamma d = \rho d * g$ KN/m3	$\gamma d(av)$
RSS1	S-11	669.9	270	2.48	24.8	25.7
	S-12	1045	400	2.61	26	
	S-13	725.0	305	2.38	23.7	
	S-14	1023.7	360	2.84	28.4	
RSS2	S-21	595.7	210	2.84	28.3	30.4
	S-22	648.2	220	2.95	29.4	
	S-23	351.7	100	3.52	35.2	
	S-24	661.8	230	2.88	28.7	
RSS3	S-31	761.8	240	3.17	31.7	27.1
	S-32	549.8	195	2.82	28.2	
	S-33	500.6	160	3.13	31.2	
	S-34	589.8	200	2.95	29.5	
RSS4	S-41	495.7	230	2.16	21.5	21.8
	S-42	438.8	170	2.58	25.8	
	S-43	477.9	243	1.97	19.6	
	S-44	765.0	370	2.07	20.6	
RSS5	S-51	550.1	212	2.59	25.9	26
	S-52	859.5	302	2.85	28.4	
	S-53	778.1	280	2.78	27.8	
	S-54	570.4	260	2.19	21.9	
RSS6	S-61	735.1	270	2.72	27.2	25.7
	S-62	646.2	260	2.49	24.8	
	S-63	585.7	230	2.55	25.4	
	S-64	462.8	280	1.65	25.7	
RSS7	S-71	725.2	250	2.90	29	23.6
	S-72	722.4	270	2.68	26.7	
	S-73	300.7	150	2.00	20	
	S-74	810.8	425	1.91	19	

Appendix F: Saturated unit weight of rock sample collected from field in laboratory results

Slope sections	Sample Code	m	ΔV	ρb = M/ΔV g/cm3	γsat = ρb * g KN/m3	γsat(av)
RSS1	S-11	714.1	270	2.64	26.4	26.6
	S-12	1080.7	400	2.70	27	
	S-13	755.3	305	2.48	24.7	
	S-14	130.1	360	0.36	28.6	
RSS2	S-21	603.2	210	2.87	28.7	30.6
	S-22	651	220	2.96	29.6	
	S-23	353.8	100	3.54	35.4	
	S-24	667.3	230	2.90	29	
RSS3	S-31	763.9	240	3.18	31.8	27.3
	S-32	553.9	195	2.84	28.4	
	S-33	502.7	160	3.14	31.4	
	S-34	592.3	200	2.96	29.6	
RSS4	S-41	543.7	230	2.36	23.6	23.9
	S-42	475.6	170	2.80	27.9	
	S-43	529.3	243	2.18	21.8	
	S-44	828.6	370	2.24	22.4	
RSS5	S-51	561.5	212	2.65	26.5	26.7
	S-52	876	302	2.90	29	
	S-53	808.6	280	2.89	28.8	
	S-54	587.9	260	2.26	22.6	
RSS6	S-61	770	270	2.85	28.5	27.1
	S-62	672.8	260	2.59	25.8	
	S-63	612.8	230	2.66	26.6	
	S-64	495	280	1.77	27.5	
RSS7	S-71	740	250	2.96	29.6	25.2
	S-72	735.7	270	2.72	27.2	
	S-73	338.3	150	2.26	22.5	
	S-74	913.5	425	2.15	21.5	

Appendix G: Point Load tests Results

Slope sections	Sample code	Length	width	height	De2	p	Is=p/De2	Is(50)	Is(50)av
RSS1	S-11	10	7	5		11.36	2.5	2.8	3.5
	S-12	12	8	6		12	1.96	2.4	
	S-13	9	7	5		6.48	1.45	1.65	
	S-14	14	5.5	4		19.65	7.1	7.8	
RSS2	S-21	11	7	4.2		32.13	8.6	9.4	8.2
	S-22	9	8	3		25.59	8.4	8.7	
	S-23	10	8	4		24.5	6.01	6.6	
RSS3	S-31	10	7.4	4		28.2	7.5	8.1	6.9
	S-32	9	6	4		23.13	7.4	7.9	
	S-33	11	5	3		13.58	7.1	6.39	
	S-34	10	6.5	4.4		18.4	5.1	5.5	
RSS4	S-41	10	6	4		14.9	4.8	4.9	4.4
	S-42	11	5.2	3		7.8	3.9	3.51	
	S-43	10	5.5	4		7.29	2.6	2.65	
	S-44	11	6.5	4.5		22.5	6.04	6.5	
RSS5	S-51	10	6	3		14	6.1	5.7	6.9
	S-52	11	6	4.5		21.4	6.2	6.6	
	S-53	12	6	5		20	5.2	5.6	
RSS6	S-61	12	6	5		14.4	3.7	3.9	3.12
	S-62	8	6	5		10.5	2.7	2.9	
	S-63	9	7	4		7.8	2.2	2.3	
	S-64	10	7	3		9.3	3.4	3.4	
RSS7	S-71	10	6	3.5		20.12	7.5	7.5	4.15
	S-72	9	7.5	4		12.45	3.2	3.4	
	S-73	9	5	3		5.96	3.1	2.7	
	S-74	12	7	5		12.36	2.7	3.02	

Appendix H: Basic rock mass rating system (Beinswski, 1989)

Strength of intact rocks	Uniaxial compressive strength (Mpa)	>250	100-2500	50-100	25-50	5-25	1-5	<1
1	Rating	15	12	7	4	2	1	0
	RQD%	90 - 100%	75 - 90%	50 - 75%	25 - 50%	<25		
2	Rating	20	17	13	8	3		
	Condition of discontinuities	Very rough discontinuo us No separation Un weathered	Rough walls Separation < 0.1mm Slightly weathered	Slightly rough Separation<1 mm Highly weathered	Slicken sides or gouge<5mm thick or continuous separation 1-5mm	Soft gouge>5mm thick or separation>5mm continuous decomposed wall rock		
3	Rating	30	25	20	10	0		
	Spacing discontinuities in m	>2	0.6-2	0.2-0.6	0.06-0.2	<0.06		
4	Rating	20	15	10	8	5		
	Ground water condition	Completely dry	Damp	wet	Dipping	Flowing		
5	Rating	15	10	7	4	0		
	RMR rating	100 - 81	80 - 61	60 - 41	40 - 21	<20		
	Class	A	B	C	D	E		
	Description	Very good rock	Good rock	Fair rock	Poor rock	Very poor rock		

Appendix I: Estimated shear strength parameters of rock mass using RocData software for the critical slope sections of rocks

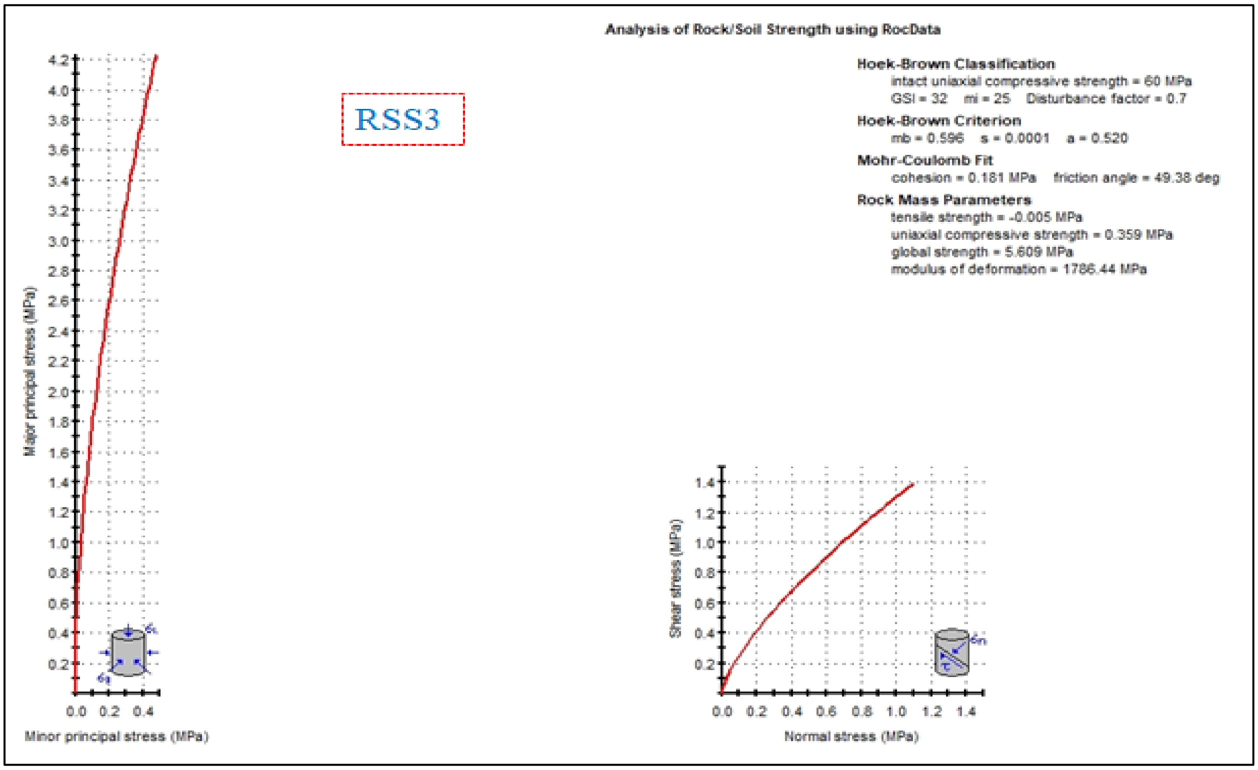

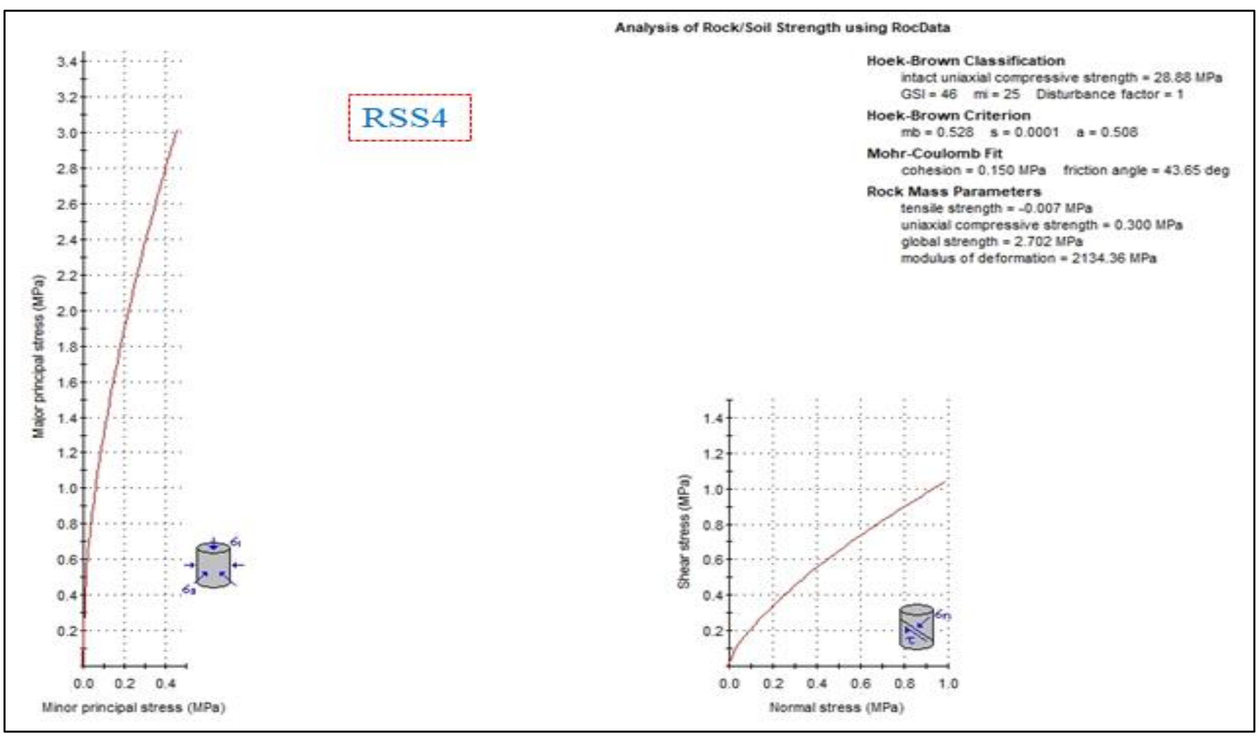

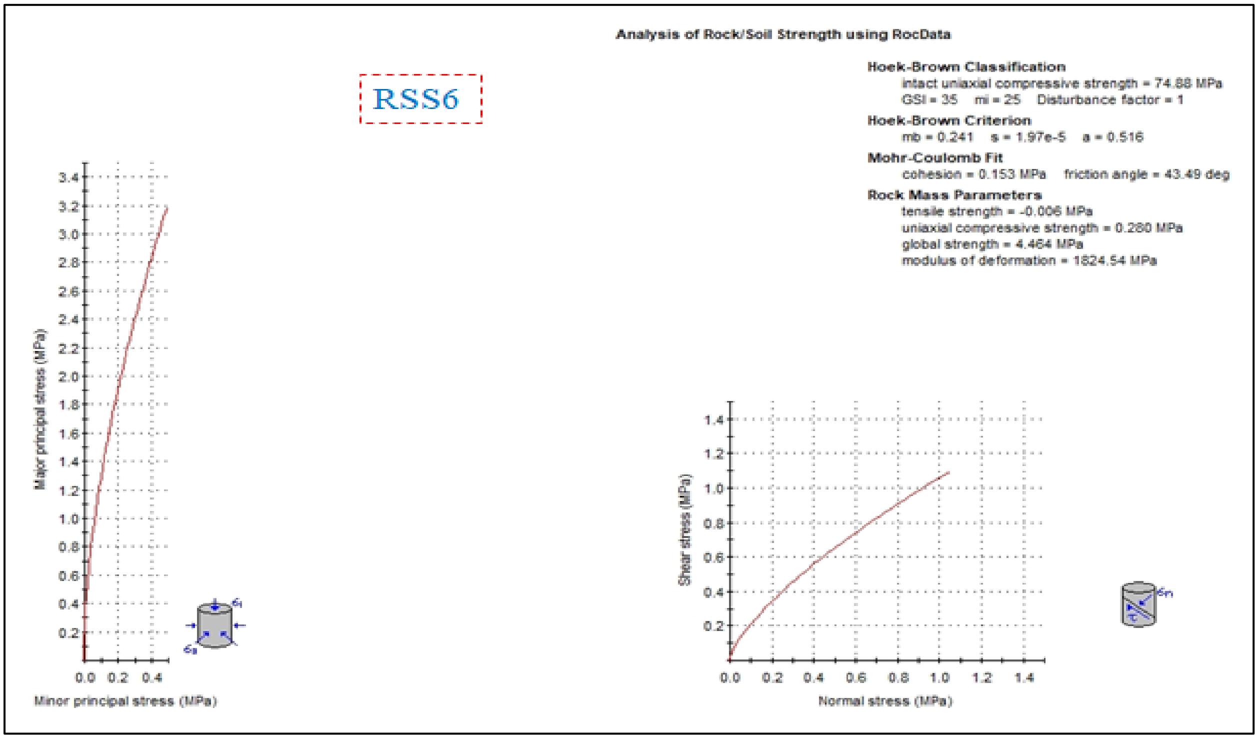

Analysis of Rock/Soil Strength using RocData
RSS6
Hoek-Brown Classification
intact uniaxial compressive strength = 74.88 MPa
GSI = 35 mi = 25 Disturbance factor = 1
Hoek-Brown Criterion
mb = 0.241 s = 1.97e-5 a = 0.516
Mohr-Coulomb Fit
cohesion = 0.153 MPa friction angle = 43.49 deg
Rock Mass Parameters
tensile strength = -0.006 MPa
uniaxial compressive strength = 0.280 MPa
global strength = 4.464 MPa
modulus of deformation = 1824.54 MPa
Major principal stress (MPa)
Minor principal stress (MPa)
Shear stress (MPa)
Normal stress (MPa)

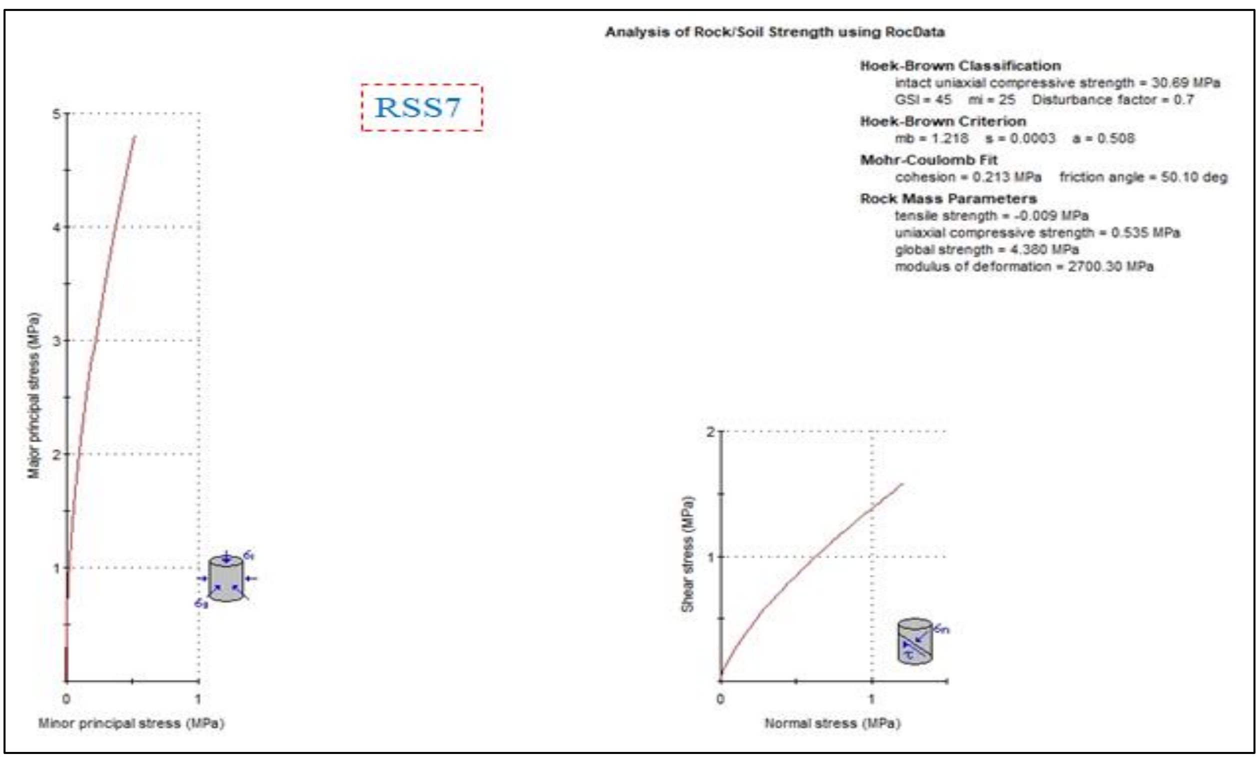

Analysis of Rock/Soil Strength using RocData
RSS7
Hoek-Brown Classification
intact uniaxial compressive strength = 30.69 MPa
GSI = 45 mi = 25 Disturbance factor = 0.7
Hoek-Brown Criterion
mb = 1.218 s = 0.0003 a = 0.508
Mohr-Coulomb Fit
cohesion = 0.213 MPa friction angle = 50.10 deg
Rock Mass Parameters
tensile strength = -0.009 MPa
uniaxial compressive strength = 0.535 MPa
global strength = 4.380 MPa
modulus of deformation = 2700.30 MPa
Major principal stress (MPa)
Minor principal stress (MPa)
Shear stress (MPa)
Normal stress (MPa)

Appendix J: The evaluated shear strength parameters of critical failure planes (joints) using Barton Bandis

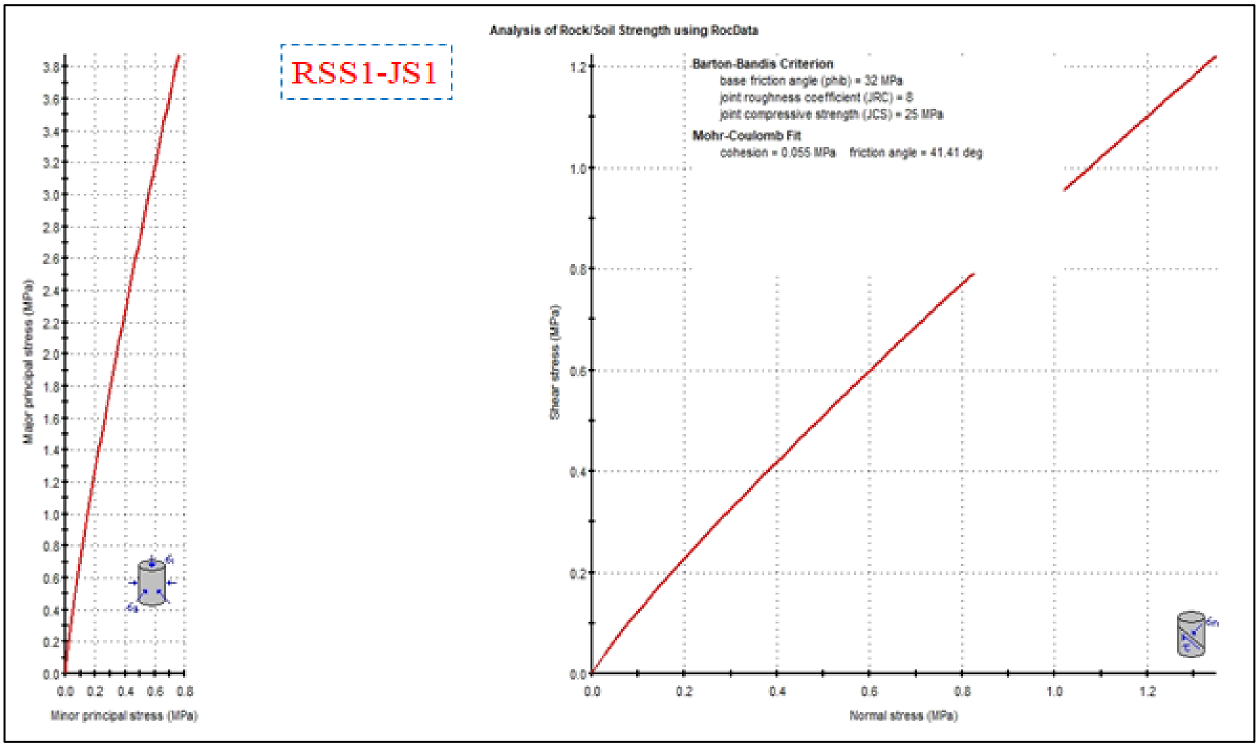

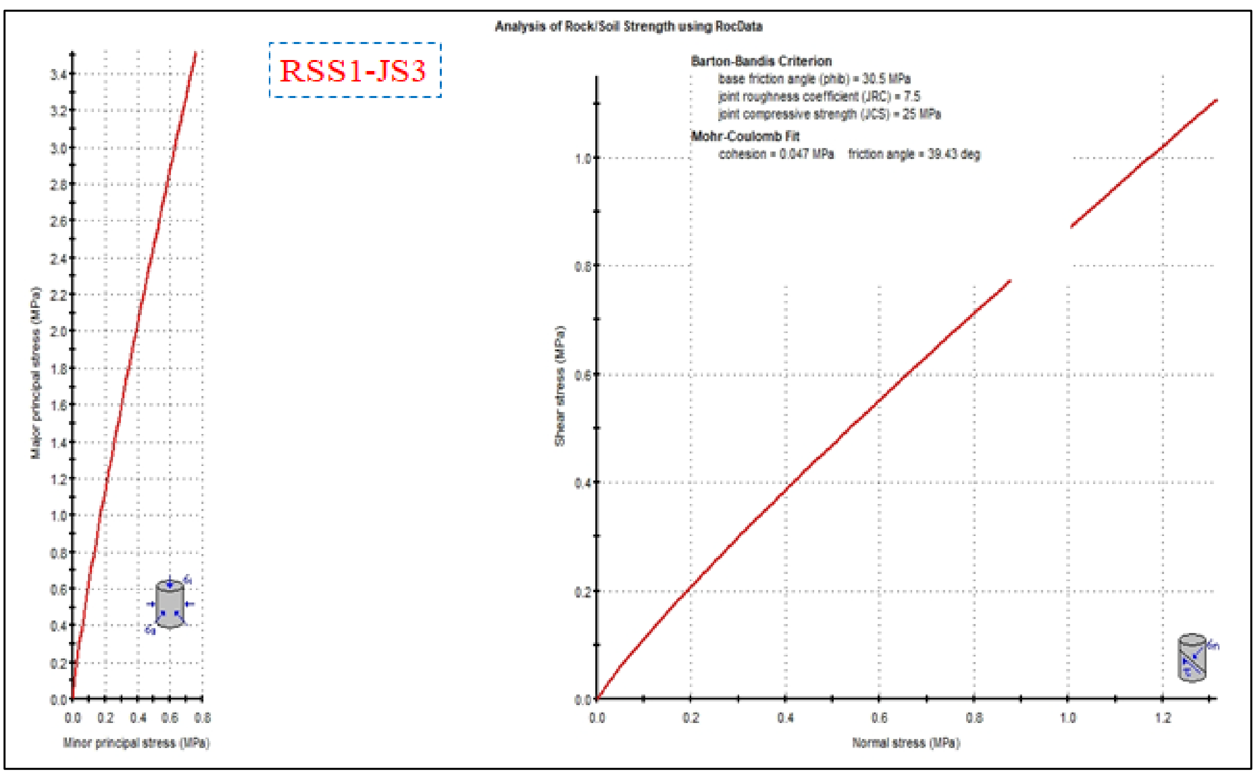

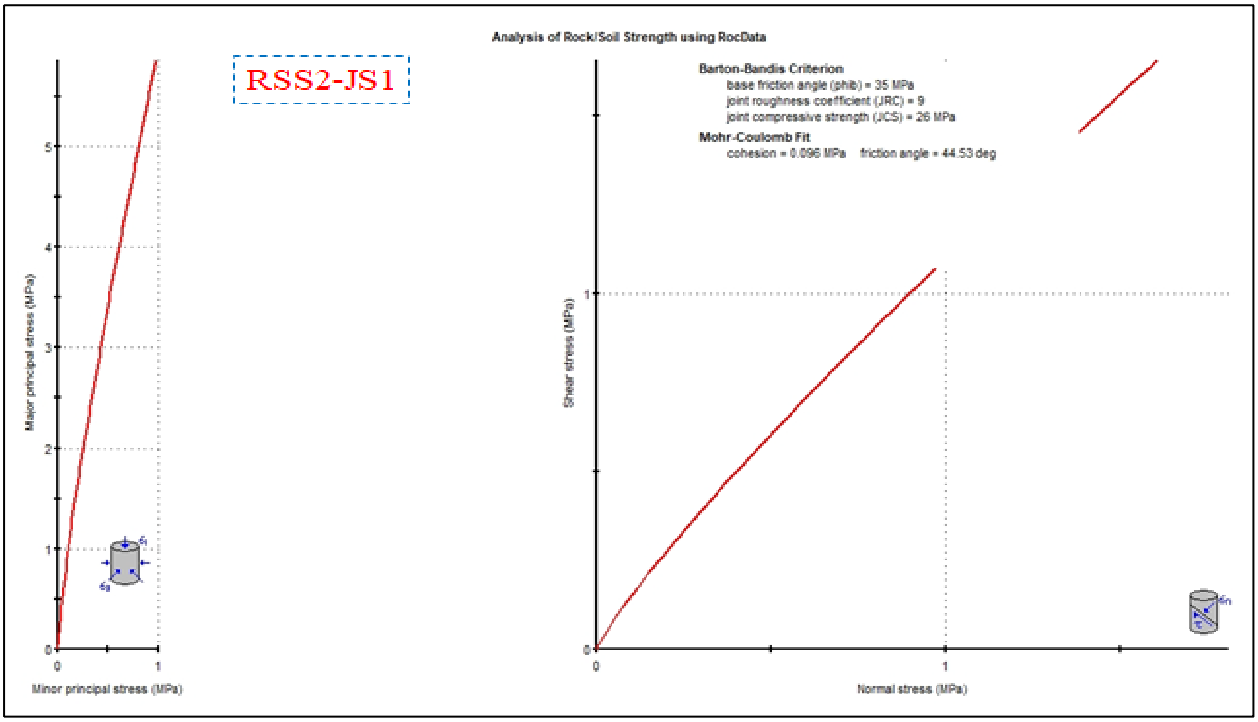
Analysis of Rock/Soil Strength using RocData
RSS2-JS1
Barton-Bandis Criterion
base friction angle (phib) = 35 MPa
joint roughness coefficient (JRC) = 9
joint compressive strength (JCS) = 26 MPa
Mohr-Coulomb Fit
cohesion = 0.096 MPa friction angle = 44.53 deg
Major principal stress (MPa)
Minor principal stress (MPa)
Shear stress (MPa)
Normal stress (MPa)

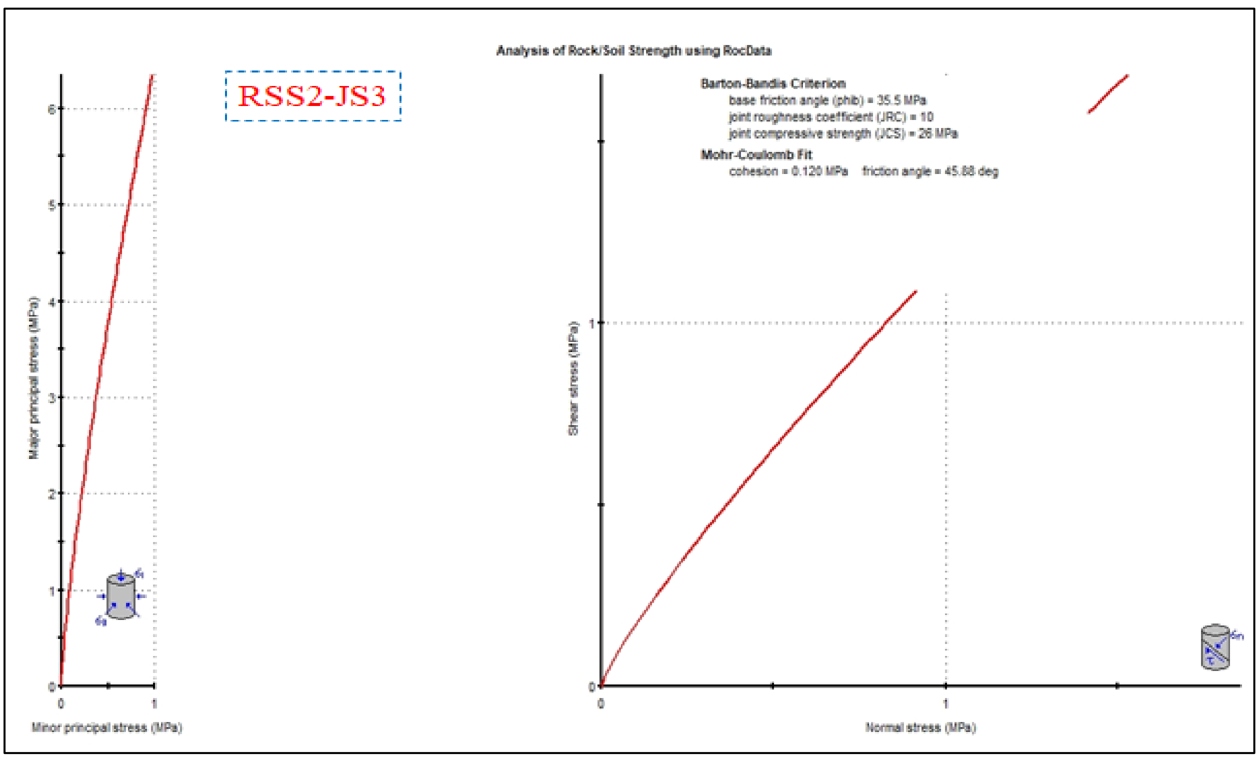
Analysis of Rock/Soil Strength using RocData
RSS2-JS3
Barton-Bandis Criterion
base friction angle (phib) = 35.5 MPa
joint roughness coefficient (JRC) = 10
joint compressive strength (JCS) = 26 MPa
Mohr-Coulomb Fit
cohesion = 0.120 MPa friction angle = 45.88 deg
Major principal stress (MPa)
Minor principal stress (MPa)
Shear stress (MPa)
Normal stress (MPa)

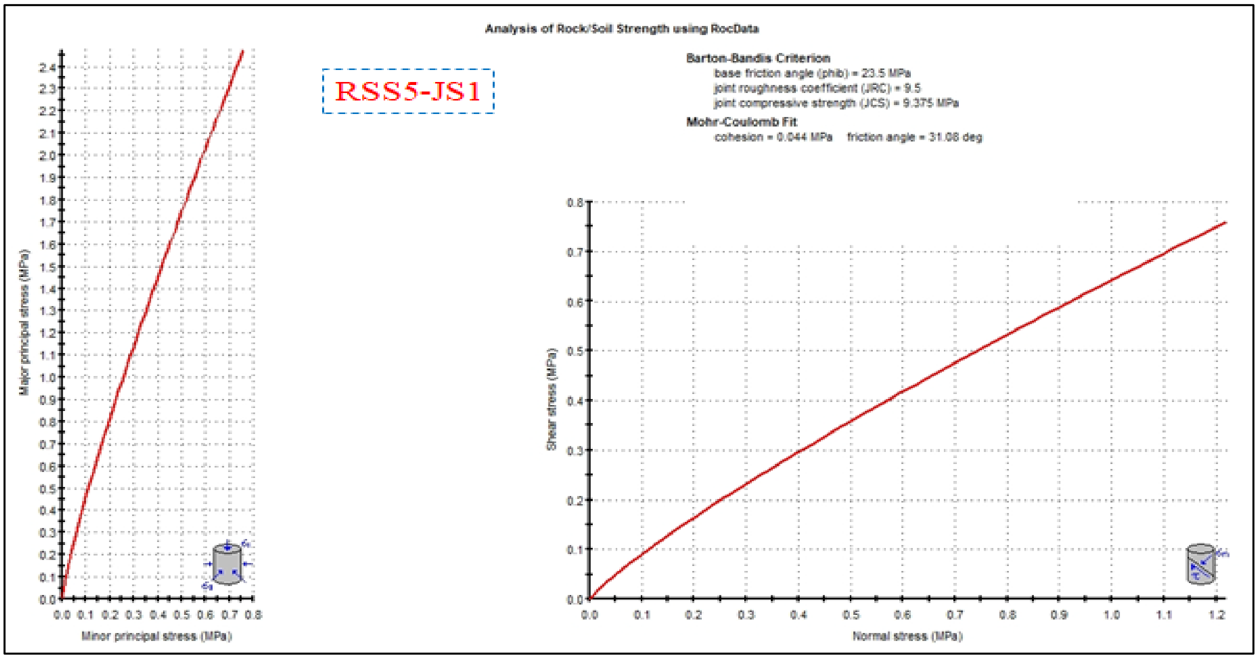

Appendix K: The Chart and table built in Rocdata software used for modelling

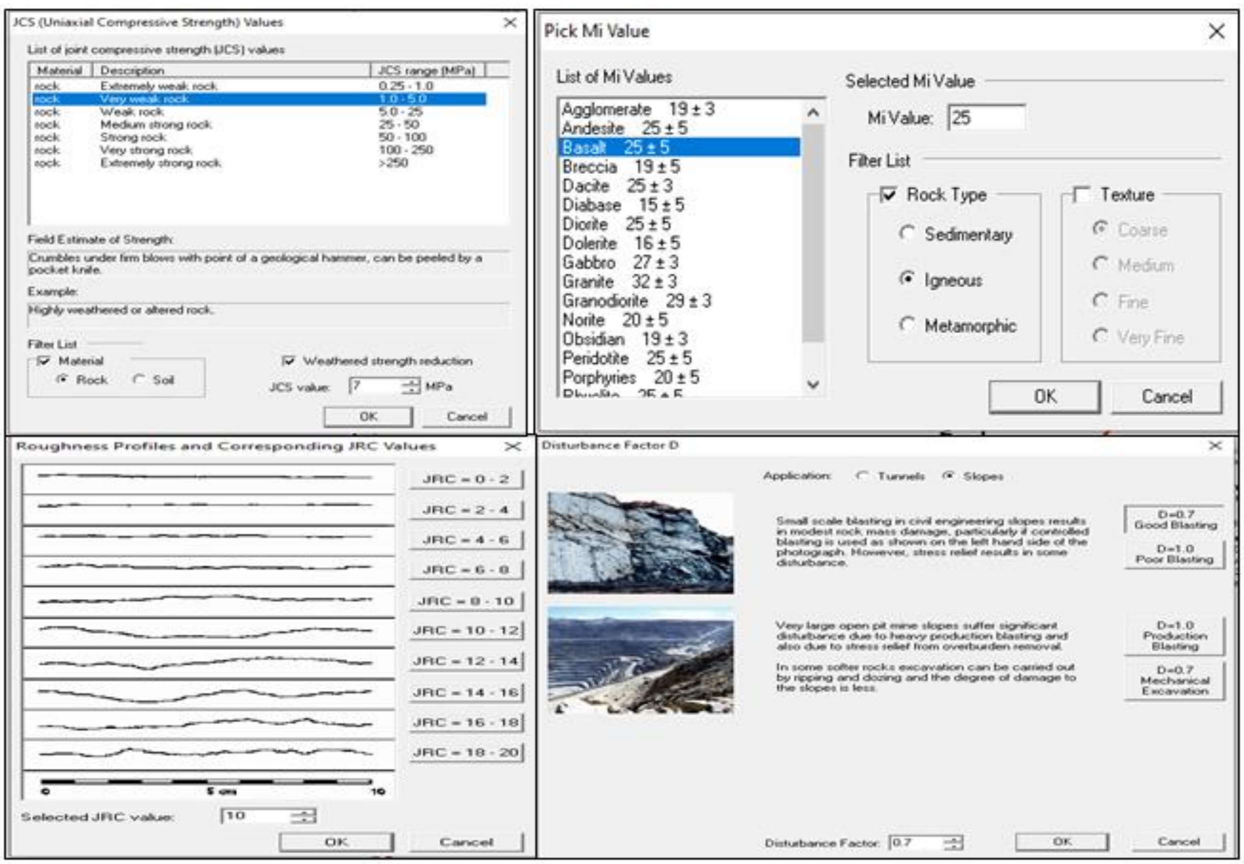

Appendix L: Soil Particle Size Analysis Result (Sieve and Hydrometer analysis)

Sieve No.	Test pit one (SS1)		Test pit two (SS2)	
	Opening (mm)	% Passing	Opening (mm)	% Passing
4	4.75	89.93	4.75	69.14
10	2.00	68.5	2.00	49.69
16	1.18	45.06	1.18	25.71
20	0.60	27.15	0.60	13.76
40	0.425	20.27	0.425	9.72
60	0.25	15.18	0.25	6.84
200	0.075	3.46	0.075	1.89
	0.020	2.50	0.02	1.50
	0.010	2.20	0.01	1.20
	0.002	2.00	0.002	1.00
	0.001	1.50	0.001	0.50

Appendix M: Atterberg limit test results at SS1 and SS2

Test pit 1(SS1) at depth 1m	Liquid Limit tests			Plasticity limit tests		
Sample number	S-1	S-2	S-3	S-01	S-02	S-03
Moisture can and lid number	A-1	A 3	S 2	R30	M32	N20
M_{SC} = Mass of empty, clean can + lid (grams)	22.1	22.4	22.7	9.5	9.3	9.4
M_{CMS} = Mass of can, lid, and moist soil (grams)	63.8	68.4	65.5	13.1	12.5	12.8
M_{CDS} = Mass of can, lid, and dry soil (grams)	51.2	54.3	52.2	12.3	11.8	12.1
M_S = Mass of soil solids (grams)	29.1	31.9	29.5	2.8	2.5	2.7
M_W = Mass of pore water (grams)	12.6	14.1	13.3	0.8	0.7	0.7
w = Water content, w%	43.3	44.2	45.1	28.6	28.0	25.9
No. of blows (N)	32	26	21	Average of PL % $= \frac{\mathbf{28.6+28+25.9}}{\mathbf{3}} =$ 27.5%		
	LL at 25 blows = 44.417					
PI	PI=LL-PL=44.417-27.5=16.917					

Test pit 2(SS2) at depth 1m	Liquid Limit tests			Plasticity limit tests	
Sample number	1	2	3	1	2
Moisture can and lid number	M67	M60	M10	N10	M100
M_{SC} = Mass of empty, clean can + lid (grams)	22.1	22.6	22.3	9.86	9.41
M_{CMS} = Mass of can, lid, and moist soil (grams)	50.5	59.1	55.2	14.21	13.6
M_{CDS} = Mass of can, lid, and dry soil (grams)	39.3	44.5	41.9	13.16	12.63
M_S = Mass of soil solids (grams)	17.2	21.9	19.6	3.3	3.22
M_W = Mass of pore water (grams)	11.2	14.6	13.3	1.05	0.97
w = Water content, w%	65.1	66.6	67.8	31.8	30.1
No. of blows (N)	34	29	22	Average PL % = $\frac{31.8+30.1}{2}$ = 30.95%	
	LL at 25 blows = 67.238				
PI	PI = LL-PL=67.238-30.95=36.288				

Appendix N: Natural Moisture contents of soil results (NMC) at slope section SS1 and SS2

Determination of Water (Moisture) Content of Soil	For pit 1 at SS1			For pit 2 at SS2		
Specimen number	1			2		
Moisture can and lid number	B-20	A-40	S-10	A-3	N-2	O
M_{SC} = Mass of empty, clean can + lid (grams)	29.3	26.5	30.3	42.7	43.8	39.6
M_{CMS} = Mass of can, lid, and moist soil (grams)	58.1	50.4	68.8	80.2	84.8	94.8
M_{CDS} = Mass of can, lid, and dry soil (grams)	52.1	45.5	60.7	75.9	80	88.9
M_S = Mass of soil solids (grams)	28.8	23.9	38.5	37.5	41	52.2
M_W = Mass of pore water (grams)	6	4.9	8.1	4.3	4.8	5.9
W= Water content, w%	20.8	20.5	21.04	11.5	11.7	11.3
Average of water contents (W %)	W1 = 20.78%			W2= 11.5%		

Appendix O: Specific Gravity tests results of SS1 and SS2

SPECIFIC GRAVITY DETERMINATION	For pit 1 at SS1			For pit 2 at SS2		
Specimen number	1			2		
Pycnometer bottle number	a	b	c	1	2	3
WP = Mass of empty, clean pycnometer (grams)	109.1	108	109.4	109.3	107.9	109.4
WPS = Mass of empty pycnometer + dry soil (grams)	116.6	115.6	119.4	116.9	117.4	119.5

WB = Mass of pycnometer + dry soil + water (grams)	385	386	387	384.8	390.4	387.1
WA = Mass of pycnometer + water (grams)	380.2	381.3	381	379.6	384.3	381
Specific Gravity (GS)	2.8	2.62	2.5	3.16	2.79	2.525
Average of Specific Gravity (G1+G2+G3)/3	$G_{s1}=\frac{2.8+2.62+2.5}{3}= 2.64$			$G_{s2}=\frac{3.16+2.79+2.525}{3}=$ 2.83		

Appendix P: Compaction tests results of SS1 and SS2

Laboratory Compaction test of Soil	For pit 1 at SS1				For pit 2 at SS2			
Compacted Soil - Sample no.	1	2	3	4	1	2	3	4
w = Assumed water content, w%	4	6	8	10	10	12	14	16
Actual average water content, w%	17.1	18.1	19.6	21.7	19.07	20.9	27.4	32.7
Mass of compacted soil and mold (grams)	9467	9601	9793	9711	9041	9211	9396	9297
Mass of mold (grams)	5172	5172	5172	5172	5172	5172	5172	5172
Wet mass of soil in mold (grams)	4295	4429	4621	4539	3869	4039	4224	4125
Volume of mold(cm3)	2137				2137			
Wet density, ρ , (g/cm3)	2.01	2.07	2.16	2.12	1.71	1.79	1.95	1.93
Dry density, ρd , (g/cm3)	1.68	1.77	1.81	1.74	1.43	1.45	1.53	1.45
Optimum Moisture Content	19.8%				28%			
Maximum Dry Density	1.81				1.532			

Appendix Q: Plasticity Chart (Das, 2002)

Plasticity index (PI)	Descriptions
0	Non plasticity
1-5	Slight plasticity
5-10	Low plasticity
10-20	Medium plasticity
20-40	High plasticity
>40	Very high plasticity

Appendix R: Temperature recorded in the study area (2000-2021)

ST. Name	Tep.Max	Years	Jan	Feb	Mar	Apr	May	Jun	Jul	Aug	Sep	Oct	Nov	Des
Qune	Tep.Max	2000	30	30.4	29.2	28.2	28.2	29	30	30	31	30.4	30.4	29
Qune	Tep.Max	2001	30.2	31.2	31.5	29	31.2	29.5	30.8	31.1	32.6	32.2	31.5	29
Qune	Tep.Max	2002	28.4	29.6	31	33	35	33	32.2	30	30	30	29	29.5
Qune	Tep.Max	2003	30	31.2	31	30.4	32.2	31.8	28.6	28	29.4	30.4	30.2	30
Qune	Tep.Max	2004	30.2	28.8	30	29.8	32	31.2	29	27.4	28.2	28.4	30.2	31
Qune	Tep.Max	2005	30	33	31	30	30.2	30	31	31	30.2	30	30	27
Qune	Tep.Max	2006	29.8	30.2	31.2	31	31	31	29	29	29.2	30.4	28.8	28.4
Qune	Tep.Max	2007	27.8	31	32	30.2	29.4	29.6	29.8	28.2	28.4	29.2	28.4	28
Qune	Tep.Max	2008	29	30.1	32	31.2	32	37.3	33.6	26.8	29.4	28.2	28.2	28.8
Qune	Tep.Max	2009	33	31	33	31.5	32.4	34.8	33.6	26.8	29.4	28.2	28.2	28.8
Qune	Tep.Max	2010	28.2	28	28.4	29	29.4	29.4	30	28.2	29	29	28	29
Qune	Tep.Max	2011	29	29.4	30	31.2	32	30	30.5	30.5	30	30	29.5	27.5
Qune	Tep.Max	2012	26.5	29.5	30	29.5	29.5	31.2	30.5	30	30.5	30	30	29.5
Qune	Tep.Max	2013	30.5	29.5	30	30.8	30.2	31	31.5	30	30	31	31	29.6
Qune	Tep.Max	2014	30	31.6	32.6	31.1	30.3	32.8	30.6	29	30.3	30.4	30.3	28.1
Qune	Tep.Max	2015	27.4	32.7	32.7	32.6	31.6	32	30.3	29.7	29.3	30.4	29.7	28.4
Qune	Tep.Max	2016	29	31.2	33.6	32.2	29.4	29.4	28.8	30.2	32.5	29	27.4	28
Qune	Tep.Max	2017	28.5	29.4	32.8	31.5	31.4	32.2	31.4	31	27.5	29.2	27.4	27
Qune	Tep.Max	2018	28.6	31.3	28.6	28.6	28.6	28.6	29.4	28.7	28.6	31.3	28.6	28.7
Qune	Tep.Max	2019	31.4	32.3	34.2	33.4	33.6	32.1	30.9	27.8	28.2	28	28.2	25.6
Qune	Tep.Max	2020	28.1	29.3	27.8	31	31.1	30.1	30.2	29.6	28.7	28.1	29.3	27.8
Qune	Tep.Max	2021	27.4	29.2	31	32.3	32.1	29.2	31	32.3	32.1	31.2	29.1	30
Qune	Tep.Max	2022	29	29.2	29.9	28.7	28.9	30	32.4	29.9	28.7	29.4	29.4	29.4
		Average	29.22	30.40	31.02	30.70	30.94	31.10	30.66	29.36	29.70	29.76	29.25	28.61

ST. Name	Tep. Min	Years	Jan	Feb	Mar	Apr	May	Jun	Jul	Aug	Sep	Oct	Nov	Des
Qune	Tep. Min	2000	12	15.2	14	14.5	13	15.4	16	14	16	15	14.3	14.8
Qune	Tep. Min	2001	10.4	15	10	15	9.4	11	14	14.8	11	12.5	12.4	11.8
Qune	Tep. Min	2002	9	8.6	13	13	14.2	16	15	14.2	11.8	11.2	14	11.9
Qune	Tep. Min	2003	14.4	15	13.6	14.2	14.8	13.8	14	14.6	15.6	12	14.6	10.8
Qune	Tep. Min	2004	10	11.2	10.4	14.4	12.6	12	10.2	1.2	13.6	13.6	10.6	12.8
Qune	Tep. Min	2005	10.2	11.2	15	14.6	14.8	15.2	15	15	15	14.8	10.1	8.4
Qune	Tep. Min	2006	12	17	10	14	14.2	14	14	14	14.2	13.4	12	10.8
Qune	Tep. Min	2007	10.2	15.2	15	14.2	14.4	14.5	14.2	14.7	13	10.1	9.2	8
Qune	Tep. Min	2008	9	7.3	9.4	11.2	14	13	7.5	8.5	9	10	10.2	11
Qune	Tep. Min	2009	9.5	11	11	14.5	14	15.4	14.2	15	15	10.2	10.5	13.5
Qune	Tep. Min	2010	9.5	13.2	14	15	15	16	15	14	15	15	12	10
Qune	Tep. Min	2011	12	14.8	14.8	12.8	12	14	14	13.5	14	13.5	13.5	8.5
Qune	Tep. Min	2012	9.5	9.8	11	12	13	14	11.5	14	14	12	13	13
Qune	Tep. Min	2013	13.5	11.5	12.5	13.5	14	15	14	14	14	12	12	8.4
Qune	Tep. Min	2014	8.5	11.3	12.4	13	13.8	14.3	14	14	14	10.4	9.5	7
Qune	Tep. Min	2015	7	8.2	11.8	12	14	14.8	14.6	13.8	13.7	13	10.2	10.6
Qune	Tep. Min	2016	10	10	14.8	15.2	15	15	14.8	14	14	13	11.2	12
Qune	Tep. Min	2017	11	10.2	11.8	13.7	14.8	15	14.3	13.5	13	10	7.8	5.5
Qune	Tep. Min	2018	11	12	13	10.4	9	9.6	13.4	12	8.4	9.2	8.7	10
Qune	Tep. Min	2019	7	10	13.5	12.5	13.7	14.4	13.2	13	13.1	9.8	9.7	8
Qune	Tep. Min	2020	12	11	10.2	12.4	13.5	13.8	13	11.8	13	9.9	7.8	6.8
Qune	Tep. Min	2021	4.1	4.3	10	13	12.1	12.5	12	11	12	8	6.5	6
Qune	Tep. Min	2022	7	7.2	7.2	7.2	7.2	13	12	13	12	13	12	13
		Average	9.95	11.31	12.10	13.14	13.15	13.99	13.47	12.94	13.23	11.81	10.95	10.11

ST. Name	Tep. Max	Years	Jan	Feb	Mar	Apr	May	Jun	Jul	Aug	Sep	Oct	Nov	Des
Badesa	Tep. Max	2000	29	29.6	28.4	28	31.5	29.9	28.7	30.4	29.3	27.5	28.6	31.3
Badesa	Tep. Max	2001	29.5	31	29	29	30.3	37.2	32.5	29.9	30.2	30	31.3	31.3
Badesa	Tep. Max	2002	29.4	32.4	32.2	31.4	32.2	32	30.4	30	30	31	31	30.4
Badesa	Tep. Max	2003	32	32.8	33	33	32	32	28.4	30	30	31.4	33	32
Badesa	Tep. Max	2004	31.4	32.2	34	29.4	31.5	31.5	30.3	29	28.9	29.2	30.4	29
Badesa	Tep. Max	2005	29.8	33.5	31.5	37	29.3	29.6	29	29.6	28.6	30.4	29.4	29.4
Badesa	Tep. Max	2006	30.6	31.7	31.5	29.8	29.8	31	30	28.4	27.6	29.2	29.2	27.6
Badesa	Tep. Max	2007	30.7	32.6	33	30.4	31.6	30.4	29.5	28	28.2	28.8	29	29.2
Badesa	Tep. Max	2008	30.7	31.2	33	31.3	30.8	32.2	29.8	29.5	29.4	30.8	28.2	29.4
Badesa	Tep. Max	2009	29.8	32.2	33.8	31.2	39.8	32.4	30.4	29.9	30.1	30.4	30.5	29.2
Badesa	Tep. Max	2010	30.4	32.2	29	29.4	30.4	31.2	29.4	28.7	29	29.3	29.5	29.8
Badesa	Tep. Max	2011	30.7	32.2	32.6	33	34	31.4	30.4	30.4	28.4	30.8	31	29.8
Badesa	Tep. Max	2012	30	31.8	32.2	30.2	33.8	32.8	30.4	29.3	28.8	29.3	30	29.8
Badesa	Tep. Max	2013	32.6	32.8	32.5	29.6	28.8	28.6	31.5	27.5	29.6	29.4	29	28.7
Badesa	Tep. Max	2014	29.9	31.5	32	30	29.4	32.6	31.6	28.6	28.8	30	30.3	29.6
Badesa	Tep. Max	2015	30.6	32.3	32.7	33.5	32.1	31	31.6	31.3	30.4	31.3	37.2	31.3
Badesa	Tep. Max	2016	33.4	32.5	34.6	32.5	30.4	30	29.8	29.7	30.6	32	32.5	32.3
Badesa	Tep. Max	2017	30	32.5	33.7	32	31	32.5	30.8	31.2	32	31.2	29.9	30.7
Badesa	Tep. Max	2018	31	31	31	31	30.9	29.7	29.3	30	30.2	31.3	30.2	32
Badesa	Tep. Max	2019	32.7	33	33.8	33.8	34.4	30	30	28.7	28.7	30	30	29.5
Badesa	Tep. Max	2020	32	33	33.5	32.2	29.4	30.4	30.4	30.4	28.7	31	30.3	30.4
Badesa	Tep. Max	2021	30.2	31.3	32	30	30	29.4	29.4	29.4	29.4	31.5	31.5	31.5
Badesa	Tep. Max	2022	34.5	34.5	34.5	34.5	34.5	30	29.2	29.3	29.3	29.3	29.3	29.3
		Average	30.91	32.17	32.33	31.40	31.65	31.21	30.12	29.53	29.40	30.22	30.49	30.15

ST. Name	Tep. Min	Years	Jan	Feb	Mar	Apr	May	Jun	Jul	Aug	Sep	Oct	Nov	Des
Badesa	Tep. Min	2000	11.5	10	11.7	12	11.6	10.3	12	10.2	12.3	11.8	13.2	12.5
Badesa	Tep. Min	2001	11	10.5	10	10	8.5	11	12	10.5	8.4	13.7	13.5	11.9
Badesa	Tep. Min	2002	6.5	6	7	11.5	13	11.5	13	13.2	9.5	6	7	9.5
Badesa	Tep. Min	2003	5	10	11	11.8	10	12	13	10	11.5	5.5	6.5	4.5
Badesa	Tep. Min	2004	7	6	5	9	10	11.4	12.5	11	11	10	5.9	5.3
Badesa	Tep. Min	2005	7	5	8.9	10	11.5	11.8	11.2	11.7	9.7	6.5	5	3
Badesa	Tep. Min	2006	5.3	9.4	8	10	10	10.9	9.5	11.5	11	8.4	7.2	6.7
Badesa	Tep. Min	2007	6.2	9	8.8	7.2	11.7	12	10.2	11.7	10.5	4.6	4.5	4.3
Badesa	Tep. Min	2008	5.4	5.5	6	8	12	10.5	11	8.9	10	7.2	4.5	3.7
Badesa	Tep. Min	2009	4.5	7	9.5	11.3	11.6	8.4	13.2	12.5	10	6.5	5.4	10
Badesa	Tep. Min	2010	4.4	9.4	7.2	6.8	10.3	13.7	13.3	12.2	8.5	9	6	2.5
Badesa	Tep. Min	2011	5.5	6.7	9.4	11	12	13.5	13	10.7	11	7.5	5	4.5
Badesa	Tep. Min	2012	6	6.5	7.5	12.5	10.2	11.9	11.5	12	11.6	5.3	4.9	6.4
Badesa	Tep. Min	2013	4.5	6.3	10.2	12.6	12.3	13	13.6	10	11.2	7	6	5
Badesa	Tep. Min	2014	5.3	8.4	10.6	12	11.8	11	13	11.2	12.5	7.2	7.6	5.6
Badesa	Tep. Min	2015	5.9	6.4	10.4	11.5	13.2	13.6	13	13.4	12.5	9.2	7.5	9.5
Badesa	Tep. Min	2016	15.4	7.5	14.3	14.8	12.5	10	13.6	12.8	11.9	11	7.2	7
Badesa	Tep. Min	2017	9	9.4	11	11.4	12	13.7	13.2	9	8	8.4	5.5	3.6
Badesa	Tep. Min	2018	2	5	6	9	11.6	12.5	13.2	12.2	10	8.9	7	8
Badesa	Tep. Min	2019	5	7.5	11	12.9	12	12.9	12	12.9	13.9	9	5.2	4.5
Badesa	Tep. Min	2020	9	8	10.5	12.3	11.3	12	12	13	13	13	6.3	5
Badesa	Tep. Min	2021	6.5	7	12.3	12.2	10.7	8.5	7	7.5	10	8.3	9	10
Badesa	Tep. Min	2022	12	12.2	12.6	14	13	13	11	11	12	12	12	12
		Average	6.95	7.77	9.52	11.03	11.43	11.70	12.04	11.27	10.87	8.52	7.04	6.74

Appendix S: Rainfall recorded in the study area (2000-2021)

ST. Name	Prcip	Years	Jan	Feb	Mar	Apr	May	Jun	Jul	Aug	Sep	Oct	Nov	Des
Qune	Prcip	2000	50.5	40	124	39.7	70.1	101.9	27.6	135.8	17.4	27.4	35	10
Qune	Prcip	2001	36.1	98.4	47	0	9.7	51.8	49	46	33.7	123	31.5	101.8
Qune	Prcip	2002	70.5	0	174	49.7	73.1	121.9	27.6	145.8	17.4	17.4	25	20
Qune	Prcip	2003	3.2	53.1	54.5	112.7	25.2	105	205.4	225	140.8	0	30	15.8
Qune	Prcip	2004	51.4	0	73.4	164.8	2.4	36.1	125.6	1446	246.8	99	17	28
Qune	Prcip	2005	0	14.8	107.6	173.6	208.8	98.4	215.6	87.6	171	4.8	12.4	0
Qune	Prcip	2006	12	33.4	130	88	63.4	47	140.8	243.3	101.1	133	0	73.2
Qune	Prcip	2007	18.2	0	148.4	285.4	43.4	0	192.3	200.9	147.2	16.2	0	0
Qune	Prcip	2008	11.6	0	18.5	105.4	118.9	9.7	0	0	0	0	0	0
Qune	Prcip	2009	32	10.1	42.2	71.1	0	51.8	93.7	95.6	58.2	59.9	54.5	63.3
Qune	Prcip	2010	2.5	85.8	199.2	87.2	65.1	49	133	103	211.2	0	3	0
Qune	Prcip	2011	0	0	43.2	36	110.4	46	98.5	141.5	57.5	0	0	0
Qune	Prcip	2012	0	0	0	95.5	44	33.7	88.5	192	108.5	13	1.6	7
Qune	Prcip	2013	26.7	2	7	51.5	20	123	58	69	146.5	5	41	40
Qune	Prcip	2014	0	3.1	172.9	174.8	190.7	31.5	181.5	205	108.4	147.3	8.9	3.1
Qune	Prcip	2015	0	0	9	42.6	131	101.8	49.8	236.5	105.2	2.6	0	18.8
Qune	Prcip	2016	5.3	36.6	39.6	254.4	220.8	87.7	205.8	119.1	116.2	28.2	12	0
Qune	Prcip	2017	0	39.1	24.5	35.5	77.6	20.9	86.2	162.9	186.9	11	0	0
Qune	Prcip	2018	0	0	0	0	0	0	67.2	50	102.7	69.2	29.9	0
Qune	Prcip	2019	0	12.7	56.8	90.2	188.4	138.6	130.6	194.8	209.4	95.5	91.4	25.8
Qune	Prcip	2020	0	0	0	56.5	162.1	143.7	60.8	175.1	263.4	119.8	13.4	4.4
Qune	Prcip	2021	11.5	0	4.7	3.8	98.9	0	0	176.2	138.1	0	0	0
Qune	Prcip	2022	131.3	0	0	0	0	89.3	110.4	83.1	0	0	0	0
		Average	20.12	18.66	64.20	87.76	83.65	64.73	102.08	197.13	116.85	42.27	17.68	17.88

ST. Name	Prcip	Years	Jan	Feb	Mar	Apr	May	Jun	Jul	Aug	Sep	Oct	Nov	Des
Badesa	Prcip	2000	31.5	140.5	84.5	0	37.9	9.8	105.6	201.8	54.1	38	12	22.9
Badesa	Prcip	2001	126.7	335.9	144.8	18.7	77.4	99.3	149.5	147.7	51.6	121.4	110.7	92.1
Badesa	Prcip	2002	16.5	0	69.6	48.2	106	56.3	108.1	150.8	94.9	50.5	0	72.2
Badesa	Prcip	2003	1.5	0	55.2	117.2	65.9	136.2	211.8	149.1	106.3	3.2	18.3	10.8
Badesa	Prcip	2004	20.5	0	55	338	33.7	77.2	153.3	117.3	258.1	135.2	18.8	31.2
Badesa	Prcip	2005	9.3	2.1	99.3	191.1	215.2	66.3	178.7	138.2	152	50	58	0
Badesa	Prcip	2006	2.6	8.9	71.4	187.9	101.4	73.8	127.1	215.1	212.4	92.5	1	75.4
Badesa	Prcip	2007	0	11.9	55.4	126.9	105.1	98.4	166	190.9	309	53.8	5.3	0
Badesa	Prcip	2008	0	0	0	165.1	172.2	41.3	152.9	222	140.5	50.7	93.4	0
Badesa	Prcip	2009	20.5	0.7	54	126.7	45.4	67.9	134.7	148.1	84.5	29.9	22.6	2.2
Badesa	Prcip	2010	87.7	202.5	280	335.9	48.2	278.5	162.3	254.7	0	0	0	0
Badesa	Prcip	2011	0	16.4	19	144.8	244.6	99.5	223.8	280.3	37.9	25.8	0	0.2
Badesa	Prcip	2012	0	18	123.3	18.7	185.6	178.6	195.4	322.6	9.8	1.2	15.7	17.2
Badesa	Prcip	2013	0	144.8	183.4	77.4	52.8	205.6	139.9	276.3	105.6	63.6	0	0
Badesa	Prcip	2014	0	152.8	119.4	99.3	32.6	105.6	275.3	166.6	201.8	16	0	0.3
Badesa	Prcip	2015	0	22.3	24.6	149.5	140.3	53	109.2	113.2	54.1	37	24	68.6
Badesa	Prcip	2016	0	14.6	225.4	147.7	58.5	147.3	41.5	103.7	38	0	0	0
Badesa	Prcip	2017	0	49.4	77.2	51.6	68.5	5.1	3.2	3.5	0	0	0	22.7
Badesa	Prcip	2018	50.1	196.7	144.1	121.4	57.3	109.1	54.3	79.4	22.9	1.1	20.4	22
Badesa	Prcip	2019	0.5	73.6	115.6	110.7	140.6	171.4	241.3	115.6	67.6	36.7	89.8	189.2
Badesa	Prcip	2020	0	0	240.1	92.1	135.7	68.4	0	0	31.7	10.9	0	0
Badesa	Prcip	2021	10.9	0	0	171.5	205.4	94.3	95	80	86	95	80	59
Badesa	Prcip	2022	0.4	0.4	0.4	9.5	9.5	135.8	143.2	102.7	102.7	102.7	102.7	102.7
		average	16.47	60.50	97.47	123.91	101.73	103.42	137.92	155.63	96.59	44.14	29.25	34.29